THE QUARTERLY JOURNAL OF
MECHANICS AND APPLIED MATHEMATICS

VOLUME VIII PART 3
SEPTEMBER 1955

OXFORD
AT THE CLARENDON PRESS
1955.

Price 15*s. net*

PRINTED IN GREAT BRITAIN BY CHARLES BATEY AT THE UNIVERSITY PRESS, OXFORD

THE QUARTERLY JOURNAL OF MECHANICS AND APPLIED MATHEMATICS

THE QUARTERLY JOURNAL OF MECHANICS AND APPLIED MATHEMATICS is published at 15*s.* net for a single number with an annual subscription (for four numbers) of 50*s.* post free.

NOTICE TO CONTRIBUTORS

1. *Communication.* Papers should be communicated to one or other of the Executive Editors, by name, at King's College, Strand, London, W.C. 2.

2. *Presentation.* Manuscripts should preferably be typewritten, and each paper should be preceded by a summary not exceeding 300 words in length. References to literature should be given in standard order, *author, title of journal, volume number, date, page.* These should be placed at the end of the paper and arranged according to the order of reference in the paper.

3. *Diagrams.* The number of diagrams should be kept to the minimum consistent with clarity. The lines of the figures should be drawn in ink either on draughtsman's paper or on good quality white paper. Each individual line in the figure should bear reducing to one-half of the size of the original, and great care should be exercised to see that the lines are regular in thickness, especially where they meet. Lettering of the figure should be in pencil and should be sufficient to define clearly the lines and curves in it. The writing of formulae or of explanations on the diagram itself should be avoided. All explanations of symbols, etc., should be given in underline. Contributors should indicate on their manuscripts where figures should be inserted.

4. *Tables.* Tables should preferably be arranged so that they can be printed with the columns parallel to the longer edge of the page.

5. *Notation.* All single letters used to denote vectors in the manuscript should be marked by underlining with a wavy line. Scalar and vector products should be denoted by $\underset{\sim}{a} . \underset{\sim}{b}$ and $\underset{\sim}{a} \wedge \underset{\sim}{b}$ respectively. Real and imaginary parts of complex quantities should be denoted by re and im respectively.

6. *Offprints.* Authors of papers will be entitled to 25 free offprints. This number is available for sharing between authors of joint papers.

7. All correspondence other than that dealing with contributions should be addressed to the Publisher:

GEOFFREY CUMBERLEGE
OXFORD UNIVERSITY PRESS
AMEN HOUSE, LONDON, E.C. 4

NICS

ICS is
n (for

cutive

hould
rature
page.
der of

t with
paper
ucing
at the
hould
The
All
hould

n the

d be
oted
ould

er is

ssed

The s
for the
this equ
this agr

1. Int

In a se
second
motion
this w
accura
metho
and fo
makes
of prob

2. The

We
the rea
Und
potenti

We use

γ is
c_∞ is
U is
We sha

[Quart. J
5092.3

SECOND-ORDER METHODS IN INVISCID SUPERSONIC THEORY

By J. FELL *and* D. C. M. LESLIE

(*Sir W. G. Armstrong Whitworth Aircraft Ltd., Coventry: Armaments Division*)

[Received 21 October 1954]

SUMMARY

The second-order perturbation equation for the velocity potential is written down for the steady supersonic flow of an inviscid polytropic gas. A particular integral of this equation is obtained for the general three-dimensional case, and it is shown that this agrees with the known result of Van Dyke for the axisymmetric problem.

1. Introduction

In a series of papers (**1**, **2**, **3**, **4**) Van Dyke has studied the application of second-order methods to the solution of problems in the steady supersonic motion of an inviscid polytropic gas past one or more slender bodies. From this work it is clear that this approach gives results of very satisfactory accuracy for many common wing and body shapes, but so far practical methods of calculation have only been available for two-dimensional wings and for bodies of revolution at zero yaw. The work described in this paper makes it possible to develop second-order solutions for a much wider class of problems.

2. The perturbation equations

We shall briefly deduce the relevant second-order equations, referring the reader to Van Dyke (**1**, **2**) for a detailed discussion of their validity.

Under the assumption of steady irrotational flow, there exists a velocity potential $\Omega(x, y, z)$ which satisfies

$$\left.\begin{aligned}(c^2\delta_{ij}-\Omega_i\,\Omega_j)\Omega_{ij} &= 0\\ c^2 = c_\infty^2-\tfrac{1}{2}(\gamma-1)(\Omega_i\,\Omega_i-U^2)&\end{aligned}\right\}. \tag{2.1}$$

We use a summation convention and define

$$\Omega_i = \frac{\partial\Omega}{\partial x_i}, \qquad \Omega_{ij} = \frac{\partial\Omega}{\partial x_i\,\partial x_j};$$

γ is the adiabatic exponent,
c_∞ is the velocity of sound in the free stream,
U is the velocity of the free stream.

We shall define the quantities M and β by

$$M = U/c_\infty, \qquad \beta^2 = M^2-1.$$

If we approximate to Ω by the expression

$$\Omega = U(x+\phi) \tag{2.2}$$

and assume that ϕ is so small that we may neglect all terms which are $o(\phi^2)$, (2.1) reduces to the linearized equation

$$L(\phi) \equiv \phi_{yy}+\phi_{zz}-\beta^2\phi_{xx} = 0, \tag{2.3}$$

where suffixes denote partial derivatives. This is not sufficiently accurate for many purposes, and so we consider the second-order approximation in which we write

$$\Omega = U(x+\phi+\varphi). \tag{2.4}$$

In this expression we assume that ϕ still satisfies (2.3) but that we now neglect only terms which are $o(\varphi^2)$. Substituting in (2.1), we find

$$L(\varphi) = M^2[\tfrac{1}{2}(\gamma-1)M^2(2\phi_x+\phi_i\phi_i)\phi_{jj}+2\phi_i\phi_{xi}+\phi_i\phi_j\phi_{ij}], \tag{2.5}$$

where i and j are dummy suffixes and denote derivatives.

A careful examination of orders of magnitude shows that we may drop from the right-hand side all triple products involving streamwise derivatives: thus we may write

$$L(\varphi) = 2M^2[(N-1)\beta^2\phi_x\phi_{xx}+\phi_y\phi_{xy}+\phi_z\phi_{xz}+\tfrac{1}{2}(\phi_y^2\phi_{yy}+\phi_z^2\phi_{zz})+\phi_y\phi_z\phi_{yz}], \tag{2.6}$$

where

$$N = \frac{(\gamma+1)M^2}{2\beta^2}.$$

This equation for φ is linear, and, if we can find a particular integral (p.i.), the complementary function will satisfy the linearized equation (2.3) and can be treated by standard methods.

Before attempting to find such a particular integral we shall make the further simplification of neglecting the triple terms. This is the correct procedure for planar systems, and in many other problems the use of an approximate particular integral for the triple terms can be justified.

We finally reduce our problem to that of finding a p.i. of the equation

$$L(\varphi) = 2M^2[(N-1)\beta^2\phi_x\phi_{xx}+\phi_y\phi_{xy}+\phi_z\phi_{xz}], \tag{2.7}$$

where

$$L(\phi) = 0.$$

Stated in this form the problem is independent of the derivation sketched above. We may write the general solution of

$$L(\phi) = 0$$

in the form

$$\phi = -\frac{1}{\pi}\int\!\!\int\!\!\int_{\Sigma_1}\frac{f(x_1,y_1,z_1)}{|\mathbf{R}-\mathbf{R}_1|}\,d\tau_1, \tag{2.8}$$

where we are using the hyperbolic vector notation

$$\mathbf{A}.\mathbf{B} = A_x B_x - \beta^2(A_y B_y + A_z B_z),$$

$$|\mathbf{A}| = \sqrt{(\mathbf{A}.\mathbf{A})},$$

and $f(x, y, z)$ is an arbitrary function defined over the region Σ_1.

This does not restrict our analysis to those cases in which ϕ is generated by simple source distributions, since, if we allow $f(x, y, z)$ to include singular functions such as the Dirac delta function and its derivatives, the field due to a system of transverse doublets, etc., can be included in the same formulation.

Thus (2.7) can be formally written as

$$L(\varphi) = \iiint_{\Sigma_1} d\tau_1 \iiint_{\Sigma_2} d\tau_2 \frac{F(\mathbf{R}_1, \mathbf{R}_2)}{|\mathbf{R}-\mathbf{R}_1||\mathbf{R}-\mathbf{R}_2|}, \tag{2.9}$$

and, provided that we can find a p.i. $\lambda(\mathbf{R}, \mathbf{R}_1, \mathbf{R}_2)$ satisfying

$$L(\lambda(\mathbf{R}, \mathbf{R}_1, \mathbf{R}_2)) = \frac{1}{|\mathbf{R}-\mathbf{R}_1||\mathbf{R}-\mathbf{R}_2|}, \tag{2.10}$$

we can write the p.i. of (2.9) as

$$\psi = \iiint_{\Sigma_1} d\tau_1 \iiint_{\Sigma_2} d\tau_2 \, F(\mathbf{R}_1, \mathbf{R}_2)\lambda(\mathbf{R}, \mathbf{R}_1, \mathbf{R}_2). \tag{2.11}$$

3. Evaluation of the particular integral

Since both sides of (2.10) are invariant to a shift of origin, we can write

$$\lambda(\mathbf{R}, \mathbf{R}_1, \mathbf{R}_2) = \mu(\mathbf{R}-\mathbf{R}_1, \mathbf{R}-\mathbf{R}_2).$$

Furthermore, since (2.10) is Lorentz invariant and the right-hand side of this equation transforms as a tensor of order zero, we can further reduce this to

$$\lambda(\mathbf{R}, \mathbf{R}_1, \mathbf{R}_2) = \nu(|\mathbf{R}-\mathbf{R}_1|, |\mathbf{R}-\mathbf{R}_2|, |\mathbf{R}_1-\mathbf{R}_2|). \tag{3.1}$$

This relation has been used to simplify some of the algebra of this section.

Method 1

In two dimensions, a p.i. can be found without difficulty since the introduction of characteristic coordinates allows us to write the analogue of (2.9) as

$$\frac{\partial^2 \varphi}{\partial\lambda\partial\mu} = F(\lambda, \mu),$$

which can be integrated directly.

The analogue of this procedure in three dimensions is to use Whittaker's general solution of the wave equation (**5**). Let

$$\left.\begin{aligned}\phi_1 &= \int_{-\pi}^{\pi} f(x-\beta y\cos\theta-\beta z\sin\theta,\theta)\,d\theta\\ \phi_2 &= \int_{-\pi}^{\pi} g(x-\beta y\cos\omega-\beta z\sin\omega,\omega)\,d\omega\end{aligned}\right\}, \tag{3.2}$$

where f and g are arbitrary functions, be two solutions of the linearized equation (2.3). It may then be readily verified that the p.i. of

$$L(\varphi)=\phi_1\phi_2$$

is formally

$$\varphi=-\frac{1}{2\beta^2}\int_{-\pi}^{\pi}d\theta\int_{-\pi}^{\pi}d\omega\,\operatorname{cosec}^2\tfrac{1}{2}(\theta-\omega)F(x-\beta y\cos\theta-\beta z\sin\theta,\theta)\times$$
$$\times G(x-\beta y\cos\omega-\beta z\sin\omega,\omega), \tag{3.3}$$

where

$$F(r,s)=\int^{r} f(t,s)\,dt,$$

and similarly for $G(r,s)$. Now Jones (**6**) has shown that

$$\begin{aligned}\frac{1}{2\pi}\int_{-\pi}^{\pi}&\frac{d\theta}{x-\beta y\cos\theta-\beta z\sin\theta}\\ &=\frac{1}{\{x^2-\beta^2(y^2+z^2)\}^{\frac{1}{2}}} \quad \text{if } x>\beta(y^2+z^2)^{\frac{1}{2}}\\ &=0 \quad \text{if } \beta(y^2+z^2)^{\frac{1}{2}}>x>-\beta(y^2+z^2)^{\frac{1}{2}}\\ &=\frac{-1}{\{x^2-\beta^2(y^2+z^2)\}^{\frac{1}{2}}} \quad \text{if } x<-\beta(y^2+z^2)^{\frac{1}{2}}.\end{aligned} \tag{3.4}$$

From this result we can evaluate f and g in our special case, and can write

$$\lambda=-\frac{1}{8\pi^2\beta^2}\int_{-\pi}^{\pi}d\theta\int_{-\pi}^{\pi}d\omega\,\operatorname{cosec}^2\left(\frac{\theta-\omega}{2}\right)\log(X_1-\beta Y_1\cos\theta-\beta Z_1\sin\theta)\times$$
$$\times\log(X_2-\beta Y_2\cos\omega-\beta Z_2\sin\omega), \tag{3.5}$$

where $X_1=x-x_1$, etc. This result is only formally correct since the integral has a non-integrable singularity at $\theta=\omega$. However, the expression

$$\chi=-\frac{1}{8\pi^2\beta^2}\int_{-\pi}^{\pi}d\theta\int_{-\pi}^{\pi}d\omega\,\operatorname{cosec}^2\left(\frac{\theta-\omega}{2}\right)\log(X_1-\beta Y_1\cos\theta-\beta Z_1\sin\theta)\times$$
$$\times\log(X_2-\beta Y_2\cos\theta-\beta Z_2\sin\theta)$$

cancels the singularity and is formally a complementary function. Thus the expression

$$\lambda=-\frac{1}{4\pi^2\beta^2}\int_{-\pi}^{\pi}\log(X_1-\beta Y_1\cos\theta-\beta Z_1\sin\theta)J(\theta)\,d\theta,$$

where

$$J(\theta) = \frac{1}{2}\int_{-\pi}^{\pi} \operatorname{cosec}^2\left(\frac{\theta-\omega}{2}\right)\{\log(X_2-\beta Y_2\cos\omega-\beta Z_2\sin\omega)- \\ -\log(X_2-\beta Y_2\cos\theta-\beta Z_2\sin\theta)\}\,d\omega, \quad (3.6)$$

is finite and is a p.i. of (2.10). The evaluation of this integral is simplified if we put $Z_1 = Z_2 = 0$ and use the group properties of the solution to restore the general values of Z_1 and Z_2 in the final answer.

Integrating by parts,

$$J(\theta) = \beta Y_2 \int_{-\pi}^{\pi} \frac{\cot\frac{1}{2}(\theta-\omega)\sin\omega\,d\omega}{X_2-\beta Y_2\cos\omega} = -\pi\left[1-a_2\frac{1+t^2}{a_2^2+t^2}\right],$$

where $$a_2^2 = \frac{X_2-\beta Y_2}{X_2+\beta Y_2}, \qquad t = \tan\tfrac{1}{2}\theta.$$

Integrating by parts again,

$$\lambda = \frac{1}{2\pi\beta^2}\int_{-\infty}^{\infty}\left(\tan^{-1}t-\tan^{-1}\frac{t}{a_2}\right)\left(\frac{2t}{1+t^2}-\frac{2t}{a_1^2+t^2}\right)dt,$$

where $$a_1^2 = \frac{X_1-\beta Y_1}{X_1+\beta Y_1}.$$

Defining $$g(s) = \int_{-\infty}^{\infty}\tan^{-1}st\left(\frac{1}{1+t^2}-\frac{1}{a_1^2+t^2}\right)t\,dt,$$

we have $$\lambda = \frac{1}{\pi\beta^2}\int_{1/a_2}^{1} g'(s)\,ds.$$

But $$g'(s) = \int_{-\infty}^{\infty}\left(\frac{1}{1+t^2}-\frac{1}{a_1^2+t^2}\right)\frac{t^2\,dt}{1+s^2t^2} = \pi\left(\frac{a_1}{1+a_1 s}-\frac{1}{1+s}\right),$$

so that

$$\lambda = -\frac{1}{2\beta^2}\log|X_1X_2-\beta^2Y_1Y_2+\{X_1^2-\beta^2Y_1^2\}^{\frac{1}{2}}\{X_2^2-\beta^2Y_2^2\}^{\frac{1}{2}}| - \frac{1}{\beta^2}\log 2 + \\ + \frac{1}{2\beta^2}\log|X_1+\{X_1^2-\beta^2Y_1^2\}^{\frac{1}{2}}| + \frac{1}{2\beta^2}\log|X_2+\{X_2^2-\beta^2Y_2^2\}^{\frac{1}{2}}|.$$

Making the obvious generalization to $Z_1 \neq Z_2 \neq 0$, we see that the last three terms are complementary functions while the first becomes

$$\lambda = -\frac{1}{2\beta^2}\log|(\mathbf{R}-\mathbf{R}_1).(\mathbf{R}-\mathbf{R}_2)+|\mathbf{R}-\mathbf{R}_1||\mathbf{R}-\mathbf{R}_2|| = \lambda_m. \quad (3.7)$$

Method 2

From the lemma $$\frac{1}{\pi}\int_{-\infty}^{\infty}\frac{dt}{at^2+b}=\frac{1}{(ab)^{\frac{1}{2}}},$$

we can write (2.10) as

$$L(\varphi)=\frac{1}{|\mathbf{R}-\mathbf{R}_1||\mathbf{R}-\mathbf{R}_2|}=\frac{1}{\pi}\int_{-\infty}^{\infty}\frac{dt}{(1+t^2)[(\mathbf{R}-\mathbf{R}_t)^2+A_t^2]}, \tag{3.8}$$

where $$\mathbf{R}_t=\frac{\mathbf{R}_1t^2+\mathbf{R}_2}{1+t^2}, \qquad A_t=\frac{t}{1+t^2}|\mathbf{R}_1-\mathbf{R}_2|.$$

But, using the fact that the solution of

$$L(\chi)=\frac{1}{R^2+A^2}, \quad \text{where } R=\sqrt{(|\mathbf{R}|^2)},$$

is a function of R only, we readily derive

$$\chi=-\frac{1}{\beta^2}\left(\frac{A}{R}\tan^{-1}\frac{R}{A}+\tfrac{1}{2}\log\frac{R^2+A^2}{A^2}-1\right), \tag{3.9}$$

and therefore

$$\lambda=-\frac{1}{\pi\beta^2}\int_{-\infty}^{\infty}\left\{\frac{1}{Q}\tan^{-1}Q+\tfrac{1}{2}\log(1+Q^2)-1\right\}\frac{dt}{1+t^2}, \tag{3.10}$$

where $$Q=\left\{\frac{[(\mathbf{R}-\mathbf{R}_1)^2t^2+(\mathbf{R}-\mathbf{R}_2)^2][1+t^2]-t^2(\mathbf{R}_1-\mathbf{R}_2)^2}{t^2(\mathbf{R}_1-\mathbf{R}_2)^2}\right\}^{\frac{1}{2}}.$$

Define $$f(s)=-\frac{1}{\pi\beta^2}\int_{-\infty}^{\infty}\left\{\frac{1}{Q}\tan^{-1}sQ+\tfrac{1}{2}\log(1+s^2Q^2)-s\right\}\frac{dt}{1+t^2}$$

and then $$\lambda=\int_0^1 f'(s)\,ds.$$

But

$$f'(s)=\frac{s(1-s)}{\pi\beta^2}\int_{-\infty}^{\infty}\frac{Q^2\,dt}{(1+s^2Q^2)(1+t^2)}=-\frac{1}{\beta^2}\left[\frac{s}{1+s}+\frac{(B^2+1)^{\frac{1}{2}}}{(1+s)(B^2S^2+1)^{\frac{1}{2}}}\right],$$

where $$B^2=\frac{\{|\mathbf{R}-\mathbf{R}_1|+|\mathbf{R}-\mathbf{R}_2|\}^2-|\mathbf{R}_1-\mathbf{R}_2|^2}{|\mathbf{R}_1-\mathbf{R}_2|^2}.$$

Hence

$$\lambda=\int_0^1 f'(s)\,ds=-\frac{1}{\beta^2}\log\left|\frac{|\mathbf{R}-\mathbf{R}_1|+|\mathbf{R}-\mathbf{R}_2|+|\mathbf{R}_1-\mathbf{R}_2|}{2|\mathbf{R}_1-\mathbf{R}_2|}\right|=\lambda_1, \tag{3.11}$$

neglecting an irrelevant constant. The connexion between (3.11) and (3.7) will be explained in the next section.

4. The looping technique

One further difficulty still remains. We have formally written our p.i. of (2.9) as

$$\psi = \iiint_{\Sigma_1} d\tau_1 \iiint_{\Sigma_2} d\tau_2 \, F(\mathbf{R}_1, \mathbf{R}_2)\lambda(\mathbf{R}, \mathbf{R}_1, \mathbf{R}_2), \tag{4.1}$$

where λ is defined in (2.10). If β^2 is negative, then the integrations in (2.11) are carried out over the whole of Σ_1 and Σ_2. In this case, the limits of integration are independent of $\mathbf{R}$ and formal differentiation under the integral sign is sufficient to show that (2.11) is a p.i. of (2.9).

In supersonic problems, however, β^2 is positive and Σ_1 and Σ_2 are typically either lines or surfaces in $z = 0$. The obvious procedure in this case is to limit the region of integration to those points on Σ_1 for which $(\mathbf{R}-\mathbf{R}_1)^2 > 0$, and similarly for Σ_2, but, since the limits of integration now depend on $\mathbf{R}$, formal differentiation gives contributions from the limits, and, in fact, these cannot be ignored.

We can avoid these difficulties very simply, and in order to demonstrate our method we shall assume that $F(\mathbf{R}_1, \mathbf{R}_2)$ is a single-valued, analytic function of x_1 and x_2 and that Σ_1 and Σ_2 are the half-planes $z_1 = z_2 = 0$, $x_1 > 0$, $x_2 > 0$. These restrictions are not essential but will serve for purposes of illustration.

In this case we would expect to take the x_1 integral from $x_1 = 0$ to the branch point at

$$x_1 = x-\beta[(y-y_1)^2+z^2]^{\frac{1}{2}},$$

and similarly for x_2. If we could replace these variable limits of integration by fixed limits, the present difficulty would disappear. This can be done by regarding x_1 and x_2 as complex variables; a suitable path of integration for x_1, say, is then a fixed contour C_1 which loops the branch point and passes through the origin at $x_1 = 0$.

Since the path of integration is now independent of $\mathbf{R}$, the operator L, applied to (2.11), gives

$$\iint_{\Sigma_1} dS_1 \iint_{\Sigma_2} dS_2 \frac{F(\mathbf{R}_1, \mathbf{R}_2)}{|\mathbf{R}-\mathbf{R}_1|\,|\mathbf{R}-\mathbf{R}_2|}, \tag{4.2}$$

where the integrals are defined over these loop paths.

Since $F(\mathbf{R}_1, \mathbf{R}_2)$ is an analytic function of x_1 and x_2 and $|\mathbf{R}-\mathbf{R}_1|$ merely changes sign on looping a branch point, (4.2) is four times the real integral over the regions of integration defined by

$$\Sigma_1, \quad (\mathbf{R}-\mathbf{R}_1)^2 > 0,$$

$$\Sigma_2, \quad (\mathbf{R}-\mathbf{R}_2)^2 > 0.$$

The paths C_1 and C_2 are, however, the fundamental ones, and it is only

when the singularity at the branch point is of a sufficiently low order that we can use real paths in (4.2). The looping technique can also be used when we have non-integrable singularities at the branch point, and it is then equivalent to the method of finite parts devised by Hadamard (7).

Thus, if (4.1) is interpreted on a loop path, it is, at least formally, a p.i. of (4.2). Introduction of these loop paths shows that the four functions

$$\lambda_1, \lambda_2 = -\frac{1}{\beta^2}\log\left|\frac{|\mathbf{R}-\mathbf{R}_1|+|\mathbf{R}-\mathbf{R}_2|\pm|\mathbf{R}_1-\mathbf{R}_2|}{2|\mathbf{R}_1-\mathbf{R}_2|}\right|,$$
$$\lambda_3, \lambda_4 = \frac{1}{\beta^2}\log\left|\frac{|\mathbf{R}-\mathbf{R}_1|-|\mathbf{R}-\mathbf{R}_2|\pm|\mathbf{R}_1-\mathbf{R}_2|}{2|\mathbf{R}_1-\mathbf{R}_2|}\right| \tag{4.3}$$

are all p.i.s of (2.10). We note that λ_m is given by

$$\lambda_m = \tfrac{1}{2}(\lambda_1+\lambda_2).$$

If we use the special form

$$\lambda_r = \tfrac{1}{4}(\lambda_1+\lambda_2+\lambda_3+\lambda_4), \tag{4.4}$$

then, on looping the branch points, λ_r merely changes sign in the same way as

$$\frac{1}{|\mathbf{R}-\mathbf{R}_1|\,|\mathbf{R}-\mathbf{R}_2|}.$$

Thus if we use the special form λ_r in (4.1), that integral too may be taken along real paths. λ_r also has the useful property that it vanishes on the two Mach cones

$$|\mathbf{R}-\mathbf{R}_1| = 0, \qquad |\mathbf{R}-\mathbf{R}_2| = 0.$$

One further point is worth making. Since L is a linear operator, we may differentiate both sides of (2.10) with respect to y_1, say, and obtain

$$L\left\{\frac{\partial\lambda}{\partial y_1}\right\} = -\frac{\beta^2(y-y_1)}{|\mathbf{R}-\mathbf{R}_1|^3|\mathbf{R}-\mathbf{R}_2|}.$$

We may similarly integrate both sides of this equation with respect to x_1 over a loop path. Using such techniques it is a simple matter to extend our p.i. so that we can deal directly with those cases in which the field is generated by multipoles rather than by simple sources.

5. Relation to known solutions

It may readily be shown that

$$L(M^2\phi\phi_x) = 2M^2\{-\beta^2\phi_x\phi_{xx}+\phi_y\phi_{xy}+\phi_z\phi_{xz}\},$$

which allows us to reduce (2.7) to the simpler equation

$$L(\phi) = 2M^2\beta^2N\phi_x\phi_{xx}. \tag{5.1}$$

Van Dyke has obtained a particular integral of this equation in the axisymmetric case, and we shall show how this may be obtained by our method.

In axisymmetric flow the potential is given by

$$\phi = -\int \frac{f(\xi)\,d\xi}{\{(x-\xi)^2-\beta^2r^2\}^{\frac{1}{2}}},$$

so that

$$\psi = -\frac{M^2N}{2}\int\int f'(\xi)f''(\eta)\lambda_r[x-\xi, x-\eta, r]\,d\xi d\eta.$$

Integrating by parts, and using the symmetry of the integrand in ξ and η, we have

$$\psi = -\frac{M^2N}{4}\int\int f'(\xi)f'(\eta)\left(\frac{\partial\lambda_r}{\partial\xi}+\frac{\partial\lambda_r}{\partial\eta}\right)d\xi d\eta,$$

which can be written as

$$\begin{aligned}\psi &= -M^2N\int \frac{(x-\xi)f'(\xi)}{\{(x-\xi)^2-\beta^2r^2\}^{\frac{1}{2}}}d\xi\int \frac{f'(\eta)\,d\eta}{\{(x-\eta)^2-\beta^2r^2\}^{\frac{1}{2}}}\\ &= M^2Nr\phi_r\phi_x,\end{aligned}$$

which is Van Dyke's result.

We have also verified that our p.i. gives the known result for two-dimensional wings and for yawed cones. This will be proved in subsequent papers.

In principle, the triple terms in equation (2.6) can be treated by these methods and an extension to higher dimensions is also possible. Preliminary examination, however, suggests that the functions involved are very complex.

The formulae obtained here have been applied to the study of second-order flow round yawed bodies of revolution and to the calculation of thickness corrections to the aerodynamic derivatives of wings of finite aspect ratio. This work will be published later.

Acknowledgements

The authors are particularly indebted to Mr. A. Lightbody of the Armaments Division, Sir W. G. Armstrong Whitworth Aircraft Ltd., for the encouragement he has given throughout the course of this work. This work forms parts of the research programme of this Division and is published by permission of the firm.

REFERENCES

1. M. D. Van Dyke, *N.A.C.A.* (*U.S.A.*) Report **1081**.
2. —— *J. Aero. Sci.* **18** (1951), 161.
3. —— ibid. **20** (1953), 61.
4. —— *N.A.C.A.* (*U.S.A.*) Tech. Note 2982.
5. E. T. Whittaker and G. N. Watson, *Modern Analysis* (Cambridge, 1940), p. 383.
6. R. T. Jones, *J. Aero. Sci.* **19** (1952), 813.
7. J. Hadamard, *Lectures on Cauchy's Problem* (Yale, 1923).

ROTATIONAL FLOW THROUGH CASCADES

PART I. THE COMPONENTS OF VORTICITY

By W. R. HAWTHORNE

(*Department of Engineering, University of Cambridge*)

[Received 25 June 1954]

SUMMARY

The flow of a fluid with a non-uniform velocity passing through a cascade of turbine or compressor blades is examined theoretically to determine the nature of the components of vorticity in the direction of flow. Three such components are found, two lying in the stagnation streamline leaving the blade, and one distributed in the stream. The distributed secondary circulation is that due to the curving of the flow in a bend, or passage between the blades, as described by Squire and Winter. The trailing shed circulation is due to the change in circulation along the blade as found in the flow of a uniform fluid about a wing of finite span. The third component—the trailing filament circulation—is due to the stretching of the vortex filaments carried with the flow between the upper and lower stagnation streamlines in the wake of each blade. The application of these results to cascades and isolated aerofoils is discussed briefly.

1. Introduction

When a fluid with a non-uniform total pressure flows around a bend, secondary flows may be generated which can materially alter the character of the flow. Such flows have been studied by several authors (**1**–**5**) and a satisfactory theory obtained for the flow of a non-uniform inviscid incompressible fluid when the secondary flows are not large.

These flows are of particular interest in cascades of turbine and compressor blades where non-uniform approaching flows of considerable extent may be found on the walls bounding the cascade. Recently Preston (**6**), using a simplified approach, has discussed the generation of the component of vorticity in the direction of flow, which gives rise to the secondary flows. Preston starts with the concept that the vortex filaments carried with the rotational flow may be followed in the Lagrangian manner as the flow passes through a cascade. Kronauer (**3**) and Hawthorne (**5**) have also made some use of this approach. When studying the flow past a cascade, Preston assumes that in addition to the components of vorticity present in the vortex filaments, a change in circulation about the blade or aerofoil will cause circulation to be shed off into the stream. The existence of this shed vorticity has been demonstrated in the theory of finite wings in a uniform flow. The concepts are, however, less familiar

in non-uniform flow and there is a need for an analytical proof of the existence of the different components of vorticity. Such a proof is attempted in this paper.

Two analytical approaches are made. One is based on the equations for the flow of an inviscid, incompressible fluid in a force field. In the other the vortex filaments are followed as the fluid passes through the cascade. By demonstrating the equivalence of the two results various features of the flow are explained.

2. Secondary vorticity in a flow with a force field

An expression for the change of the component of vorticity in the direction of flow is derived in (**1**) for inviscid, incompressible flow in the absence of body forces. A similar method may be used for the case when body forces are present.

The vorticity $\boldsymbol{\Omega} = \operatorname{curl} \mathbf{V}$, where $\mathbf{V}$ is the velocity vector (scalar q), may be split into two components, namely a component

$$\frac{(\boldsymbol{\Omega}.\mathbf{V})}{(\mathbf{V}.\mathbf{V})}\mathbf{V} = \left(\frac{\xi}{q}\right)\mathbf{V}$$

along a streamline, where ξ is the scalar of the component of vorticity in the direction of flow, and a component

$$\frac{(\mathbf{V}\wedge\boldsymbol{\Omega})\wedge\mathbf{V}}{(\mathbf{V}.\mathbf{V})}$$

normal to the streamline. Since

$$\operatorname{div}\boldsymbol{\Omega} = 0,$$

it follows that
$$\operatorname{div}(\xi\mathbf{V}/q) - \operatorname{div}\frac{\mathbf{V}\wedge(\mathbf{V}\wedge\boldsymbol{\Omega})}{(\mathbf{V}.\mathbf{V})} = 0; \tag{1}$$

and since
$$\operatorname{div}(\xi\mathbf{V}/q) \equiv (\xi/q)\operatorname{div}\mathbf{V} + \mathbf{V}.\operatorname{grad}(\xi/q)$$

and
$$\operatorname{div}\mathbf{V} = 0,$$

we have
$$\mathbf{V}.\operatorname{grad}(\xi/q) = \operatorname{div}\frac{\mathbf{V}\wedge(\mathbf{V}\wedge\boldsymbol{\Omega})}{q^2}. \tag{2}$$

From the Euler equation

$$(\mathbf{V}.\operatorname{grad})\mathbf{V} = -\frac{1}{\rho}\operatorname{grad} p + \mathbf{F} \tag{3}$$

where $\mathbf{F}$ is the vector representing the body forces, and using the identity

$$\operatorname{grad}(\mathbf{V}.\mathbf{V}) \equiv 2(\mathbf{V}.\operatorname{grad})\mathbf{V} + 2\mathbf{V}\wedge\operatorname{curl}\mathbf{V}$$

or
$$(\mathbf{V}.\operatorname{grad})\mathbf{V} \equiv \operatorname{grad}\tfrac{1}{2}q^2 - \mathbf{V}\wedge\boldsymbol{\Omega}. \tag{4}$$

we have by subtracting (3) from (4)

$$\mathbf{V}\wedge\boldsymbol{\Omega} = \frac{1}{\rho}\operatorname{grad} p_0 - \mathbf{F}, \tag{5}$$

where p_0 is the total pressure ($= p+\frac{1}{2}\rho q^2$).

Substituting the expression (5) for $\mathbf{V}\wedge\boldsymbol{\Omega}$ in equation (2), we find that

$$\mathbf{V}.\operatorname{grad}(\xi/q) = \operatorname{div}\left\{\frac{1}{q^2}\left(\mathbf{V}\wedge\frac{1}{\rho}\operatorname{grad} p_0\right)\right\} - \operatorname{div}\left\{\frac{1}{q^2}(\mathbf{V}\wedge\mathbf{F})\right\}. \tag{6}$$

Now the circulation round any stream tube of cross-sectional area dA is $\xi\,dA$ and, since $q\,dA$, the volume flow along the stream tube, is constant, ξ/q is the secondary circulation per unit volume flowing. The term on the left-hand side of (6) is then proportional to the gradient of the secondary circulation in the direction of flow.

If no component of force exists in the direction of flow (inviscid flow),

$$\mathbf{V}.\mathbf{F} = 0, \tag{7}$$

and, therefore,

$$\mathbf{V}.\operatorname{grad}\left(\frac{p_0}{\rho}\right) = 0. \tag{8}$$

Condition (8) expresses the fact that the total pressure remains unchanged along a streamline. The second term in equation (6) then represents the divergence of a quantity f/q, where f is the scalar of $\mathbf{F}$. This quantity is analogous to the circulation about an aerofoil which the force field may be supposed to represent. Applying equation (6) to the case of a wing in a flow with p_0 everywhere constant, the right-hand side becomes equal to the rate of change of circulation along the span of the wing (since the first term disappears) and the well-known result that the strength of the trailing vortex sheet is equal to this rate of change of circulation follows at once.

The first term on the right-hand side of equation (6) may be expanded as follows:

$$\operatorname{div}\left\{\frac{1}{q^2}\left(\mathbf{V}\wedge\operatorname{grad}\left(\frac{p_0}{\rho}\right)\right)\right\} = \frac{1}{q^2}\boldsymbol{\Omega}.\operatorname{grad}\left(\frac{p_0}{\rho}\right) - \mathbf{V}\left\{\operatorname{grad}\left(\frac{1}{q^2}\right)\wedge\operatorname{grad}\left(\frac{p_0}{\rho}\right)\right\}. \tag{8a}$$

Substituting for $\operatorname{grad} q^2$ from (4), (8 a) becomes

$$\frac{1}{q^2}\boldsymbol{\Omega}.\operatorname{grad}\left(\frac{p_0}{\rho}\right) - \\ -\frac{1}{q^4}\left\{2\mathbf{V}\wedge\operatorname{grad}\left(\frac{p_0}{\rho}\right)\right\}.(\mathbf{V}.\operatorname{grad})\mathbf{V} - \frac{1}{q^4}\left\{2\mathbf{V}\wedge\operatorname{grad}\left(\frac{p_0}{\rho}\right)\right\}.\mathbf{V}\wedge\boldsymbol{\Omega}. \tag{8b}$$

Expanding the last term and noting (8), (8 b) becomes

$$\frac{1}{q^2}\boldsymbol{\Omega}.\operatorname{grad}\left(\frac{p_0}{\rho}\right)-\frac{1}{q^4}\left\{2\mathbf{V}\wedge\operatorname{grad}\left(\frac{p_0}{\rho}\right).(\mathbf{V}.\operatorname{grad})\mathbf{V}\right\}-$$

$$-\frac{1}{q^4}\left\{2(\mathbf{V}.\mathbf{V})\left(\operatorname{grad}\left(\frac{p_0}{\rho}\right).\boldsymbol{\Omega}\right)\right\}. \quad (9)$$

The last term may be rewritten, using (5), in the form

$$\frac{1}{q^2}\operatorname{grad}\left(\frac{p_0}{\rho}\right).\boldsymbol{\Omega}=\frac{1}{q^2}(\mathbf{V}\wedge\boldsymbol{\Omega}.\boldsymbol{\Omega}+\mathbf{F}.\boldsymbol{\Omega})=\frac{1}{q^2}(\mathbf{F}.\boldsymbol{\Omega}). \quad (10)$$

Equation (6) may therefore be written

$$\mathbf{V}.\operatorname{grad}\left(\frac{\xi}{q}\right)=-\frac{1}{q^4}\left\{2\mathbf{V}\wedge\operatorname{grad}\left(\frac{p_0}{\rho}\right)\right\}.(\mathbf{V}.\operatorname{grad})\mathbf{V}-\frac{1}{q^2}\mathbf{F}.\boldsymbol{\Omega}-\operatorname{div}\left(\frac{\mathbf{V}\wedge\mathbf{F}}{q^2}\right). \quad (11)$$

In the absence of body forces this equation reduces to that derived previously by the author (**1**). It describes the generation of a component of vorticity in the direction of flow in a curved duct, first noted by Squire and Winter (**2**) and later discussed by other authors (**1**, **3**, **4**, **5**). In a cascade the first term on the right-hand side of equation (11) describes the component of secondary circulation due to the bending of the flow in the passage between the blades. From this must be subtracted a term (the last term on the right-hand side of (11)) which represents the rate of change of circulation round the blades in their spanwise direction. This may be thought of as a vortex sheet trailing downstream from the blades similar to that obtained with wings of finite span in uniform flow (p_0 = constant). In non-uniform flow, however, another term (the second term on the right-hand side of (11)) must also be subtracted. The physical significance of this term will be shown later.

3. Application to cascades of aerofoils

Consider an initially quasi-two-dimensional flow (Fig. 1), in which the pressure p_1 is initially uniform and the initial velocity U_1 varies in the z-direction only. Let the components of the velocity vector $\mathbf{V}$ be C_x, C_u, and C_z in the x-, y-, z-directions respectively. Let this flow approach and be deflected by a force field (e.g. a two-dimensional cascade) of finite width in the x-direction and of infinite extent in the y-direction. In the y-direction similarity will be preserved so that all properties of the flow are independent of y.

Suppose, first, that we envisage a flow in which the original planes of constant p_0 remain planes as they pass through the force field, i.e. p_0 is

a function of z only. Also, let the angle α made by $\mathbf{V}$ with the x-axis be independent of z. By continuity there will be no acceleration in the x-direction. Hence C_x will be independent of x and y and $\alpha = \tan^{-1}(C_u/C_x)$

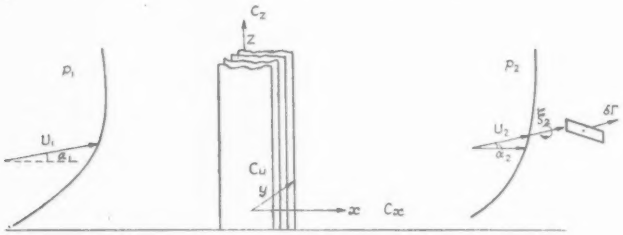

FIG. 1.

will be independent of y and z. The secondary circulation may be obtained directly from equation (2). Here

$$\mathbf{V} = \mathbf{i}C_x + \mathbf{j}C_u = \mathbf{i}C_x + \mathbf{j}C_x \tan\alpha, \tag{12}$$

$$\boldsymbol{\Omega} = \operatorname{curl}\mathbf{V} = -\mathbf{i}\tan\alpha\frac{dC_x}{dz} + \mathbf{j}\frac{dC_x}{dz} + \mathbf{k}C_x\frac{d\tan\alpha}{dx}, \tag{13}$$

where $\mathbf{i}$, $\mathbf{j}$, and $\mathbf{k}$ are unit vectors in the x-, y-, z-directions respectively. Also

$$\mathbf{V}\wedge\boldsymbol{\Omega} = \mathbf{i}C_x^2\tan\alpha\frac{d\tan\alpha}{dx} - \mathbf{j}C_x^2\frac{d\tan\alpha}{dx} + \mathbf{k}C_x\sec^2\alpha\frac{dC_x}{dz}, \tag{14}$$

$$\mathbf{V}\wedge(\mathbf{V}\wedge\boldsymbol{\Omega}) = \mathbf{i}C_x^2\tan\alpha\sec^2\alpha\frac{dC_x}{dz} + \mathbf{j}C_x^2\sec^2\alpha\frac{dC_x}{dz} - \mathbf{k}C_x^3\sec^4\alpha\frac{d\alpha}{dx}, \tag{15}$$

and

$$\frac{\mathbf{V}\wedge(\mathbf{V}\wedge\boldsymbol{\Omega})}{q^2} = \frac{\mathbf{V}\wedge(\mathbf{V}\wedge\boldsymbol{\Omega})}{C_x^2\sec^2\alpha} = \mathbf{i}\tan\alpha\frac{dC_x}{dz} + \mathbf{j}C_x\frac{dC_x}{dz} - \mathbf{k}C_x\sec^2\alpha\frac{d\alpha}{dx}. \tag{16}$$

Hence

$$\operatorname{div}\left(\frac{\mathbf{V}\wedge(\mathbf{V}\wedge\boldsymbol{\Omega})}{q^2}\right) = \frac{dC_x}{dz}\sec^2\alpha\frac{d\alpha}{dx} - \frac{dC_x}{dz}\sec^2\alpha\frac{d\alpha}{dx} = 0. \tag{17}$$

Hence the component of vorticity in the direction of flow which is initially zero remains zero in this type of flow.

Such a force field does not, however, correctly represent a two-dimensional cascade since, in such a cascade, there is no component of force exerted by the blades in the z-direction, i.e. along the span. There will therefore be an acceleration in this direction, since in any surface of constant p_0

$$\frac{p}{\rho} + \tfrac{1}{2}q^2 = \frac{p_1}{\rho} + \tfrac{1}{2}U_1^2. \tag{18}$$

Furthermore, q in any such surface tends to be proportional to U_1, and there will therefore usually be a component of the pressure gradient normal to the surface. In the absence of any other force this component of the pressure gradient will cause an acceleration and the surface of constant p_0 will no longer remain plane but will be displaced in the z-direction. Such displacements have been observed in the flow through cascades immediately upstream and downstream of the blades as well as within the blade passages.

In order to develop a first-order theory it will be assumed as in references (**2**) and (**5**) that the basic flow at each value of z has a constant axial velocity C_x and an angle α independent of y and z. The velocity components of this basic flow are then given by equation (12). Superimposed on such a basic flow will be small perturbation velocities which are so small that the value of p_0 at each value of z remains constant. This supposition affects the value of the vorticity component, Ω_{xy}, the component of $\mathbf{\Omega}$ in the xy-plane and normal to the velocity vector. In the flow described above, with no component of acceleration in the z-direction, Ω_{xy} from equations (3) and (5) is given by

$$q\Omega_{xy} = \frac{1}{\rho}\frac{dp_0}{dz} - \frac{1}{\rho}\frac{dp}{dz} = q\frac{dq}{dz}, \tag{19}$$

which agrees with the value deduced from equation (13).

In the absence of a force in the z-direction equation (5) yields the result

$$q\Omega_{xy} = \frac{1}{\rho}\frac{dp_0}{dz}$$

or

$$\Omega_{xy} = \frac{U_1}{q}\frac{dU_1}{dz}. \tag{20}$$

This is different from the value deduced in equation (13) from the components of the basic flow only. This difference may be explained by showing, as in reference (**5**), that the component of vorticity due to the small perturbations is of the same order as the vorticity in the approaching flow and may not, therefore, be neglected.

In the first approximation the force f acts in the xy-plane normal to a streamline of the basic two-dimensional flow and is approximately related to Ω_z, the vorticity component in the z-direction, by the equation

$$f \doteq q\Omega_z. \tag{21}$$

The force exerted by a cascade of blades on a non-uniform flow is not readily predictable. The flow presumably leaves the trailing edges of the blades so that Joukowski's hypothesis is satisfied, or approximately satisfied.

Hence this condition becomes one of the boundary conditions of the problem and enables the blade force to be determined.

The vorticity component Ω_z comprises a component due to the basic two-dimensional flow and a component due to the small perturbations which may be of the same order. A knowledge of the perturbation velocities which satisfy all the boundary conditions is therefore needed to calculate Ω_z and thence f. As the perturbations may be regarded as due to the additive effect of the secondary components of vorticity generated in all the surfaces of constant total pressure, the effect of one surface on another must be considered. This problem is considered further in Part II of this paper.

For the purposes of this part of the paper it will be assumed in both analytical approaches that in each surface of constant total pressure the force field exerted is that corresponding to the component of Ω_z due to the basic two-dimensional flow only. This implies that at a given value of z the circulation about each blade of the cascade will be that which would be obtained in a two-dimensional flow with an approach velocity equal to the value of U_1 corresponding to that z. This assumption is valid in that it is possible to conceive of a cascade of twisted blades producing such a field of force.

Alternatively, a limiting cascade may be envisaged in which closely spaced blades fix the outlet angle of the perturbed flow at a value independent of z. The perturbation velocities are, thereby, controlled in such a way that the component of vorticity, ξ, at outlet from the cascade force field can have no value other than zero. In other words, one surface of constant total pressure cannot slide over the other. The force field required to produce this effect will now be different from the previous one. This example is, however, not as useful for analysis here as the one chosen above.

The acceleration of the basic flow in the xy-plane is $C_x^2(d\tan\alpha/dx)$ in the y-direction, whence the force is $C_x^2\sec\alpha(d\tan\alpha/dx)$. Hence, inserting appropriate values in equation (11), we find

$$q\frac{d(\xi/q)}{ds}=\frac{2q}{q^4}U_1\frac{dU_1}{dz}C_x^2\cos\alpha\frac{d\tan\alpha}{dx}-\frac{1}{q^3}C_x^2\sec\alpha\frac{d\tan\alpha}{dx}U_1\frac{dU_1}{dz}-$$
$$-\frac{d}{dz}\left(\frac{C_x^2\sec\alpha}{q}\frac{d\tan\alpha}{dx}\right), \qquad (22)$$

where $ds=dx\sec\alpha$ is an element of length in the direction of flow. Substituting $q=C_x\sec\alpha$ and noting that α is assumed to be independent of z and C_x to be independent of x,

$$d(\xi/q)=2U_1\frac{dU_1}{dz}\left(\frac{d\alpha}{C_x^2\sec^2\alpha}\right)-U_1\frac{dU_1}{dz}\frac{d\alpha}{C_x^2}-C_x\frac{dC_x}{dz}\frac{\sec^2\alpha\,d\alpha}{C_x^2}. \qquad (22a)$$

The first term on the right-hand side of this equation is identical with the expression obtained in (**5**) for the secondary circulation in a similar flow in the absence of body forces. It is the expression which is required to determine the secondary circulation obtained by the bending of the flow between the blades of a cascade. The integration of this equation will be performed after the discussion of the vortex filament theory.

4. Vortex filament theory

Fig. 2 shows a surface of constant p_0 passing through a section of a two-dimensional cascade. It will be assumed that the basic flow in this surface

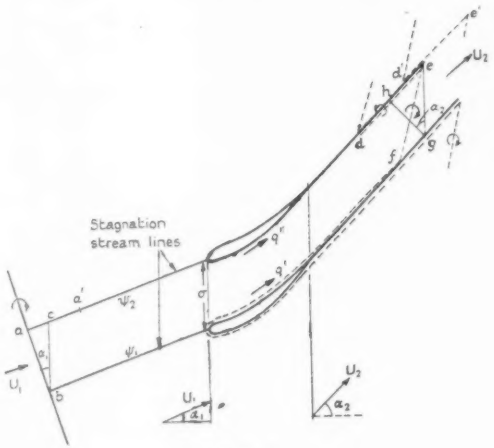

FIG. 2.

is that of two-dimensional potential flow and that flows due to the variation of p_0 normal to the paper may be regarded as perturbations of this flow. The analysis of (**6**) and the earlier sections of this paper may then be applied to the flow. In the flow there will be vortex filaments moving with the fluid and satisfying the theorems of Kelvin and Helmholtz. One such vortex filament, *ab*, lying in the plane of constant p_0, is shown in Fig. 2. The vortex filament will always be composed of the same particles and its motion may be followed until it is downstream of the cascade. Owing to the differing velocities on the convex and concave surfaces of the blades, it will take up a position *def*, Fig. 2. The filament may stretch directly from *d* to *e* along the stagnation streamline or, as is suggested in (**6**) for rounded leading edges, the filament may stretch upstream from *d* round the nose of the blade and back along the convex surface as is shown for the lower blade in Fig. 2. The portion *ef* of the vortex filament

contributes a component of vorticity in the direction of flow. The secondary circulation due to this vorticity component in a plane strip normal to the flow stretching between streamlines ψ_1 and ψ_2 and of unit height normal to the paper is, from equation (2.4) of (**5**),†

$$\delta\Gamma_1 = -\frac{dU_1}{dz}\left\{\int_{-\infty}^{+\infty}(U_1/q)^2_{\psi_2}\,d\phi - \int_{-\infty}^{+\infty}(U_1/q)^2_{\psi_1}\,d\phi\right\}, \tag{23}$$

where ϕ is the potential function for the basic two-dimensional motion and

$$d\phi = (q/U_1)\,ds. \tag{24}$$

The integral is in each case taken along a streamline. Denoting by q'' the velocity on the stagnation streamline ψ_2 taken along the *convex* surface of the blade and by q' the velocity along stagnation streamline ψ_1 taken along the *concave* surface of the blade (Fig. 2), the equation becomes

$$\delta\Gamma_1 = -\frac{dU_1}{dz}\left\{\int_{-\infty}^{+\infty}\left(\frac{U_1}{q''}\right)^2 d\phi - \int_{-\infty}^{+\infty}\left(\frac{U_1}{q'}\right)^2 d\phi\right\}. \tag{25}$$

Far upstream and downstream the potential lines such as ab and gh will be normal to the flow. Taking the integrals over such limits and substituting for $d\phi$, we obtain

$$\delta\Gamma_1 = -\frac{dU_1}{dz}\left\{\int_a^h \frac{U_1\,ds}{q''} - \int_b^g \frac{U_1\,ds}{q'}\right\}.$$

† The equation of (**5**) needs slight modification. It was originally applied to a strut or isolated aerofoil for which $U_2 = U_1$. The modification for $U_2 \neq U_1$ is as follows: From (**5**), equations (1.18), (1.20), and (2.3) yield the downstream vorticity,

$$\xi_2 = 2\frac{U_2}{U_1}\frac{dU_1}{dz}\int_{-\infty}^{+\infty}\frac{1}{(q/U_1)^3}\frac{\partial(q/U_1)}{\partial n}\,ds,$$

where the integral is taken along the streamline and n is a coordinate normal to the streamline lying in the plane of constant p_0. Now

$$\delta\Gamma_1 = \int_{\psi_1}^{\psi_2}\xi_2\,dn, \quad \text{and} \quad d\phi = (q/U_1)\,ds, \quad d\psi = (q/U_1)\,dn.$$

Hence downstream at infinity

$$\delta\Gamma_1 = \frac{U_1}{U_2}\int_{\psi_1}^{\psi_2}\xi_2\,d\psi.$$

On substitution for dn and ds, the expression for ξ_2 may be used to obtain the expression for $\delta\Gamma_1$, equation (23), by integrating once with respect to ψ.

Because of the periodic repetition of the flow in each blade passage, the last integral has the same value as a similar integral taken from c to e along the stagnation streamline passing along the concave surface of the blade; hence

$$\delta\Gamma_1 = -\frac{dU_1}{dz}\left\{\int_a^h \frac{U_1\,ds}{q''} - \int_a^h \frac{U_1\,ds}{q'} + \int_a^c \frac{U_1}{q'}\,ds - \int_h^e \frac{U_1}{q'}\,ds\right\}.$$

The first two integrals cancel out except at the blade and the last two may be evaluated from the geometry of Fig. 2, thus giving

$$\delta\Gamma_1 = -\frac{dU_1}{dz}\left\{U_1 \oint \frac{ds}{q} + \sigma \sin\alpha_1 - \sigma(U_1/U_2)\sin\alpha_2\right\}, \tag{26}$$

where σ is the pitch of the blades and $\oint \frac{ds}{q}$ is taken from the leading edge along the convex surface to the trailing edge and back along the concave surface. It is therefore a negative quantity.

Noting that, by continuity, the downstream velocity U_2 is given by

$$U_1 \cos\alpha_1 = U_2 \cos\alpha_2, \tag{27}$$

then

$$\delta\Gamma_1 = \frac{dU_1}{dz}\left[-U_1 \oint \frac{ds}{q} + \frac{\sigma}{2}\frac{\sin 2\alpha_2 - \sin 2\alpha_1}{\cos\alpha_1}\right]. \tag{28}$$

The positive direction of $\delta\Gamma_1$ is that of a right-handed screw advancing downstream.

Each vortex filament has a portion de (Fig. 2), which produces a secondary circulation opposite in sign to that produced by fe. Only one filament is drawn in Fig. 2 but, in fact, a succession of them could be drawn between d and e (one such is partly shown at d' and e'), all of which will contribute to the circulation about the stagnation streamline at e. The circulation at e is the sum of the circulations in all the filaments such as $d'e'$, where d' lies between d and c. The filament starting as ab reaches de in a given time. Since the time t taken by a particle starting at a and reaching d via the concave surface of the blade is the same as the time taken by a particle starting at a and reaching e by the convex surface, we find that

$$t = \int_a^d \frac{ds}{q'} = \int_a^e \frac{ds}{q''} = \int_a^d \frac{ds}{q''} + \int_d^e \frac{ds}{q}, \tag{29}$$

where superscripts $'$ and $''$ refer to the concave and convex surfaces respectively. Consider a filament such as $d'e'$ which starts from a' so that d' arrives at e in the same time t. Then the total circulation at e will be the

circulation associated with all the vortex filaments between a and a' and since

$$\int_a^{a'} \frac{ds}{q} = \int_d^e \frac{ds}{q} \tag{30}$$

and, from (29),

$$\int_a^{a'} \frac{ds}{q} = -\oint \frac{ds}{q}$$

or

$$aa' = -U_1 \oint \frac{ds}{q}. \tag{31}$$

Hence the circulation about e is given by

$$\delta\Gamma_2 = -aa' \frac{dU_1}{dz} = U_1 \frac{dU_1}{dz} \oint \frac{ds}{q}. \tag{32}$$

The equivalence of this term and the $\mathbf{F}.\boldsymbol{\Omega}$ term in equation (11) may be approximately established as follows. From Fig. 3 the force exerted by

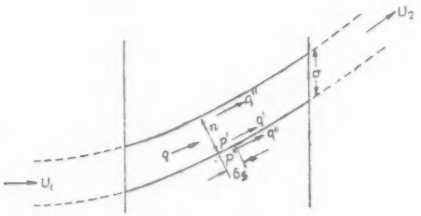

FIG. 3.

an element of blade (assumed to be thin) of length ds on the fluid is given by $(p'-p'')\,ds = \frac{1}{2}\rho(q''^2-q'^2)\,ds$, since p_0 is constant in the surface. The force f per unit mass of fluid is then given by

$$f = \frac{q''+q'}{2} \frac{q''-q'}{n}. \tag{33}$$

Noting that $\frac{1}{2}(q''+q')$ is approximately the average flow velocity q and substituting this expression for $\mathbf{F}$ and equation (20) for $\boldsymbol{\Omega}$ in equation (11), the contribution to the secondary circulation from the $\mathbf{F}.\boldsymbol{\Omega}$ term is given by

$$q \frac{d(\xi/q)}{ds} = -U_1 \frac{dU_1}{dz} \frac{1}{q^3} \frac{q(q''-q')}{n}. \tag{34}$$

By continuity nq is constant and equal to $U_2 \sigma \cos \alpha_2$. Hence

$$U_2 \sigma \cos \alpha_2 \frac{\xi_2}{U_2} = -U_1 \frac{dU_1}{dz} \int \frac{(q''-q')\,ds}{q^2}$$

or

$$\delta\Gamma_2 = -U_1 \frac{dU_1}{dz} \int \frac{q''-q'}{q^2}\,ds. \tag{35}$$

The equivalence of this with the expression for $\delta\Gamma_2$, equation (32), is obtained by noting that

$$\oint \frac{ds}{q} = \int \left(\frac{1}{q''} - \frac{1}{q'}\right) ds = -\int \frac{q''-q'}{q'q''}\, ds \approx -\int \frac{q''-q'}{q^2}\, ds. \qquad (36)$$

It follows that the physical significance of the second term on the right-hand side of equation (11) is that it represents the component of vorticity

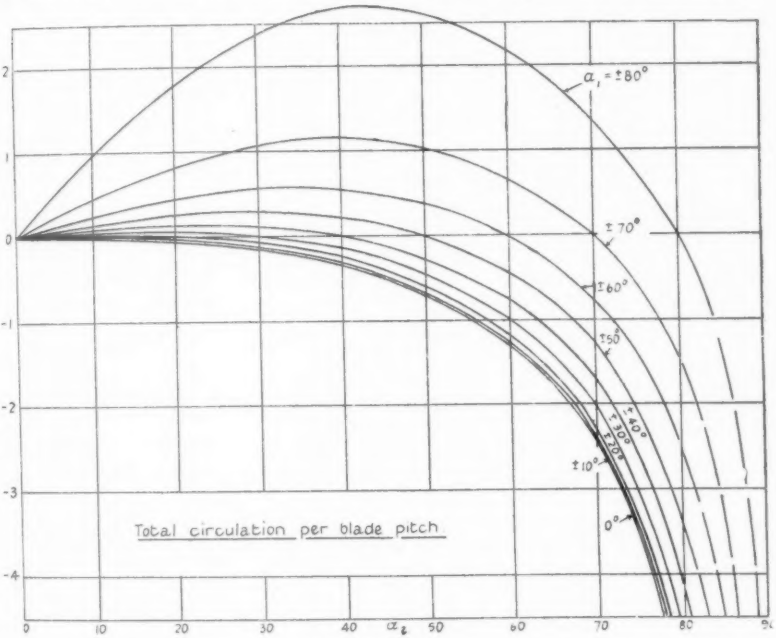

FIG. 4.

due to the stretching of the vortex filaments along the streamline from the trailing edge, as shown by de in Fig. 2.

To complete the analysis it is evident from equation (11) that the component due to the change of circulation about the blade must be added. This is given by

$$\delta\Gamma_3 = -\frac{d}{dz}(\sigma C_x(\tan\alpha_2 - \tan\alpha_1)) = -\sigma\cos\alpha_1 \frac{dU_1}{dz}(\tan\alpha_2 - \tan\alpha_1). \qquad (37)$$

Summing, we obtain

$$\delta\Gamma = \delta\Gamma_1 + \delta\Gamma_2 + \delta\Gamma_3 = \sigma\frac{dU_1}{dz}\left\{\frac{\sin 2\alpha_2 - \sin 2\alpha_1}{2\cos\alpha_1} - \cos\alpha_1(\tan\alpha_2 - \tan\alpha_1)\right\}. \qquad (38)$$

This is identical to the expression obtained as follows by integrating equation (22a) from far upstream to a section far downstream. Noting that C_x is independent of x, we obtain

$$\xi_2/U_2 = \frac{U_1}{C_x^2}\frac{dU_1}{dz}\int_1^2 (2\cos^2\alpha - 1)\,d\alpha - \frac{1}{C_x}\frac{dC_x}{dz}\int_1^2 \sec^2\alpha\,d\alpha,$$

$$\xi_2 = \frac{1}{\cos\alpha_1\cos\alpha_2}\frac{dU_1}{dz}[\tfrac{1}{2}(\sin 2\alpha_2 - \sin 2\alpha_1)] - \frac{\cos\alpha_1}{\cos\alpha_2}\frac{dU_1}{dz}(\tan\alpha_2 - \tan\alpha_1). \tag{39}$$

Hence

$$\begin{aligned}\delta\Gamma &= \xi_2\sigma\cos\alpha_2 \\ &= \sigma\frac{dU_1}{dz}\left\{\frac{\sin 2\alpha_2 - \sin 2\alpha_1}{2\cos\alpha_1} - \cos\alpha_1(\tan\alpha_2 - \tan\alpha_1)\right\} \\ &= \sigma\frac{dU_1}{dz}\sin\alpha_2\left(\frac{\cos\alpha_2}{\cos\alpha_1} - \frac{\cos\alpha_1}{\cos\alpha_2}\right).\end{aligned} \tag{40}$$

Values of $\delta\Gamma\Big/\sigma\dfrac{dU_1}{dz}$ from the above expression are shown graphically in Fig. 4.

5. Isolated aerofoils

For an isolated aerofoil the vortex filament approach leads to the same values for the trailing shed circulation and the trailing component of the vortex filaments as those given in equations (32) and (37). Equation (37) has, however, to be modified. The circulation K about the blade is given by

$$K = \sigma U_1\cos\alpha_1(\tan\alpha_2 - \tan\alpha_1), \tag{41}$$

so that, for the isolated aerofoil, we obtain

$$\delta\Gamma_3 = -\frac{K}{U}\frac{dU}{dz}, \tag{42}$$

where U is the velocity approaching the isolated aerofoil. An expression for the net distributed circulation has been obtained in (**5**), equation (2.8), and in terms of the sign convention used here it is

$$\delta\Gamma_1 = \frac{dU}{dz}\left[-U\oint\frac{ds}{q} - \frac{K}{U}\right]. \tag{43}$$

The net value of secondary circulation is then

$$\delta\Gamma = \delta\Gamma_1 + \delta\Gamma_2 + \delta\Gamma_3 = -2\frac{K}{U}\frac{dU}{dz}, \tag{44}$$

i.e. twice the trailing shed circulation.

The assumption that the circulation in each surface of constant total pressure is that corresponding to two-dimensional flow with the corresponding value of U must, however, be remembered. It is not valid in the theory of wings of finite span and is unlikely to be valid here.

6. Conclusions

The analysis shows that the components of vorticity in the direction of flow produced when a non-uniform stream flows through a cascade or passes an aerofoil, may be divided into three parts. The first is that due to the bending of the flow in such a way that the streamlines are no longer geodesics on the surfaces of constant total pressure (see (**1**)). This is the secondary circulation described by Squire and Winter (**2**). The streamwise components of vorticity are distributed throughout the flow. This *distributed secondary circulation* is the result of a distortion of the vortex filaments carried with the stream and arises in flow around bends, through the passages between blades in cascades, and in the flow about obstacles.

The second component—the *trailing shed circulation*—is that due to the change of circulation about bodies immersed in the flow. This is a familiar concept in the theory of wings of finite span immersed in a uniform stream. The analysis shows that the concept may be extended to non-uniform flows, and confirms the assumption made in Preston's simplified treatment (**6**).

The third component—the *trailing filament circulation*—arises because, in passing round the aerofoil or blade, the vortex filament on the convex surface moves ahead of that on the concave surface so that the filament has to stretch in the wake. The stretched filaments lying in the trailing stagnation streamline contribute a vorticity of the same sign as the trailing shed circulation and, together with the latter, form a trailing vortex sheet separating the flow over the upper surface from that over the lower surface.

REFERENCES

1. W. R. Hawthorne, 'Secondary circulation in fluid flow', *Proc. Roy. Soc.* A, **206** (1951), 374.
2. H. B. Squire and K. G. Winter, 'The secondary flow in a cascade of aerofoils in a non-uniform stream', *J. Aero. Sci.* **18** (1951), 271.
3. R. E. Kronauer, 'Secondary flow in fluid dynamics', *Proc. 1st U.S. National Congress of App. Mech.* (1952), 747–56.
4. H. Eichenberger, 'Secondary flow within a bend', *J. Math. Phys.* **32** (1953), 34.
5. W. R. Hawthorne, 'The secondary flow about struts and aerofoils', *J. Aero. Sci.* **21** (1954), 588.
6. J. H. Preston, 'A simple approach to the theory of secondary flows', *Aeronautical Quarterly*, **5** (1954), 218.

ROTATIONAL FLOW THROUGH CASCADES

PART II. THE CIRCULATION ABOUT THE CASCADE

By W. R. HAWTHORNE *and* W. D. ARMSTRONG

(*Department of Engineering, University of Cambridge*)

[Received 25 June 1954]

SUMMARY

The variation in circulation about aerofoils in cascade when the approaching stream has a non-uniform velocity is determined by assuming that the secondary flow is confined to the rectangular passages between, and extending downstream from, the blades. The strength of the trailing vortex sheet separating each blade passage is estimated from the secondary flow. From this is deducted the trailing filament circulation, defined in Part I, to give the trailing shed circulation from which the variation in blade circulation can be determined. Measurements of pressure distribution on a cascade of impulse turbine blades confirm experimentally the variation of lift and circulation predicted by the theory. It is shown that the secondary flow tends to cause a stalling of the blades near the wall. A similar behaviour for isolated aerofoils in non-uniform flow is predicted.

1. Introduction

To demonstrate the existence of three constituents to the component of vorticity in the direction of flow produced when a non-uniform flow passes through a cascade, a simplifying assumption was made in Part I (**1**). It was assumed that the forces exerted on the fluid at any point on the blade span would be the same as those obtained in a two-dimensional flow with the same velocity of approach. While it is possible to conceive of a cascade of twisted blades producing such a force, the assumption is clearly not generally valid for an untwisted two-dimensional cascade as normally used in cascade wind tunnels. Even in non-uniform flow it may be presumed that the circulation about a well-designed aerofoil in a given cascade will tend to adjust itself so that Joukowski's hypothesis, that the velocity at the trailing edge is finite, will be satisfied.

Regarding the flow as a basic quasi-two-dimensional flow upon which are superimposed perturbations induced by the secondary vorticities, this boundary condition at the trailing edges of the blades must be satisfied not only by the basic flow but also by the secondary induced velocities.

The basic flow fulfils the required condition since it is a series of layers of two-dimensional flow in each of which the outlet angle and blade circulation are determined by the condition that there are no infinite velocities at the trailing edge. The boundary condition for the secondary flow may be obtained by making the simplifying assumption that the sheet of fluid leaving the trailing edge of the blade remains, at least for an

appreciable distance, the boundary separating the flow from adjacent passages. Some distance downstream a diagram of the secondary flows in a plane normal to the main flow would appear as in Fig. 1. The secondary flow between the sheets of fluid trailing from the blades will

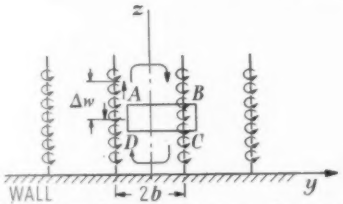

FIG. 1. Secondary flow downstream of cascade.

be similar to that in a passage after a bend and there will be no velocities at the sheets normal to or across them. With the above assumption the secondary flow may be calculated by the methods used in (**2**) for calculating the velocities induced by the distributed secondary vorticity generated in the flow of a non-uniform stream around a bend (**2**, **3**, **4**). The strength of the trailing vortex sheets situated at $y = \pm b, \pm 3b, \pm 5b$, etc. (Fig. 1), can be determined by calculating Δw, the change in spanwise secondary velocity, w, across them.

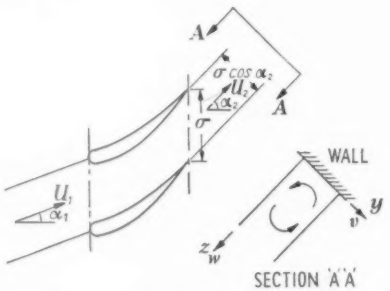

FIG. 2. Notation.

As shown in Part I, the sheets of fluid leaving the trailing edges are vortex sheets consisting of the trailing shed and trailing filament vorticity. If the trailing filament vorticity is estimated and deducted from the total strength of the vortex sheet, the trailing shed circulation, and thence the variation of circulation along the span of the blades, may be obtained. This method has been applied to some experimental results from a turbine cascade in which such estimates of the variation in circulation can be compared with values obtained from measured pressure distributions.

The notation used is shown in Fig. 2. Following references (**2**) and (**4**),

the secondary velocities v and w may be described by a stream function ψ ($w = \partial\psi/\partial y$ and $v = -\partial\psi/\partial z$), whence ξ_∞, the vorticity in the direction of flow downstream of the passage between the blades, is given by

$$\xi_\infty = \frac{\partial^2\psi}{\partial y^2} + \frac{\partial^2\psi}{\partial z^2}. \tag{1}$$

The value of ξ_∞ for a rectangular bend such as an impulse turbine blade passage was shown by Squire and Winter (**2**) to be

$$\xi_\infty \doteqdot 2\epsilon \frac{dU_1}{dz}, \tag{2}$$

where ϵ is the deflexion and U_1 the velocity far upstream. Equations (1) and (2) have been solved for the experimental variation of U_1 with z to give the stream-function ψ and thence the value of w on either side of the trailing vortex sheet (Fig. 1). The solution was obtained by the relaxation method. The value of deflexion, ϵ, used was the experimental value obtained from two-dimensional cascade tests in which the approach velocity was uniform.

2. Theory applied to impulse turbine cascade

A cascade of (approximately) impulse turbine blades shown in Fig. 3, of 6-in. chord and 18-in. span, was tested with the non-uniform approach

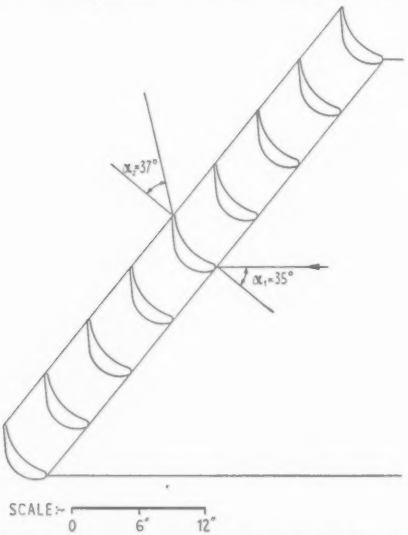

FIG. 3. Turbine cascade. Chord 6 in., pitch 6 in., span 18 in.

velocity shown in Fig. 4. Measurements of secondary velocities were made in a plane a short distance downstream of the trailing edge, and pressure

distributions on the surface of the blades were measured at various spanwise positions. The direction and magnitude of the resultants of the pressure forces are shown in Fig. 4. As the flow was symmetrical about the midspan position, the curves in Fig. 4 are drawn for only half the span. The subscript ℄ is used in the figure to signify conditions at the midspan position.

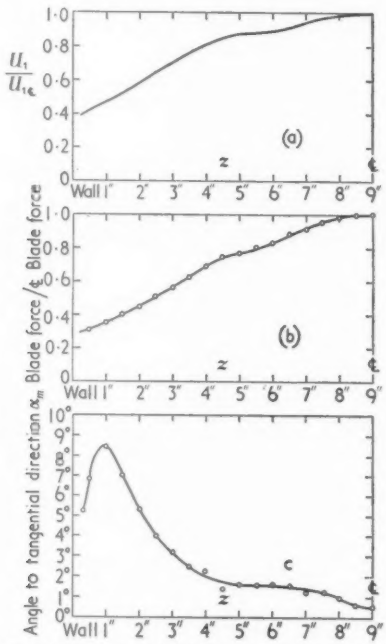

FIG. 4. Experimental results: (*a*) inlet velocity profile; (*b*) force on blade from pressure distributions; (*c*) direction of force on blade.

The secondary velocities were calculated from equations (1) and (2) where ϵ, the deflexion, was assumed constant at the two-dimensional flow value. Theoretical and experimental values of w, the spanwise velocity, are compared at two spanwise positions in Fig. 5.

The values of Δw, the strength of the trailing vortex sheet, were calculated from the theoretical values of w. They are shown in Fig. 6, curve A, as integrated values, the value at any z being the total strength of the trailing vortex sheet from the midspan position to the spanwise position z.

With the results obtained from the pressure plots it is possible to show that the trailing vortex sheet consists of components due to the trailing filament circulation and the trailing shed circulation. The trailing filament circulation has been estimated from the theory of Part I and is

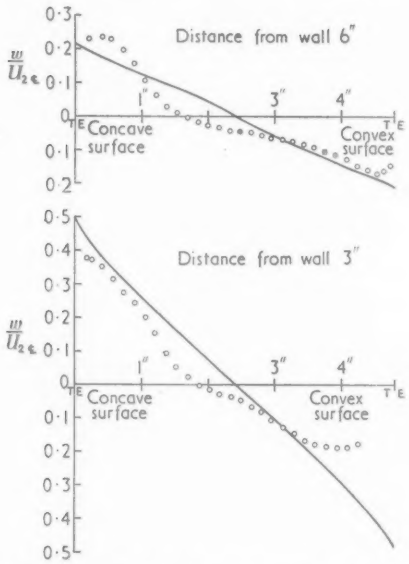

FIG. 5. Comparison of theoretical and experimental values of the secondary spanwise velocity, w. Theoretical ——. Experimental oooooooo.

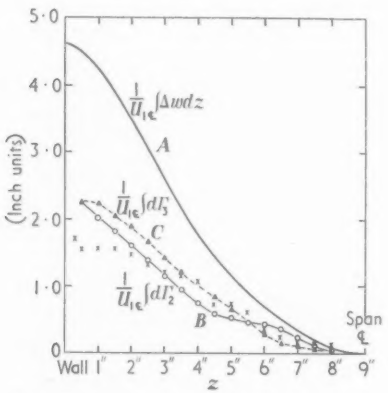

FIG. 6. Values of trailing circulation (ξ_∞ from equation (2), $\oint ds/q$ from equation (4)). A. Trailing vortex sheet from Δw ——. B. Trailing filament vorticity o—o—o. C. Shed circulation by difference ▶—▶—▶. Blade circulation from measured pressure distribution x x x. All curves show integrated value from midspan to position z.

shown as curve B, Fig. 6. The trailing shed circulation is theoretically given by the difference between curves B and A shown as curve C, Fig. 6. This is compared with experimental values of the blade circulation obtained from pressure plots and shown as experimental points in Fig. 6. The method of calculation is as follows.

The trailing filament circulation from equation (32), Part I, is

$$\delta\Gamma_2 = U_1 \frac{dU_1}{dz} \oint \frac{ds}{q}. \tag{3}$$

But the distributed secondary circulation from equation (28), Part I, is

$$\delta\Gamma_1 = \frac{dU_1}{dz}\left\{-U_1 \oint \frac{ds}{q} + \frac{\sigma}{2}\frac{\sin 2\alpha_2 - \sin 2\alpha_1}{\cos \alpha_1}\right\}$$
$$= \xi_x \sigma \cos \alpha_2. \tag{4}$$

Squire and Winter's (**2**) estimate for ξ_x given in equation (2) has been made and hence from equations (2), (3), and (4) we have

$$\delta\Gamma_2 = \sigma \frac{dU_1}{dz}\left\{\frac{1}{2}\frac{\sin 2\alpha_2 - \sin 2\alpha_1}{\cos \alpha_1} - 2\epsilon \cos \alpha_2\right\}. \tag{5}$$

The value of $\delta\Gamma_2$ for values of ϵ and α_2 appropriate to two-dimensional flow have been calculated and are shown in Fig. 6, curve B, as integrated values from the midspan position to spanwise position z.

The difference between the curves for Δw and $\delta\Gamma_2$ is shown as curve C in Fig. 6. It should give the total circulation *shed* off the blade between the midspan position and z and hence the difference in circulation about the blade at these two positions. For a blade in cascade the circulation Γ_3 is related to the lift L by

$$L = \rho U_m \Gamma_3, \tag{6}$$

where ρ is the fluid density and U_m is the vector mean of the velocities of entry and exit, U_1 and U_2. Changes in Γ_3 from the centre span value have been determined from equation (6) and the lift and velocity values shown in Fig. 4.† These values are shown as experimental points in Fig. 6. They are to be compared with the curve C, showing the difference between Δw and $\delta\Gamma_2$. Considering the approximations made and the large variation in α_2 and ϵ due to the secondary effects, the agreement is satisfactory.

A second set of curves have been drawn in which ξ_∞ has been based, not on equation (2), but on the more exact equation (4). The value of $\oint ds/q$ has been determined from measurements of the pressure distribution

† It has been assumed that the blade force measured from the pressure plots is approximately equal to the lift. When the blade is stalled and the drag is large, this approximation may be unsatisfactory.

about the blade in two-dimensional flow. The results are shown in Fig. 7, and indicate a fair agreement between theory and experiment.

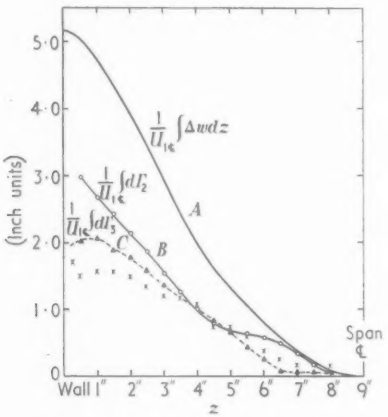

FIG. 7. Values of trailing circulation (ξ_∞ from equation (4), $\oint ds\, q$ from pressure distribution). *A*. Trailing vortex sheet from Δw ——. *B*. Trailing filament vorticity o—o—o. *C*. Shed circulation by difference ▶—▶—▶. Blade circulation from measured pressure distribution x x x. All curves show integrated value from midspan to position *z*.

The existence of a trailing filament component of the trailing vortex sheet is clearly indicated by the results shown in Figs. 6 and 7. In this instance it is of the same order of magnitude as the shed circulation and is, therefore, about half the strength of the trailing vortex sheet. Experimental confirmation of curve *A* in Fig. 6 is obtained indirectly by the comparison of measured and calculated values of the spanwise velocity w shown in Fig. 5.

3. Modifications to circulation and lift due to secondary flow

In Part I it was arbitrarily assumed that the circulation about the blade at any spanwise position would be that obtained in a two-dimensional flow with approach velocity U_1. This gave a value of trailing shed circulation

$$\delta\Gamma_3 = -\sigma \cos\alpha_1 \frac{dU_1}{dz} (\tan\alpha_2 - \tan\alpha_1), \tag{7}$$

where α_1 and α_2 were assumed invariant with z. The circulation based on this equation is compared with the result obtained from the measured pressure distributions in Fig. 8. The actual change in circulation is much smaller than that given in equation (7).

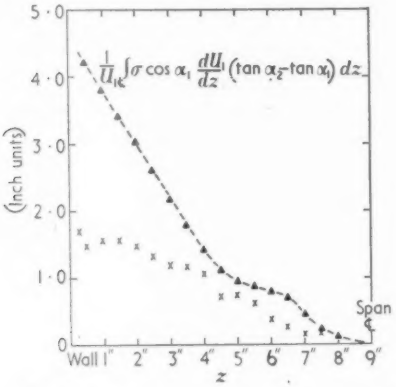

FIG. 8. Comparison between experimental circulation and circulation based on two-dimensional flow only.

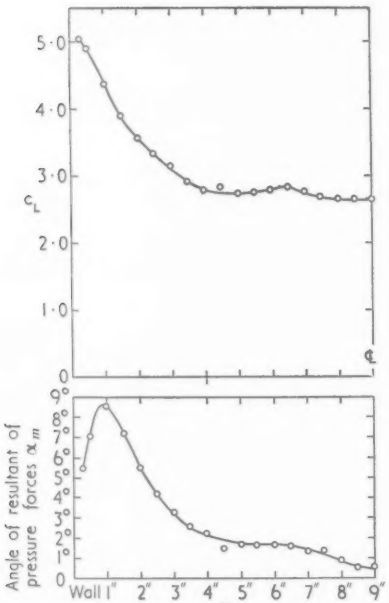

FIG. 9. Experimental lift coefficient C_L and direction of force on blade α_m.

If the assumptions of Part I were made for the lift, the value of the lift coefficient C_L, defined from

$$L = \tfrac{1}{2}\rho U_m^2 C_L c, \tag{8}$$

would be uniform along the span. Values calculated from the pressure plots are shown in Fig. 9. The increase of C_L towards the wall can be regarded as due to an *upwash*. It is accompanied by the increased angle of attack α_m (i.e. angle of resultant of pressure forces) reproduced in Fig. 9 from Fig. 4. The results of Fig. 9 are replotted in Fig. 10 as a curve of C_L against α_m. Both Figs. 9 and 10 show that very near the wall C_L continues to increase with decreasing distance from the wall. The angle of the resultant pressure forces, however, after increasing, suddenly decreases.

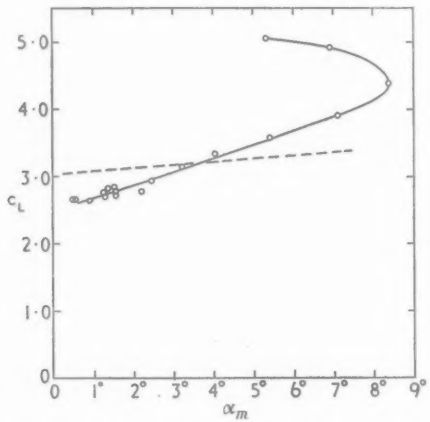

FIG. 10. Variation of C_L with α_m. From Fig. 9 o—o—o. From experiments with uniform flow – – – –.

The results of tests of the cascade in uniform two-dimensional flow show that this profile begins to show increased losses at a C_L of about 3·3. On stalling it is to be expected that, owing to the increase of drag, the angle of the resultant pressure forces will become less than the vector mean of the inlet and outlet air angles normally used to define angle of attack in cascade theory. At large values of angle of attack the reversal of α_m and C_L in Figs. 9 and 10 respectively can be partially accounted for by this effect. The agreement between the two curves in the unstalled region is fair.

4. Total secondary circulation

The total secondary circulation $\delta\Gamma$ embraced by a circuit such as $ABCD$, Fig. 1, where $AB = CD = 2b$ and $AD = BC = \delta z$, is given by the sum of the distributed and trailing vorticities, i.e.

$$\delta\Gamma = -\int_{-b}^{+b} \xi_x \, \delta z \, dy + \Delta w . \delta z, \tag{9}$$

and, since the velocities along BC and AD are the same, by

$$\begin{aligned} \delta\Gamma &= \int_{A}^{B} v \, dy + \int_{C}^{D} v \, dy \\ &= \int_{-b}^{+b} \frac{\partial v}{\partial z} \, \delta z \, dy \\ &= -\int_{-b}^{+b} \frac{\partial^2 \psi}{\partial z^2} \, \delta z \, dy. \end{aligned} \tag{10}$$

This is identical with equation (9), as may be shown by substituting for $(\partial^2\psi/\partial z^2)$ from equation (1). For $\delta\Gamma$ to be zero it is sufficient for $(\partial^2\psi/\partial z^2)$ to be zero or an odd function of y. The latter does not satisfy the physical conditions of symmetry about the y-axis implied in equation (2). Examination of equations (1) and (2) leads to the result that the condition $\delta\Gamma = 0$ is satisfied by a solution of the form

$$\psi = (y^2 - b^2)\epsilon \frac{dU_1}{dz} \tag{11}$$

provided that dU_1/dz is either linear in z or a constant. While this solution satisfies the boundary conditions $\psi = 0$ at $y = \pm b$, it does not satisfy the normal conditions that $\psi = 0$ at two values of z. It may be concluded, therefore, that the conditions for $\delta\Gamma = 0$ are too restrictive to be met in any practical case.

In Part I the particular assumption for the blade forces led to the result that $\delta\Gamma = 0$ when $\alpha_1 = \pm\alpha_2$. A similar conclusion was reached in **(5)**. However, this conclusion is not of much practical interest on account of the specialized character of the blade forces.

5. Trailing circulation outside a wall boundary layer

In the experiments described, the non-uniformity in the approaching flow extended to the midspan position. More commonly the flow is only non-uniform in a boundary layer on the walls. In such a case vortex

filaments giving rise to distributed secondary vorticity and trailing filament vorticity appear only within the boundary layer region. Owing to the distributed secondary vorticity in the blade passage, secondary vorticities are, however, induced outside the boundary layer. Across the boundaries to the 'passages' formed by the sheets of fluid leaving the trailing edges a change in w (Δw) will occur, and these trailing sheets will, therefore, contain vorticity. Since there is no trailing filament vorticity outside the wall boundary layer, the only component of trailing circulation present must be shed circulation due to a change in circulation about the blades.

Experiments with the same turbine cascade and a thin approaching boundary layer on the walls have shown that the measured circulation varies outside the wall boundary layer. Good agreement was obtained between measurements of change in the blade circulation and experimental values of Δw in this region of uniform approaching velocity. It was noted that in this region, as the boundary layer was approached, C_L decreased, indicating the existence of an apparent 'downwash' outside the boundary layer. As the boundary layer was entered, C_L increased and the major effects noted in the previous section were reproduced.

6. Isolated aerofoils

Isolated aerofoils may be treated by the same method as cascades by calculating, as shown in (**4**), the distributed secondary vorticity and, thence, the secondary flows in regions on either side of the sheet of fluid leaving the trailing edge. Values of Δw and the trailing filament circulation (equation (32), Part I) can then be estimated and the shed circulation obtained by subtraction as before. Difficulties may arise on aerofoils with well-rounded leading edges owing to the inadequacy of theoretical methods for calculating the distributed secondary vorticity (**4**).

The strength of the trailing vortex sheet can be estimated approximately from equation (11) of Part I. This is

$$\mathbf{V}.\operatorname{grad}\left(\frac{\xi}{q}\right) = -\frac{2(\mathbf{V}\wedge\operatorname{grad}(p_0/\rho)).(\mathbf{V}.\operatorname{grad})\mathbf{V}}{q^4} - \frac{\mathbf{F}.\boldsymbol{\Omega}}{q^2} - \operatorname{div}\left(\frac{\mathbf{V}\wedge\mathbf{F}}{q^2}\right). \quad (12)$$

The last two terms on the right-hand side represent the trailing filament and trailing shed circulation respectively. If the aerofoil is regarded as a lifting line with lift L and approaching velocity U varying in a spanwise direction, the value of the last two terms, giving Δw, the strength of the trailing vortex sheet, is

$$\Delta w = -\frac{L/\rho}{U^2}\frac{dU}{dz} - \frac{d}{dz}\left(\frac{L}{\rho U}\right) = -\frac{1}{\rho U}\frac{dL}{dz}, \quad (13)$$

a result which is different from that obtained in Part I, in which L is assumed to vary as U^2.

The behaviour of the flow about an aerofoil at its junction with a wall along which a boundary layer exists, e.g. at the junction of a wing and fuselage, can be discussed qualitatively in terms of equation (13). At the wall consideration of the secondary flow shows that Δw will tend to zero and consequently the slope of the curve of lift against span will tend to be zero. If U goes to zero, then d^2L/dz^2 will also be zero. Since Δw will generally be of negative sign (**4**), L will tend to decrease as the boundary layer and wall are approached.

In general, for thin wall boundary layers, the pressure distribution, and hence the force on the aerofoil, can only vary slightly in the boundary layer region; consequently, from equation (13), the strength of the trailing vortex sheet, Δw, will be small. This conclusion is in general agreement with that reached in (**4**).

If L is relatively constant and U decreases in the boundary layer, then C_L will increase and there will be the equivalent of an upwash which may lead to stalling as in the turbine cascade. For the isolated aerofoil the upwash will be accompanied by a negative induced drag, at least in the absence of stalling.

7. Conclusions

As a vortex filament in a non-uniform flow approaching a cascade, or isolated aerofoil, passes the aerofoil, the particles of the filament on the convex surface move ahead of those on the concave surface so that the filament has to stretch in the wake. This gives rise to a component of trailing vorticity, the trailing filament vorticity, which should be added to the component due to the change of circulation along the blades, the trailing shed circulation. The analysis of some experimental results on a turbine cascade with a non-uniform approaching flow shows that the strength of the trailing vortex sheet cannot be accounted for solely by the measured change in circulation about the blade. The postulation of a component due to the trailing filament vorticity satisfactorily accounts for the discrepancy.

The change in circulation along the blade can be estimated satisfactorily from calculations of the secondary flows based on a 'passage' theory and the determination of the trailing filament vorticity from a simple perturbation theory.

The results show that the secondary flow influences the behaviour of the blade in such a way as to tend to cause a stall near the wall. Similar stalling tendencies are predicted for an isolated aerofoil in a non-uniform flow and the existence of a negative induced drag is suggested.

8. Acknowledgement

Acknowledgement is made to the Chief Scientist, Ministry of Supply, for permission to publish the experimental results described in this paper.

REFERENCES

1. W. R. Hawthorne, 'Rotational flow through cascades. Part I. The components of vorticity' (see above).
2. H. B. Squire and K. G. Winter, 'The secondary flow in a cascade of aerofoils in a non-uniform stream', *J. Aero. Sci.* **18** (1951), 271.
3. W. R. Hawthorne, 'Secondary circulation in fluid flow', *Proc. Roy. Soc.* A, **206** (1951), 374.
4. —— 'The secondary flow about struts and aerofoils', *J. Aero. Sci.* **21** (1954), 588.
5. J. H. Preston, 'A simple approach to the theory of secondary flows', *The Aeronautical Quarterly*, **5** (1954), 218.

ON THE DETERMINATION OF THE FLUTTER FORCES ON WINGS WITH SUPERSONIC LEADING EDGES

By B. A. HUNN (120A, *Richmond Hill, Surrey*)

[Received 18 February 1954. Revise received 27 July 1954]

SUMMARY

This paper is concerned primarily with the practical problem of determining the aerodynamic forces on thin wings vibrating in a supersonic main stream. The class of swept wings considered is such that both the leading and trailing edges are straight and supersonic and the tip is straight in the line of flight. Two methods are considered in relation to the computing labour necessary to calculate actual flutter speeds. The first is the comprehensive treatment valid for all frequency parameters and the second is valid only for small values of the frequency.

1. Introduction

THE evaluation of the aerodynamic forces on lifting surfaces due to their modes of vibration is a problem of considerable importance in relation to the calculation of critical flutter speeds. The classical method of performing such a calculation is to regard the lifting surfaces as of such an aspect ratio that a two-dimensional aerodynamic theory is adequate. This attitude is perhaps understandable in view of the complexity of the integral equations which are derived from a linearized theory, but it is hardly to be justified for the low aspect ratio wings now in use on modern high-speed aircraft.

The problem considered here is the evaluation of these forces on wings of finite aspect ratio which are swept, and have straight leading and trailing edges and tips straight in the line of flight. The basic theory is the linearized aerodynamic one valid for wings with supersonic leading edges, although it would be equally valid for control surfaces with supersonic hinge lines. Two methods of approach are considered, one valid for all frequency parameters, the other only for small values. The former employs a transformation of variables which permits the ultimate numerical evaluation of a certain integral, and the latter employs a set of potential functions derived by Dr. G. N. Lance and the author (unpublished work) for a prescribed set of deformation modes of the class of wings mentioned.

It has been shown by Garrick and Rubinow (**1**) that the potential ϕ_U of the flow on the upper surface of a wing which is in a truly supersonic stream may be obtained from

$$\phi_U = -\frac{1}{2\pi}\int\int \frac{W(\xi,\eta)\{\tilde{\omega}(t-\tau_1)+\tilde{\omega}(t-\tau_2)\}\,d\xi d\eta}{\sqrt{\{(x-\xi)^2-B^2(y-\eta)^2\}}} \qquad (1)$$

on using linearized aerodynamic theory. In this integral the point $(x, y, 0)$

is the one under observation and the point (ξ, η) is a current one which may traverse the area of the wing in the forward Mach cone from $(x, y, 0)$. The upwash velocity $w(x, y, t)$ on the wing is assumed to be a separable function of the form

$$w(x, y, t) = W(x, y)\tilde{\omega}(t) \tag{2}$$

and the intervals τ_1 and τ_2 are given respectively by

$$\tau_{1,2} = \frac{M}{B^2 a_0}(x-\xi) \pm \frac{(x-\xi)^2 - B^2(y-\eta)^2}{B^2 a_0} \tag{3}$$

with $B^2 = M^2 - 1$, where M is the free stream Mach number and a_0 is the free stream speed of sound.

The local perturbation pressure on the upper surface is given by

$$p_U = -\rho V\left(\frac{1}{V}\frac{\partial \phi_U}{\partial t} + \frac{\partial \phi_U}{\partial x}\right) \tag{4}$$

and the local lift per unit area by

$$P = p_L - p_U, \tag{5}$$

p_L being the pressure on the lower surface.

Finally, the section lift and moment for a wing are given by

$$\text{lift/unit length} = \int_{\text{L.E.}}^{\text{T.E.}} (p_L - p_U)\, dx, \tag{6}$$

$$\text{moment about leading edge/unit length} = \int_{\text{L.E.}}^{\text{T.E.}} (x - x_{\text{L.E.}})(p_L - p_U)\, dx. \tag{7}$$

Since, however, within the framework of thin plate theory, the perturbation pressures on the upper and lower surfaces are of equal magnitude but opposite sign, it is sufficient to consider equation (6) in the form

$$+2\rho V \int_{\text{L.E.}}^{\text{T.E.}} \left(\frac{1}{V}\frac{\partial \phi_U}{\partial t} + \frac{\partial \phi_U}{\partial x}\right) dx, \tag{8}$$

with a similar result for the moment about the leading edge.

When the motion of the wing in the stream is simple harmonic, it is convenient to write

$$\tilde{\omega}(t) = e^{i\omega t} \tag{9}$$

and

$$\phi_U(x, y, 0, t) = \phi_U(x, y)e^{i\omega t}. \tag{10}$$

It then follows that

$$p_U = -\rho V e^{i\omega t}\left(\frac{i\omega}{V}\phi_U + \frac{\partial \phi_U}{\partial x}\right), \tag{11}$$

so that the determination of the section lift and moment depends upon the quantities

$$\phi_U(x_{\text{T.E.}}, y); \quad \int_{\text{L.E.}}^{\text{T.E.}} \phi_U(x,y)\,dx; \quad \int_{\text{L.E.}}^{\text{T.E.}} x\,\phi_U(x,y)\,dx. \tag{12}$$

It is evident therefore that the determination of the unsteady aerodynamic forces on a vibrating wing can be made to depend upon the flow potential. It is similarly true for modes of vibration having chord-wise distortion, for the additional strip derivatives will depend upon

$$\int x^r(p_L - p_U)\,dx.$$

2. The evaluation of the integral for the potential

When the motion of the wing is oscillatory, the integral defining the potential may be written in the form

$$\phi_U(x,y) = -\frac{1}{\pi}\int\int \frac{W(\xi,\eta)}{\sqrt{\{(x-\xi)^2 - B^2(y-\eta)^2\}}} \times \cos\left(\frac{\omega\sqrt{\{(x-\xi)^2 - B^2(y-\eta)^2\}}}{B^2 a_0}\right) e^{-iK(x-\xi)}\,d\xi d\eta \tag{13}$$

(see equation (10)), where K is defined by

$$K = \frac{M\omega}{B^2 a_0}. \tag{14}$$

Before considering the means of evaluating this integral, it will be convenient to remove the scale effect. For this, non-dimensional coordinates are introduced, defined by

$$X = x/\bar{c},$$
$$Y = y/b = y/A\bar{c}, \tag{15}$$

where $\bar{c}$ is the geometric mean chord, b the total wing span, and A the aspect ratio. Modifying the definition for (ξ, η) and using

$$\nu = \frac{\omega\bar{c}}{V} \quad \text{and} \quad S^2 = (X-\xi)^2 - B^2A^2(Y-\eta)^2, \tag{16}$$

the integral becomes

$$\phi_U(x,y) = -\frac{b}{2\pi}\int\int \frac{W}{S}\left\{\exp\left[-i\frac{M^2}{B^2}\nu\left((X-\xi) - \frac{S}{M}\right)\right] + \exp\left[-i\frac{M^2}{B^2}\nu\left((X-\xi) + \frac{S}{M}\right)\right]\right\} d\xi d\eta. \tag{17}$$

It is convenient to split this integral into its two parts:

$$\phi_U^{(1)} = -\frac{b}{2\pi}\int\int \frac{W}{S}\exp\left\{-i\frac{M^2}{B^2}\nu\left((X-\xi) - \frac{S}{M}\right)\right\} d\xi d\eta \tag{18}$$

and $$\phi_U^{(2)} = -\frac{b}{2\pi}\iint \frac{W}{S}\exp\left\{-i\frac{M^2}{B^2}\nu\left((X-\xi)+\frac{S}{M}\right)\right\}d\xi d\eta. \tag{19}$$

Then, using the transformation

$$u = \frac{1}{2B}\sqrt{\{(M+1)\nu M\}}[\sqrt{\{(X-\xi)+BA(Y-\eta)\}}-\sqrt{\{(X-\xi)-BA(Y-\eta)\}}],$$

$$v = \frac{1}{2B}\sqrt{\{(M-1)\nu M\}}[\sqrt{\{(X-\xi)+BA(Y-\eta)\}}+\sqrt{\{(X-\xi)-BA(Y-\eta)\}}], \tag{20}$$

$\phi_U^{(1)}$ becomes $$\phi_U^{(1)} = -\frac{2\bar{c}}{\pi M\nu}\iint We^{-i(u^2+v^2)}\,dudv, \tag{21}$$

and using the transformation

$$u = \frac{1}{2B}\sqrt{\{(M+1)M\nu\}}[\sqrt{\{(X-\xi)+BA(Y-\eta)\}}+\sqrt{\{(X-\xi)-BA(Y-\eta)\}}],$$

$$v = \frac{1}{2B}\sqrt{\{(M-1)M\nu\}}[\sqrt{\{(X-\xi)+BA(Y-\eta)\}}-\sqrt{\{(X-\xi)-BA(Y-\eta)\}}], \tag{22}$$

the expression for $\phi_U^{(2)}$ becomes identical in form with that given by (21).

It should be noted particularly that points within the forward Mach cone transform from (x, y) on the wing, to points in the (u, v)-plane within the sector bounded by the transformed characteristics in the first and second quadrants in the first case, and in the first and fourth quadrants in the second case. Finally, writing

$$\left.\begin{aligned} r\cos\theta &= u \\ r\sin\theta &= v \end{aligned}\right\}, \tag{23}$$

both integrals reduce to the form

$$\phi_U = -\frac{2\bar{c}}{\pi M\nu}\iint W(r,\theta)r\,e^{-ir^2}\,drd\theta. \tag{24}$$

3. Transformation of the boundaries

(i) The transformation of the characteristics through (X, Y) given by

$$(X-\xi) = \pm BA(Y-\eta) \tag{25}$$

can be shown to give, for each transformation, the equation

$$\left\{\frac{u}{\sqrt{(M+1)}}\pm\frac{v}{\sqrt{(M-1)}}\right\}^2 = 0. \tag{26}$$

These are repeated lines whose inclinations to the u-axis are given by

$$\theta = \tan^{-1}\mp\sqrt{\left(\frac{M-1}{M+1}\right)}. \tag{27}$$

(ii) Characteristics through the point (X_0, Y_0) may similarly be seen to transform into

$$\left\{\frac{u}{\sqrt{(M+1)}} \mp \frac{v}{\sqrt{(M-1)}}\right\}^2 = [(X-X_0) \mp BA(Y-Y_0)]\frac{M\nu}{B^2}. \tag{28}$$

For each sign there are two lines, one inside the appropriate sector of the (u, v)-plane and one outside. This fact will be needed when tip corrections are to be considered. The point (X_0, Y_0) lies on the given characteristic.

(iii) The transformation of the wing leading edges may be written in the form

$$m\xi = \pm A\eta. \tag{29}$$

Again, manipulation of the transformations shows in both cases that the leading edges become

$$\frac{mu^2}{M+1} + \frac{mv^2}{M-1} \pm \frac{2uv}{B^2} = (mX \mp AY)\frac{M\nu}{B^2}. \tag{30}$$

Since $m = \cot\Lambda$, Λ being the leading edge sweep-back angle, and since further

$$Bm > 1 \tag{31}$$

for supersonic leading edges, equation (30) will be identified as a pair of ellipses centred at the origin of the (u, v)-plane with major axes inclined to the u-axis at angles

$$\theta = \tfrac{1}{2}\tan^{-1}\left(\mp\frac{1}{m}\right). \tag{32}$$

The relation between r and θ can be seen to be

$$r^2 = \frac{\nu M \sin\Lambda(mX \mp AY)}{M\cos\Lambda - \cos(2\theta \pm \Lambda)}. \tag{33}$$

The upper sign is appropriate to the starboard leading edge, the lower to the port.

Finally, using the plane polar coordinates, the θ-coordinates of the intersections of the two ellipses are given by

$$\sin(2\theta - \alpha) = -\frac{AYM}{\sqrt{(X^2 + A^2Y^2)}}, \tag{34}$$

where

$$\alpha = \tan^{-1}\frac{AY}{X} = \tan^{-1}\frac{y}{x}. \tag{35}$$

4. The transformed upwash function

For flutter purposes it is convenient to regard the wing as a lamina. Any distortions may be represented by

$$f(x, y) = \sum\sum a_{rs} x^r y^s. \tag{36}$$

The accuracy of calculation of the distortion shapes, or, for that matter,

their experimental determination, justifies limiting this series to a few terms.

The upwash condition can be shown to be

$$\frac{\partial}{\partial z}\phi(x,y,0,t) = w(x,y,t) = V\frac{\partial g}{\partial x}+\frac{\partial g}{\partial t}, \tag{37}$$

where $z = g(x,y,t)$ describes the wing motion. For the oscillatory case, separable functions can be used to give

$$\frac{\partial}{\partial z}\phi(x,y,0) = V\frac{\partial G}{\partial x}+i\omega G, \tag{38}$$

where

$$g(x,y,t) = e^{i\omega t}G(x,y). \tag{39}$$

Observing that the series form is still valid, one finds that

$$\sum\sum a_{pq}\xi^p\eta^q = \sum\sum \frac{a_{pq}}{\nu^{p+q}}\left\{X_\nu-\frac{r^2}{M}(M-\cos 2\theta)\right\}^p\left\{Y_\nu-\frac{r^2}{AM}\sin 2\theta\right\}^q, \tag{40}$$

where a_{pq} is in general complex.

Using this series for the surface configuration of the wing, it then follows immediately that

$$W \equiv W(r^2,\theta). \tag{41}$$

In this event, since

$$\int r^{2n}re^{-ir^2}\,dr$$

is immediately integrable, it is convenient to perform the integration with respect to r before θ in the determination of ϕ_U.

5. Zones of integration

It can be seen without difficulty that the total potential on the upper surface of the wing can be represented as

$$\phi_U(x,y) = \phi_U^{(1)}+\phi_U^{(2)} = -\frac{2\bar{c}}{\pi M\nu}\int_{\theta_2'}^{\theta_2''} d\theta \int_0^{R(\theta)} W(r^2,\theta)re^{-ir^2}\,dr. \tag{42}$$

where

$$\left.\begin{aligned}\theta_2' &= -\tan^{-1}\sqrt{\left(\frac{M-1}{M+1}\right)}\\ \theta_2'' &= \pi-\tan^{-1}\sqrt{\left(\frac{M-1}{M+1}\right)}\end{aligned}\right\} \tag{43}$$

and $r = R(\theta)$ is the sole means of discriminating between whether the point (x,y) is forward or aft of the Mach cone from the leading edge vertex, and whether this potential is subject to tip effects.

For points on the starboard wing forward of the Mach cone and not subject to tip effects, the zone of integration in the (u,v)-plane

corresponding to the interior of the forward Mach cone from (x, y) occupied by the wing is, in fact, that segment of the ellipse

$$\frac{mu^2}{M+1}+\frac{mv^2}{M-1}+\frac{2uv}{B^2}=\frac{M\nu}{B^2}(mX-AY) \tag{44}$$

bounded by the line

$$\frac{u}{\sqrt{(M+1)}}+\frac{v}{\sqrt{(M-1)}}=0 \tag{45}$$

and lying in the first, second, and fourth quadrants (see Fig. 1).

For points lying within the Mach cone, again not subject to tip effects, the region of integration is bounded by two ellipses. If, on the starboard side, the integral is taken over the range

$$\left.\begin{aligned} &\tan^{-1}\left\{-\sqrt{\left(\frac{M-1}{M+1}\right)}\right\} \leqslant \theta \leqslant \psi_1 \\ \text{with}\quad &0 \leqslant r^2 \leqslant \left[\frac{\nu M \sin\Lambda(mX+AY)}{M\cos\Lambda-\cos(2\theta-\Lambda)}\right] \end{aligned}\right\}, \tag{46}$$

then

$$\psi_1 \leqslant \theta \leqslant \psi_2$$

with

$$0 \leqslant r^2 \leqslant \left[\frac{\nu M \sin\Lambda(mX-AY)}{M\cos\Lambda-\cos(2\theta+\Lambda)}\right] \tag{47}$$

and finally

$$\psi_2 \leqslant \theta \leqslant \pi-\tan^{-1}\sqrt{\left(\frac{M-1}{M+1}\right)} \tag{48}$$

with r given as in inequality (46) and where ψ_1 and ψ_2 are the two roots of (34) and (35) lying in the half-plane to the right of the line given by (45) (see Fig. 2).

Finally, for points subject to tip effects, use is made of the results given by Evvard (**2**). In the (x, y)-plane the area of integration is limited by the forward Mach cone from (x, y), the characteristic from that point on the edge at the tip intersected by the complementary characteristic from (x, y) and the leading edge.

The corresponding zone in the (u, v)-plane is either of the two cases previously mentioned but with a segment sliced off by the line given by

$$\left\{\frac{u}{\sqrt{(M+1)}}+\frac{v}{\sqrt{(M-1)}}\right\}^2=[(X-X_0)-BA(Y-Y_0)]\frac{M\nu}{B^2}. \tag{49}$$

In particular, it should be observed that if Y_0 is evaluated at the tip and X_0 is the corresponding value of ξ for the intersection of the line

$$(X-\xi)=BA(Y-\eta) \tag{50}$$

with

$$Y_0=\eta, \tag{51}$$

then the nearer (X, Y) approaches the tip, the nearer the line given by

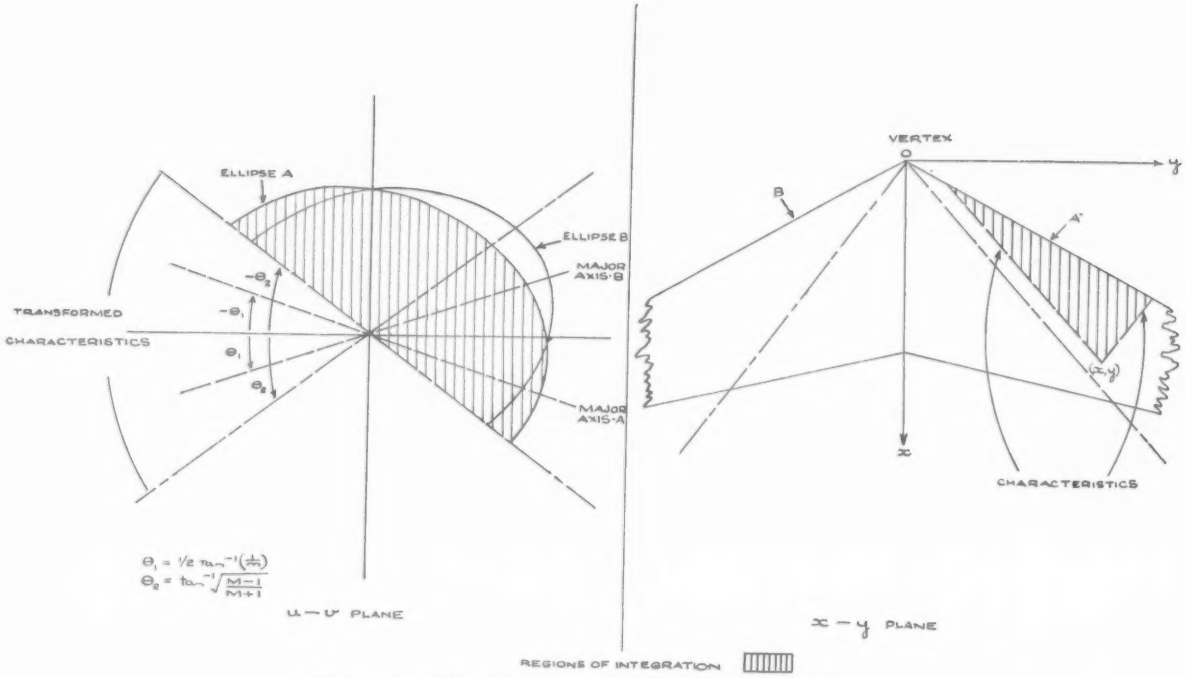

FIG. 1. Areas of integration for points outside the Mach cone.

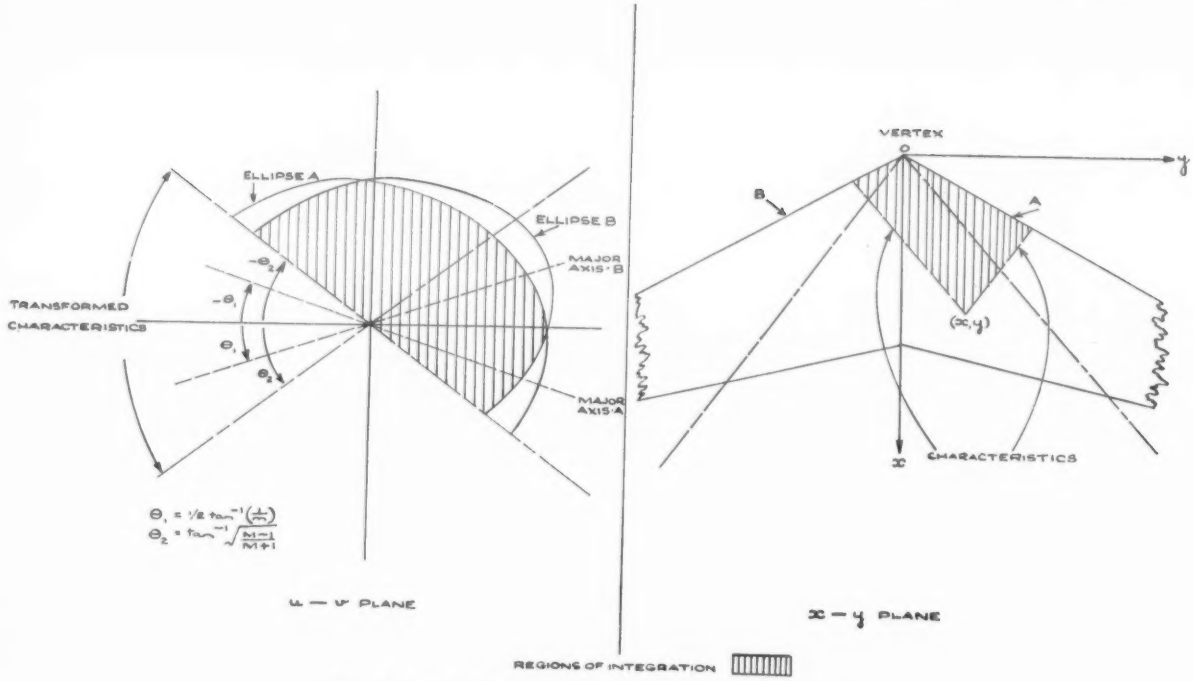

Fig. 2. Area of integration for points inside Mach cone.

(49) approaches that given by (45). Finally, when coincidence occurs the region of integration is zero (see Fig. 3).

This treatment of the tip correction needs some modification in the light of information received since the original draft of the paper was prepared. It had been stated by Stewart and Li (**3**) that the Evvard method would be suitable for oscillatory motion. This has subsequently been retracted (**4**) and they point out that errors of the second order in frequency would be introduced. Another method has been given by Stewartson (**5**).

No attempt is made in this paper to utilize their suggested method of correction. It should, however, be borne in mind that flutter usually occurs on main surfaces for frequency parameters well below unity so that the errors incurred by neglecting these effects will probably be small and restricted to small regions, but control surface flutter, occurring for values of frequency parameter usually greater than unity, will be affected more seriously.

6. The low-frequency approach

In this case the aerodynamic theory is again linearized with respect to the frequency parameter, the assumption being made that only first powers are significant. On writing

$$\phi(x, y, z, t) = \Phi(x, y, z)\exp i\omega\left(t - \frac{M^2}{B^2}\frac{x}{V}\right) \tag{52}$$

with the previous hypothesis, it can be shown that the integral defining the potential becomes

$$\Phi(x, y, 0) = -\frac{b}{2\pi}\int\int \frac{W}{S}\left(1 + i\nu\frac{M^2}{B^2}\xi\right) d\xi d\eta \tag{53}$$

using the non-dimensional variables.

An equivalent approach from the equations of fluid flow shows that Φ must be a solution of

$$\frac{\partial^2\Phi}{\partial y^2} + \frac{\partial^2\Phi}{\partial z^2} = (M^2 - 1)\frac{\partial^2\Phi}{\partial x^2}. \tag{54}$$

Using characteristic coordinates of the form

$$\left.\begin{aligned} r &= x - By \\ s &= x + By \end{aligned}\right\}, \tag{55}$$

Ward has shown (**6**) that Φ is given by

$$\Phi = -\frac{1}{2\pi B}\int\int \frac{W'}{\sqrt{\{(r - r_2)(s - s_2)\}}}\, dr_2 ds_2. \tag{56}$$

FIG. 3. Corresponding areas of integration with tip correction necessary.

Here W' has a slightly different connotation, being in fact derived from

$$\frac{\partial \Phi}{\partial z} e^{-i\nu(M^2/B^2)(x/\bar{c})} = W(x, y), \tag{57}$$

or, consistent with the low-frequency parameter approach,

$$\frac{\partial \Phi}{\partial z} = W' = W(x, y)\left(1 + i\nu \frac{M^2}{B^2} \frac{x}{\bar{c}}\right). \tag{58}$$

It is not difficult to show that (56) and (53) are identical. The form of (56) is, however, much more convenient for the determination of analytical expressions for the potential. This form has been used to compute the potentials for wings whose incidence is given by

$$\left.\begin{aligned} \frac{\partial z}{\partial x} &= -\alpha x^r |y^s| \\ \text{and} \qquad \frac{\partial z}{\partial x} &= -\alpha x^r |y^s| \operatorname{sgn}(y) \end{aligned}\right\} \tag{59}$$

for all positive and zero values of r and s such that

$$r + s \leqslant 3.$$

These include tip corrections as required for the class of wings defined in the summary. The analytical expressions obtained have been written in terms of the two parameters

$$a = Bm \quad \text{(see equation (31))}$$

and

$$\eta = B\frac{y}{x}. \tag{60}$$

Some functions have been computed for a few values of a over the corresponding ranges of η. Those omitted have necessarily been the ones concerned with tip effects, for they depend upon the geometry of the specific wing.

Using the reduced potential it is convenient to work in terms of the components defined by

$$\Phi = \Phi_1 + i\nu\Phi_2 \tag{61}$$

where

$$\left.\begin{aligned} \frac{\partial \Phi_1}{\partial z} = W_1' &= V \frac{\partial G}{\partial x} \\ \partial \Phi_2 = W_2' &= V\left(\frac{G}{\bar{c}} + \frac{M^2}{B^2} \frac{x}{\bar{c}} \frac{\partial G}{\partial x}\right) \end{aligned}\right\} \tag{62}$$

with G defined as in (39).

Further, the section lift can be shown to depend upon

$$\int_{\text{L.E.}}^{\text{T.E.}} \left\{\frac{\partial \Phi}{\partial x} - \frac{i\nu}{M^2 - 1}\left(\frac{\Phi}{\bar{c}} + M^2 \frac{x}{\bar{c}} \frac{\partial \Phi}{\partial x}\right)\right\} dx \tag{63}$$

with a similar expression for the moment. It then follows that the in-phase lift depends simply upon $\Phi_1(x_{\text{T.E.}}, y)$ while the out-of-phase lift depends upon

$$\nu\left\{\Phi_2(x_{\text{T.E.}}, y) - \frac{1}{B^2}\left(\int_{\text{L.E.}}^{\text{T.E.}} \frac{\Phi_1}{\bar{c}}\, dx + \int_{\text{L.E.}}^{\text{T.E.}} M^2 \frac{x}{\bar{c}} \frac{\partial \Phi_1}{\partial x}\, dx\right)\right\}. \tag{64}$$

Finally, it should be observed that the reduced potential can be compared with the potential given by the other method for low values of frequency parameter on the basis that

$$(\Phi_1 + i\nu\Phi_2)\left(1 - i\nu\frac{M^2}{B^2}\frac{x}{\bar{c}}\right) \doteqdot \Phi_1 + i\nu\left(\Phi_2 - \frac{M^2}{B^2}\frac{x}{\bar{c}}\Phi_1\right) \doteqdot \phi_U(x, y). \tag{65}$$

7. Numerical comparison of results

A swept wing having 44° of sweep-back on the leading edge was considered. The modes of vibration prescribed for this wing were uniform plunging motion and pitch about an axis through the leading edge vertex.

In the first case, then,

$$W(x, y) = Vi\nu\frac{z_0}{\bar{c}}, \tag{66}$$

z_0 being the amplitude of oscillation. In the second case

$$W(x, y) = -V\alpha\left(1 + i\nu\frac{x}{\bar{c}}\right). \tag{67}$$

For each of these modes the potential at two points on the same section of the wing was calculated, one outside the vertex Mach cone and the other inside.

The integrals can be shown to reduce to

$$\phi_U(x, y) =$$

$$-V\alpha\frac{\bar{c}}{\pi M\nu}\int_{\theta_1}^{\theta_2}\left[\left\{\nu x(\cos R^2 - 1) - \frac{\cos 2\theta}{M}\sin R^2 - R^2\cos R^2\left(1 - \frac{\cos 2\theta}{M}\right)\right\} + \right.$$

$$\left. + i\left\{(1 - \cos R^2)\frac{\cos 2\theta}{M} - \nu x\sin R^2 + R^2\sin R^2\left(1 - \frac{\cos 2\theta}{M}\right)\right\}\right] d\theta \tag{68}$$

for the pitching case, $R(\theta)$ being defined by

$$R^2(\theta) = \frac{\nu M\sin\Lambda(mX \mp AY)}{M\cos\Lambda - \cos(2\theta \pm \Lambda)}, \tag{69}$$

the upper sign being taken for the point outside the Mach cone on the

starboard wing and the alternating signs as defined in equations (46)–(48). The limits θ_1 and θ_2 are defined in (43). For the plunging case the integral becomes

$$\phi_U = -\frac{Vz_0}{\bar{c}} \frac{\bar{c}}{\pi M \nu} \int_{\theta_1}^{\theta_2} \{(1-\cos R^2)+i \sin R^2\}\, d\theta \qquad (70)$$

with $R(\theta)$ and the bounds of θ defined as above.

Consideration of this integral shows that the chances of deriving analytical results is small. A numerical integration was carried out using the generalized Simpson's rule. In particular for the point outside the Mach cone the integrand was evaluated for nine different values of θ, and for the point inside the numbers of values of θ taken were first three in the range defined by (46), then eleven in the range defined by (47), and finally three in the range defined by (48). The values of ν which were adopted were

$$\nu = 0,\ 0{\cdot}1,\ 0{\cdot}2,\ 0{\cdot}8, \text{ and } 1{\cdot}4.$$

The other parameters were:

$$M = 1{\cdot}84,$$
$$AY = 1{\cdot}1377,$$
$$X = 1{\cdot}9266 \text{ inside; } 1{\cdot}3994 \text{ outside,}$$
$$\bar{c} = 10{\cdot}41 \text{ ft.}$$

The rather peculiar values were chosen so as to permit comparison with a previous calculation using the low-frequency parameter theory. In particular the value of a for this aircraft at the given Mach number was 1·6.

These results were then plotted against frequency parameter and the corresponding low-frequency parameter results were superimposed. These had been obtained direct from the graphs mentioned in the previous paragraph. The slight disagreement between the two methods at $\nu = 0$ should be observed as due to the inaccuracies in graph reading and the inherent errors in numerical integration (see Figs. 4–7).

8. Discussion of results

The criteria which must be applied to any numerical technique required for practical work are that it possesses a logical simplicity, that it involves relatively simple numerical operations, and that the volume of operations is not prohibitive. With the compatible frequency parameter theory it is evident that not only must the complex potentials be evaluated at a fairly large number of points spread over the wing, but the integral involved for each point must be repeated for each new value of the

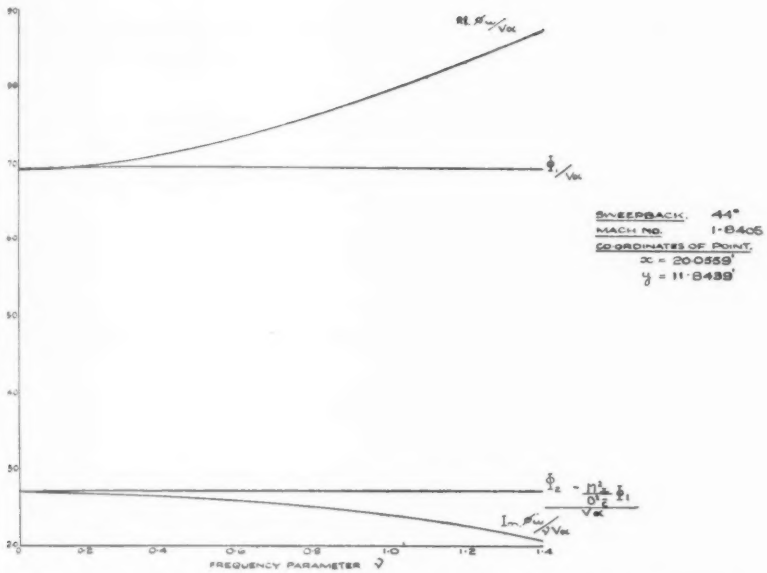

FIG. 4. Graphs of the complex potential for the case of a swept wing pitching about the vertex. Point interior to the Mach cone.

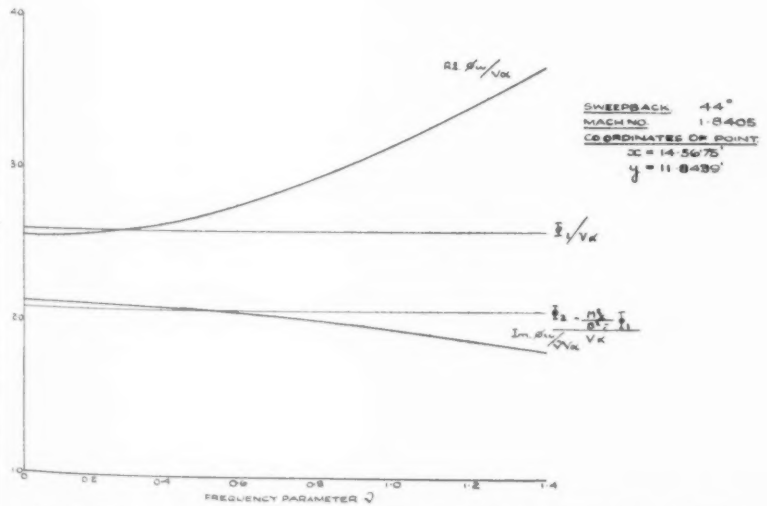

FIG. 5. Graphs of the complex potential for the case of a swept wing pitching about the vertex. Point exterior to the Mach cone.

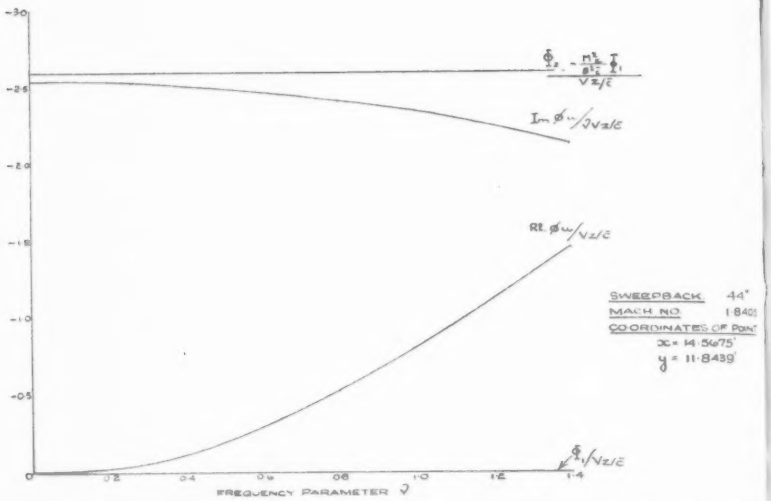

FIG. 6. Graphs of the complex potential for the case of a swept wing plunging through an amplitude z. Point exterior to the Mach cone.

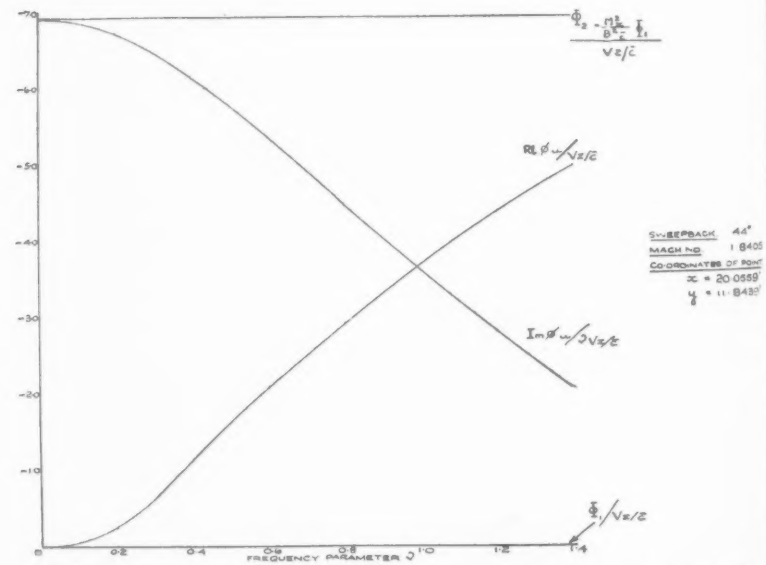

FIG. 7. Graphs of the complex potential for the case of a swept wing plunging through an amplitude z. Point interior to the Mach cone.

frequency parameter. Further, for every new mode of vibration these calculations must be repeated. It therefore follows that the volume of work involved in this comprehensive approach is large.

On the other hand, the low-frequency theory can be used for all reasonably small values of the frequency parameter, and the numerical values, except where tip corrections are involved, can be obtained from the functions already tabulated. The groundwork which has been done on tabulating these results can be regarded as common to all calculations involving the class of wings previously defined. From the numerical point of view there is therefore much to commend this method. However, from the mathematical point of view, the hypothesis that

$$\exp\left(-i\nu\frac{M^2}{B^2}\frac{x}{\bar{c}}\right)\sim 1-i\nu\frac{M^2}{B^2}\frac{x}{\bar{c}} \tag{71}$$

for sufficiently small values of ν would seem to be a very restrictive one.

Now it usually happens that main surface flutter occurs for values of frequency parameter not greater than 0·5. Referring to the graphs for the potential it will be seen that the discrepancies between the two theories is not large for $\nu = 0{\cdot}5$ except in Fig. 7. This, however, must be considered in relation to the main stream Mach number, for the basic integral involves the frequency parameter in the forms $M^2\nu/B$ and $M\nu/B$, and one would expect greater discrepancies between the two theories when the wings were only just supersonic. Bearing this in mind it can, however, be seen that if one proceeds with due caution some useful results can be obtained from low-frequency theory.

A complete flutter calculation has been performed on the wing under consideration, using the low-frequency parameter theory for comparison with results predicted by incompressible theory. Whereas the result predicted for incompressible theory gave a Mach number of 2·8, the supersonic theory gave $M = 4{\cdot}2$. This result thus appears to be rather dubious. However, it has been shown experimentally that the ratio of the experimental wing flutter speed to that calculated on a theoretical, incompressible basis in the supersonic régime increases considerably above unity with Mach number (**7**).

Finally, although specific mention has been made of wing flutter, the methods discussed can be applied to control surfaces. The chief disadvantage occurs using the low-frequency theory, for one usually finds frequency parameters greater than unity arising from control surface flutter. Therefore it would be desirable to use a third-order theory in frequency as devised by Nelson (**8**) as an alternative; but the more comprehensive method described in the earlier section of this paper should prove the more accurate.

REFERENCES

1. I. E. Garrick and S. I. Rubinow, *A Theoretical Study of Air Forces on an Oscillating or Steady Wing in a Supersonic Main Stream*, N.A.C.A., T.N. No. 1383 (July 1947).
2. J. C. Evvard, *Distribution of Wave Drag and Lift in the Vicinity of Wing Tips at Supersonic Speeds*, N.A.C.A., T.N. No. 1382 (1947).
3. H. J. Stewart and Ting-Yi Li, 'Source superposition method of solution of a periodically oscillating wing at supersonic speeds', *Quart. Applied Math.* **9** (1951), 31.
4. —— —— 'On an integral equation in supersonic oscillating wing theory', *J. Aero. Sci.* **20** (1953), 724.
5. K. Stewartson, 'On the linearized potential theory of unsteady supersonic motion, II', *Quart. J. Mech. and Applied Math.* **5** (1952), 182.
6. G. N. Ward, 'Supersonic flow past thin wings (Part 1)', ibid. **2** (1949), 136.
7. G. W. Jones and H. C. Dubose, *Investigation of Wing Flutter at Transonic Speeds for Six Systematically Varied Wing Planforms.* Restricted Report (August 1953).
8. H. C. Nelson, *Lift and Moment on Oscillating Triangular and Related Wings with Supersonic Edges*, N.A.C.A., T.N. 2494 (September 1951).

ON THE BOUNDS OF EIGENVALUES

By K. WASHIZU

(*Department of Aeronautics, University of Tokyo, Tokyo, Japan*)

[Received 23 September 1954]

SUMMARY

In this paper, formulae for locating the bounds of eigenvalues of a real symmetric matrix are treated in a unified manner. In the first part of the paper, several theorems which provide bounds for eigenvalues are represented in a geometrical space. In the second part, a generalization of Rayleigh's principle is attempted, and some theorems which provide bounds for eigenvalues are discussed as special cases of the generalized Rayleigh's principle. The system treated here has a finite number of degrees of freedom. By appropriate modifications the above principles can, however, be extended to a system with an infinite number of degrees of freedom.

1. Introduction

WHEN an eigenvalue problem can be solved only approximately, it is desirable to obtain bounds for the eigenvalues. Several theorems pertaining to such bounds have appeared in the literature (**1**). Among them Rayleigh's principle for estimating natural frequencies of vibrating systems is undoubtedly the most well established. Rayleigh's theorem shows that his approximate method always provides an upper bound for the lowest frequency and a lower bound for the highest one, and that first-order errors in the assumed mode of vibration produce only second-order errors in the estimate of the natural frequency. In practice a criterion of this kind is of limited value unless it is accompanied by another theorem which provides a lower bound for the lowest frequency or an upper bound for the highest one.

A formula giving a lower bound for the lowest eigenvalue was obtained by Temple (**2**, **3**). Kohn (**4**) and Kato (**5**) generalized his theorem so as to determine the location of any eigenvalue, i.e. not necessarily the lowest or the highest one. Later, Temple (**6**) showed that the Kohn–Kato theorem can be extended to a system with inertial couplings, while the author (**7**) showed that these theorems have definite geometrical meanings and represented them in a vector space. A brief summary of the principle of geometrical representation is given in the first part of this paper.

Recently R. V. Southwell (**8**) published a paper giving new theorems for the location of the bounds of eigenvalues. His formulae seem to suggest a method of generalizing Rayleigh's principle and have stimulated the author to write the present paper. In the second part of this

paper a generalization of Rayleigh's principle is attempted and the theorems mentioned above are discussed as special cases of the generalized Rayleigh's principle so that their mutual relations might be understood clearly. New formulae could be obtained from the generalized Rayleigh's principle, but not all, probably, will be of value for numerical computation.

2. Rayleigh's principle

Let us consider an eigenvalue problem of the type

$$Au = \lambda u, \tag{1}$$

where A is a real symmetric matrix and u is an n-dimensional vector with components

$$(u_1, u_2, ..., u_n). \tag{2}$$

Let the normal modes or eigenvectors of A be denoted by $\phi_1, \phi_2, ..., \phi_n$ and the corresponding eigenvalues by $\lambda_1, \lambda_2, ..., \lambda_n$, so that

$$A\phi_r = \lambda_r \phi_r \quad (r = 1, 2, ..., n). \tag{3}$$

All of these eigenvalues are real. Therefore, let the order of magnitude of the eigenvalues be specified so that

$$\lambda_1 \leqslant \lambda_2 \leqslant ... \leqslant \lambda_n. \tag{4}$$

The normal modes are orthogonal and normalized in the sense that

$$(\phi_r, \phi_s) = \delta_{rs}, \tag{5}$$

where δ_{rs} is Kronecker's delta, i.e.

$$\delta_{rs} = 0 \quad \text{if } r \neq s,$$
$$\delta_{rs} = 1 \quad \text{if } r = s.$$

We shall henceforth choose the n orthogonal and normalized vectors as the bases of the coordinates in the n-dimensional vector space and let w be an arbitrary vector which has components of $(c_1, c_2, ..., c_n)$ with respect to the base vectors ϕ_r, so that

$$w = \sum_{r=1}^{n} c_r \phi_r. \tag{6}$$

With the above definition, the following theorem, referred to as Rayleigh's principle in this paper, is readily obtained:

Rayleigh's principle.

$$\lambda_1 \leqslant \frac{(w, Aw)}{(w, w)} \leqslant \lambda_n. \tag{7}$$

The proof of this theorem is easy and need not be given here; the theorem holds irrespective of the signs of the eigenvalues.

For the problem of the type

$$Vv = \lambda Tv, \tag{8}$$

namely, a system having both elastic and inertial coupling, the theorem expressed in (7) can be extended with a slight modification. It is assumed that V is a real symmetric matrix and that T is a positive-definite real symmetric matrix. Now, by putting

$$T^{-\frac{1}{2}}VT^{-\frac{1}{2}} \equiv A, \qquad T^{\frac{1}{2}}v \equiv u, \tag{9}$$

(8) can be transformed to a type which is equivalent to (1). Therefore the corresponding relations can be obtained immediately. Thus, in place of (3), (5), and (6) we obtain

$$V\psi_r = \lambda_r T\psi_r, \tag{10}$$

$$\left.\begin{aligned}(\psi_r, T\psi_s) &= \delta_{rs}\\ (\psi_r, V\psi_s) &= \lambda_r\delta_{rs}\end{aligned}\right\}, \tag{11}$$

$$w = \sum_{r=1}^{n} c_r\psi_r, \tag{12}$$

and in place of (7) we get

$$\lambda_1 \leqslant \frac{(w, Vw)}{(w, Tw)} \leqslant \lambda_n. \tag{13}$$

3. Vaisey's theorem

Southwell (**8**) states Vaisey's theorem in the following manner. For a continuous system, consider a differential equation of the form

$$\vartheta w - \nu\vartheta' w = 0, \tag{14}$$

where λ of Southwell's paper is here replaced by ν. Let ϑ and ϑ' be self-adjoint linear operators and let

$$I \equiv \iint w\vartheta w\, dxdy, \tag{15}$$

$$I'/\Lambda \equiv \iint w\vartheta' w\, dxdy, \tag{16}$$

where it is assumed that I is positive definite and I'/Λ may have any sign. As a consequence, the eigenvalues ν can have both signs, but they must still be real. Let the positive eigenvalues be denoted by

$$\nu_1, \nu_2, \ldots, \nu_k, \ldots$$

and the negative ones by

$$\nu_{-1}, \nu_{-2}, \ldots, \nu_{-l}, \ldots$$

with both series in order of ascending numerical magnitude. With the above definitions, Vaisey's theorem may be stated as follows:

VAISEY'S THEOREM. *The value of ν_R defined by*

$$\nu_R \equiv \frac{\Lambda I}{I'} = \frac{\iint w\vartheta w\, dxdy}{\iint w\vartheta' w\, dxdy} \tag{17}$$

cannot lie between the least positive and the largest negative eigenvalue (ν_1 and ν_{-1}).

Now it is easy to show that there is a close similarity between (8) and (14) by writing V, T, and λ in place of ϑ', ϑ, $1/\nu$, respectively. Thus, the conditions which define each problem become equivalent, and Vaisey's theorem leads to the statement that the value of λ_R defined by

$$\lambda_R \equiv \frac{(w, Vw)}{(w, Tw)} \tag{18}$$

can only lie between the least and the largest eigenvalues (λ_1 and λ_n) if we remember that $1/\nu_1$ and $1/\nu_{-1}$ correspond to λ_n and λ_1, respectively. Thus we see that Vaisey's theorem is contained in (13).

For the sake of simplicity, we shall henceforth treat only problems of the type (1) unless special reference is made to problems of the type (8).

4. Principle of geometrical representation

We shall consider an eigenvalue problem of the type (1), and let w be an arbitrary, normalized vector as expressed by (6). Now, consider two vectors w ($\overrightarrow{OA}$) and Aw ($\overrightarrow{OB}$) in the n-dimensional vector space as shown in Fig. 1. Points P_1, P_2,..., and P_n are located on the line OA so that

$$OP_i = \lambda_i. \tag{19}$$

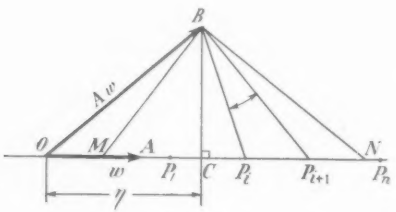

FIG. 1.

Since

$$\overline{BP_i} \cdot \overline{BP_{i+1}} \cos \angle P_i BP_{i+1} = (\overrightarrow{BP_i}, \overrightarrow{BP_{i+1}}) = (\lambda_i w - Aw, \lambda_{i+1} w - Aw)$$
$$= \sum_{r=1}^{n} (\lambda_i - \lambda_r)(\lambda_{i+1} - \lambda_r) c_r^2 \geqslant 0, \tag{20}$$

it follows that

$$\angle P_i BP_{i+1} \leqslant \tfrac{1}{2}\pi. \tag{21}$$

Now, let BC be a perpendicular from the point B to the line OA in the OAB-plane. Then

$$\eta \equiv (Aw, w) = (\overrightarrow{OB}, \overrightarrow{OA}) = OC \tag{22}$$

is the Rayleigh quotient. By using relation (7) it follows that

$$\left.\begin{aligned} &P_1 \text{ lies in } (-\infty, \eta) \\ &\text{and } P_n \text{ lies in } (\eta, +\infty) \end{aligned}\right\}, \tag{23}$$

or equivalently

$$\left.\begin{aligned} &\angle(-\infty)BP_1 \leqslant \tfrac{1}{2}\pi \\ &\text{and } \angle P_n B(+\infty) \leqslant \tfrac{1}{2}\pi \end{aligned}\right\}. \tag{24}$$

From (21) and (24) the following conclusion is derived:

Let M and N be two points on an arbitrary, normalized vector $w = \overrightarrow{OA}$ and let the point B be defined by the relation $Aw = \overrightarrow{OB}$ (Fig. 1). If

$$\angle MBN \geqslant \tfrac{1}{2}\pi, \tag{25}$$

then at least one eigenvalue must be contained in the interval MN, i.e.

$$OM \leqslant \lambda_r \leqslant ON. \tag{26}$$

A very simple example of this relation is illustrated in Fig. 2. In the case $n = 2$, we obtain

$$w = (\cos\theta, \sin\theta),$$

$$Aw = \begin{pmatrix} \lambda_2 & 0 \\ 0 & \lambda_1 \end{pmatrix}\begin{pmatrix} \cos\theta \\ \sin\theta \end{pmatrix} = \begin{pmatrix} \lambda_2 \cos\theta \\ \lambda_1 \sin\theta \end{pmatrix},$$

and $\quad \angle P_1 B P_2 = \tfrac{1}{2}\pi \quad$ (from (20)).

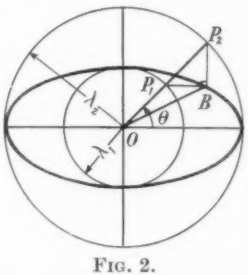

FIG. 2.

These relations are used in drawing an ellipse whose major and minor semi-axes are λ_2 and λ_1 respectively. To the problem of type (8) the above geometrical representation (26) can be extended with a slight modification. By using (9), the problem (8) can be reduced to the same type as (1), and, in this modified space, the relation (26) holds similarly.

5. Kato's theorem

One of Kato's theorems (5) can be stated as follows:

Let w be an arbitrary normalized vector, so that $(w, w) = 1$, and let η and ϵ be defined as follows:

$$(Aw, w) \equiv \eta, \qquad (Aw - \eta w, Aw - \eta w) \equiv \epsilon^2.$$

Then, for every a such that $a < \eta$, (a, b) contains a point of the spectrum, where b is defined by

$$b = \eta + \frac{\epsilon^2}{\eta - a}. \tag{27}$$

Now we find in Fig. 3 that

$$\left.\begin{aligned} \eta &= (Aw, w) = (\overrightarrow{OB}, \overrightarrow{OA}) = OC \\ \epsilon^2 &= (Aw-\eta w, Aw-\eta w) = \overline{BC}^2 \end{aligned}\right\}, \tag{28}$$

and

$$\epsilon^2+\eta^2 = (Aw, Aw)$$

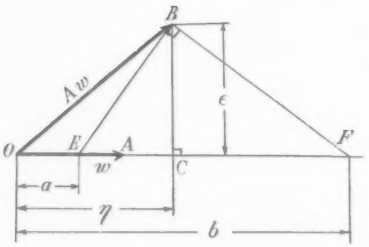

FIG. 3.

Let E and F be two points on the line OA such that $a = OE < OC$ and $\angle EBF = \frac{1}{2}\pi$. Then we get

$$EC.CF = \overline{BC}^2 = \epsilon^2,$$

and

$$OF = OC+CF = \eta+\frac{\epsilon^2}{\eta-a} = b.$$

This is the geometrical meaning of (27), which is already evident from relation (26) if the condition $\angle EBF = \frac{1}{2}\pi$ is taken into consideration.

6. Temple's theorem

Temple (**6**) extended Kato's theorem to the problem with the type

$$Vv = \lambda Tv, \tag{8}$$

namely, to a system with inertial couplings. His theorem may be stated as follows:

Let w be an arbitrary normalized vector, so that $(w, Tw) = 1$, and let ρ and ϵ be defined such that

$$\left.\begin{aligned} \rho &\equiv (w, Vw) \\ R &\equiv Vw-\rho Tw \\ \epsilon_T^2 &\equiv (R, T^{-1}R) \end{aligned}\right\}. \tag{29}$$

Then, for every a such that $a < \rho$, (a, b) contains a point of the spectrum, where b is defined by

$$(b-\rho)(\rho-a) = \epsilon_T^2. \tag{30}$$

Temple's theorem can be represented as in Fig. 4. The geometrical

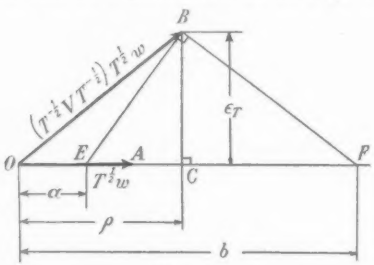

FIG. 4.

relationships are similar to those for Kato's theorem.

7. Kohn's theorem

The main parts of Kohn's theorem (**4**) can be stated as follows:

Some eigenvalue λ_i *lies in the interval,*

$$\alpha-[(A^2)_{\mathrm{av}}-2\alpha A_{\mathrm{av}}+\alpha^2]^{\frac{1}{2}} \leqslant \lambda_i \leqslant \alpha+[(A^2)_{\mathrm{av}}-2\alpha A_{\mathrm{av}}+\alpha^2]^{\frac{1}{2}}. \tag{31}$$

where α *is an arbitrary positive number,*

$$A_{\mathrm{av}} = (w, Aw) \quad \textit{and} \quad (A^2)_{\mathrm{av}} = (w, A^2 w),$$

w being an arbitrary normalized vector.

Now, by transforming (31) into the present notation, we get

$$\alpha-[\epsilon^2+(\alpha-\eta)^2]^{\frac{1}{2}} \leqslant \lambda_i \leqslant \alpha+[\epsilon^2+(\alpha-\eta)^2]^{\frac{1}{2}}. \tag{32}$$

Let us consider the geometrical meaning of (32). Take a point G on the line OA so that $OG = \alpha$, as shown in Fig. 5, and let E and F be two points on the same line on opposite sides of G so that

$$\overline{EG} = \overline{BG} = \overline{GF}. \tag{33}$$

Then the relation (32) states that

$$OE \leqslant \lambda_i \leqslant OF.$$

The equivalence of Figs. 3 and 5 is then easily seen.

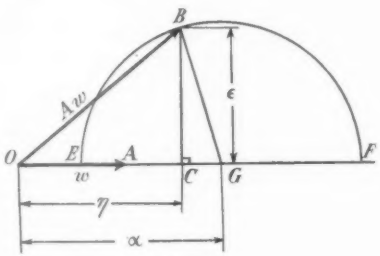

FIG. 5.

A GENERALIZATION OF RAYLEIGH'S PRINCIPLE

8. Matrix function

Consider a rational function in terms of λ such that

$$f(\lambda) = \frac{g(\lambda)}{h(\lambda)}, \tag{34}$$

where

$$g(\lambda) = \alpha_0+\alpha_1\lambda+\ldots+\alpha_m\lambda^m,$$
$$h(\lambda) = \beta_0+\beta_1\lambda+\ldots+\beta_l\lambda^l,$$

and $\alpha_0, \alpha_1, \ldots, \alpha_m, \beta_0, \beta_1, \ldots, \beta_l$ are arbitrary real constants. We can build

a matrix function to correspond to (34) in terms of a real symmetrical matrix A such that

$$f(A) = g(A)[h(A)]^{-1} = [h(A)]^{-1}g(A), \tag{35}$$

where

$$g(A) = \alpha_0 I + \alpha_1 A + \ldots + \alpha_m A^m,$$
$$h(A) = \beta_0 I + \beta_1 A + \ldots + \beta_l A^l,$$

and I is a unit matrix. Then the following theorem is obtained:

If we denote the eigenvalues of A and $f(A)$ by λ_i $(i = 1, 2, \ldots, n)$, and κ_i $(i = 1, 2, \ldots, n)$, respectively, then

$$\kappa_i = f(\lambda_i) \quad (i = 1, 2, \ldots, n). \tag{36}$$

Thus there are correspondences between λ_i and κ_i, although the orders of magnitude and degeneracies are in general completely different.

9. A generalization of Rayleigh's principle

Let us now consider how Rayleigh's principle can be generalized in the case when the matrix A is transformed into $f(A)$. For convenience, let the modified Rayleigh quotient be defined by

$$\lambda_{RM} \equiv \frac{(w, f(A)w)}{(w, w)}. \tag{37}$$

Now let the relation $\kappa = f(\lambda)$ be plotted as shown in Fig. 6, and let the minimum and maximum eigenvalues of $f(A)$ be denoted by κ_p and κ_q, respectively. A generalization of Rayleigh's principle is obtained by applying it to the matrix $f(A)$, giving

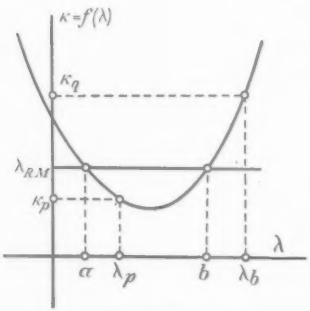

FIG. 6.

$$\kappa_p \leqslant \lambda_{RM} \leqslant \kappa_q. \tag{38}$$

Let us denote the abscissae of the points of intersection of the line $\kappa = \lambda_{RM}$ with the curve $\kappa = f(\lambda)$ by a and b.† Then a geometrical interpretation of the above relation is as follows:

If λ_{RM} is defined by (37) and two points a and b are defined as above, then at least one eigenvalue is contained in the inside and outside of the interval (a, b) respectively:

$$\left.\begin{aligned} &a \leqslant \lambda_p \leqslant b \\ &\text{and } \lambda_q \text{ lies in either } (-\infty, a) \text{ or } (b, +\infty) \end{aligned}\right\}. \tag{39}$$

† For simplicity, we consider a case in which $\kappa = \lambda_{RM}$ and $\kappa = f(\lambda)$ have only two intersection points. It is easy to extend the result (39) to cases with more intersection points.

10. Calculation of λ_{RM}

It is not usually easy to calculate the matrix $[h(A)]^{-1}$ in (35). For calculating λ_{RM} alone, however, the following transformation may be useful. First, let us assume that

$$h(\lambda_i) \quad (i = 1, 2, \ldots, n) \tag{40}$$

are all positive. Since we can find a real vector u such that

$$[h(A)]^{-\frac{1}{2}} w = u,$$

λ_{RM} can be transformed into

$$\lambda_{RM} = \frac{(w, [h(A)]^{-1} g(A) w)}{(w, w)} = \frac{(w, [h(A)]^{-\frac{1}{2}} g(A) [h(A)]^{-\frac{1}{2}} w)}{(w, w)} = \frac{(u, g(A) u)}{(u, h(A) u)}.$$

By writing w in place of u, we obtain

$$\lambda_{RM} = \frac{(w, g(A) w)}{(w, h(A) w)}. \tag{41}$$

Therefore, if assumption (40) holds, then λ_{RM} can be calculated by (41).

If assumption (40) does not hold, then we transform $f(\lambda)$ into

$$f(\lambda) = \frac{h(\lambda) g(\lambda)}{[h(\lambda)]^2}, \tag{42}$$

and by applying (41) we obtain

$$\lambda_{RM} = \frac{(h(A) w, g(A) w)}{(h(A) w, h(A) w)}. \tag{43}$$

The two relations (41) and (43) may prove convenient in practical calculations.

In the following sections it will be shown how the theorems which provide the bounds of eigenvalues can be obtained as special cases of this generalized Rayleigh's principle.

11. Case 1

$f(\lambda) = 1/(\lambda - \alpha)$, *where* α *is an arbitrary real constant.* In this case we have

$$f(A) = (A - \alpha I)^{-1} \tag{44}$$

and

$$\kappa_i = (\lambda_i - \alpha)^{-1} \quad (i = 1, 2, \ldots, n). \tag{45}$$

Let the negative eigenvalues of $A - \alpha I$ be denoted by

$$\lambda_1 - \alpha, \quad \lambda_2 - \alpha, \quad \ldots, \quad \lambda_j - \alpha,$$

and the positive ones by

$$\lambda_{j+1} - \alpha, \quad \ldots, \quad \lambda_n - \alpha,$$

then the eigenvalues of $f(A)$ are arranged in order of their algebraic magnitude, namely

$$\frac{1}{\lambda_j-\alpha},\ \frac{1}{\lambda_{j-1}-\alpha},\ \cdots,\ \frac{1}{\lambda_1-\alpha},\ \frac{1}{\lambda_n-\alpha},\ \cdots,\ \frac{1}{\lambda_{j+1}-\alpha}.$$

Therefore the generalized Rayleigh's principle leads to

$$\frac{1}{\lambda_j-\alpha} \leqslant \lambda_{RM} \leqslant \frac{1}{\lambda_{j+1}-\alpha}, \tag{46}$$

where

$$\lambda_{RM} = \frac{(w,(A-\alpha I)^{-1}w)}{(w,w)}, \tag{47}$$

or

$$\lambda_{RM} = \frac{(w,(A-\alpha I)w)}{((A-\alpha I)w,(A-\alpha I)w)}. \tag{48}$$

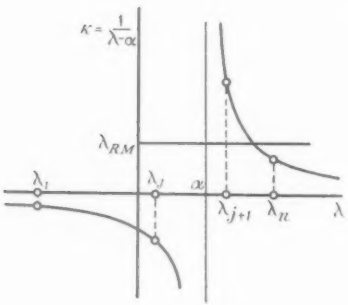

FIG. 7.

12. Case 2

$f(\lambda) = (\lambda-\alpha)^2$, *where* α *is an arbitrary real constant.* In this case we have

$$f(A) = (A-\alpha I)^2 \tag{49}$$

and

$$\kappa_i = (\lambda_i-\alpha)^2 \quad (i = 1, 2, \ldots, n). \tag{50}$$

The generalized Rayleigh's principle asserts that if λ_p and λ_q are defined so that

$$\left.\begin{aligned} \kappa_p &= (\lambda_p-\alpha)^2 \equiv \min(\lambda_i-\alpha)^2 \\ \kappa_q &= (\lambda_q-\alpha)^2 \equiv \max(\lambda_i-\alpha)^2 \end{aligned}\right\}, \tag{51}$$

then

$$(\lambda_p-\alpha)^2 \leqslant \lambda_{RM} \leqslant (\lambda_q-\alpha)^2, \tag{52}$$

where

$$\lambda_{RM} = \frac{(w,(A-\alpha I)^2 w)}{(w,w)}. \tag{53}$$

These relations are shown graphically in Fig. 8, where $\kappa = f(\lambda)$ and $\kappa = \lambda_{RM}$ have only two points of intersection, the abscissae of which are denoted by a and b, respectively. Then we get

$$a \leqslant \lambda_p \leqslant b, \tag{54}$$

and λ_q lies in either $(-\infty, a)$ or $(b, +\infty)$. (55)

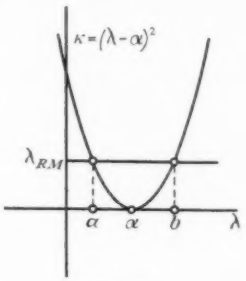

FIG. 8.

In order to calculate a and b, let us define ϵ and η so that

$$\eta \equiv (w, Aw),$$

$$\epsilon^2+\eta^2 \equiv (Aw, Aw),$$

with the normalized condition that $(w, w) = 1$. Then we obtain

$$\begin{aligned} \lambda_{RM} &= \epsilon^2+\eta^2-2\alpha\eta+\alpha^2 \\ &= \epsilon^2+(\alpha-\eta)^2, \end{aligned}$$

and

$$\left.\begin{aligned} a &= \alpha-\sqrt{\{\epsilon^2+(\alpha-\eta)^2\}} \\ b &= \alpha+\sqrt{\{\epsilon^2+(\alpha-\eta)^2\}} \end{aligned}\right\}. \tag{56}$$

It is easily seen that relation (54) combined with (56) is equivalent to Kohn's theorem, which was mentioned in section 7.

13. Case 3

$f(\lambda) = \dfrac{\lambda}{\alpha}+\dfrac{\alpha}{\lambda}$, *where* α *is an arbitrary real constant.* At the outset, let us assume that all the eigenvalues of A, namely, λ_i $(i = 1, 2, \ldots, n)$, and α are positive. In this case we have

$$f(A) = \alpha^{-1}A+\alpha A^{-1} \tag{57}$$

and

$$\kappa_i = \frac{\lambda_i}{\alpha}+\frac{\alpha}{\lambda_i} \quad (i = 1, 2, \ldots, n). \tag{58}$$

All the κ_i are positive and equal to or greater than 2. The generalized Rayleigh's principle asserts that if λ_p and λ_q are defined so that

$$\left.\begin{aligned} \kappa_p &= \frac{\lambda_p}{\alpha}+\frac{\alpha}{\lambda_p} \equiv \min\left\{\frac{\lambda_i}{\alpha}+\frac{\alpha}{\lambda_i}\right\} \\ \kappa_q &= \frac{\lambda_q}{\alpha}+\frac{\alpha}{\lambda_q} \equiv \max\left\{\frac{\lambda_i}{\alpha}+\frac{\alpha}{\lambda_i}\right\} \end{aligned}\right\}, \tag{59}$$

then

$$\frac{\lambda_p}{\alpha}+\frac{\alpha}{\lambda_p} \leqslant \lambda_{RM} \leqslant \frac{\lambda_q}{\alpha}+\frac{\alpha}{\lambda_q}, \tag{60}$$

where
$$\lambda_{RM} = \frac{(w, (\alpha^{-1}A + \alpha A^{-1})w)}{(w, w)}, \tag{61}$$

or
$$\lambda_{RM} = \frac{(Aw, Aw) + \alpha^2(w, w)}{\alpha(w, Aw)}. \tag{62}$$

These relations are shown graphically in Fig. 9, and we get
$$\alpha \leqslant \lambda_p/\alpha \leqslant b, \tag{63}$$

and
$$\lambda_q/\alpha \text{ lies in either } (0, a) \text{ or } (b, +\infty), \tag{64}$$

where
$$a = 1+\delta-\sqrt{(\delta^2+2\delta)},$$
$$b = 1+\delta+\sqrt{(\delta^2+2\delta)}, \tag{65}$$

and
$$\lambda_{RM} \equiv 2(1+\delta), \qquad \delta \geqslant 0.$$

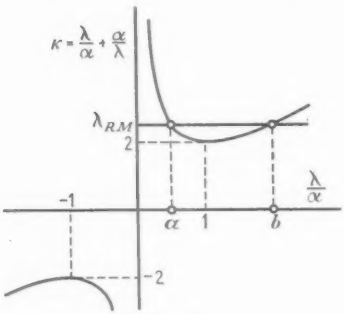

FIG. 9.

Next, let us remove the restriction that λ_i $(i = 1, 2, \ldots, n)$ and α are all positive. Unfortunately no useful criteria for the bounds of the eigenvalues are obtained in this case, as is easily shown in Fig. 9. For example, even if $\delta > 0$ still holds, λ_p/α can lie either in $(-\infty, 0)$ or in (a, b).

14. Case 4

$f(\lambda) = \left(\frac{\lambda}{\alpha} + \frac{\alpha}{\lambda}\right)^{-1} = \frac{\alpha\lambda}{\lambda^2+\alpha^2}$, *where* α *is an arbitrary real constant.* In this case the transformed matrix is
$$f(A) = (\alpha^{-1}A + \alpha A^{-1})^{-1}, \tag{66}$$

and the eigenvalues of $f(A)$ are
$$\kappa_i = \left(\frac{\lambda_i}{\alpha} + \frac{\alpha}{\lambda_i}\right)^{-1} = \frac{\alpha\lambda_i}{\lambda_i^2+\alpha^2} \quad (i = 1, 2, \ldots, n). \tag{67}$$

Clearly, $f(\lambda)$ is an odd function and bounded. Therefore we can expect to have better formulae for bounds than those given in section 13. Now the

generalized Rayleigh's principle asserts that if λ_p and λ_q are defined so that

$$\left.\begin{aligned} \kappa_p &= \frac{\alpha\lambda_p}{\lambda_p^2+\alpha^2} \equiv \min\left\{\frac{\alpha\lambda_i}{\lambda_i^2+\alpha^2}\right\} \\ \kappa_q &= \frac{\alpha\lambda_q}{\lambda_q^2+\alpha^2} \equiv \max\left\{\frac{\alpha\lambda_i}{\lambda_i^2+\alpha^2}\right\} \end{aligned}\right\}, \tag{68}$$

then

$$\frac{\alpha\lambda_p}{\lambda_p^2+\alpha^2} \leqslant \lambda_{RM} \leqslant \frac{\alpha\lambda_q}{\lambda_q^2+\alpha^2}, \tag{69}$$

where

$$\lambda_{RM} = \frac{\alpha(w, Aw)}{\alpha^2(w, w)+(Aw, Aw)}. \tag{70}$$

These relations are shown graphically in Fig. 10.

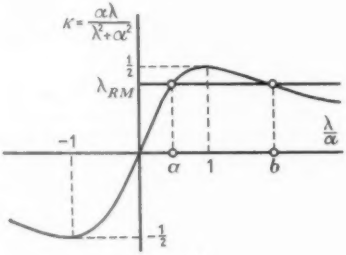

FIG. 10.

Let us define a positive quantity ϵ such that

$$\lambda_{RM} \equiv \frac{1}{2(1+\epsilon)} \qquad \text{when } \lambda_{RM} > 0,$$

$$\equiv -\frac{1}{2(1+\epsilon)} \qquad \text{when } \lambda_{RM} < 0;$$

then, after some reduction, we obtain

(1) If $\lambda_{RM} > 0$, λ_p/α lies in either $(-\infty, a)$ or $(b, +\infty)$ (71)

and

$$a \leqslant \lambda_q/\alpha \leqslant b, \tag{72}$$

where

$$\left.\begin{aligned} a &= 1+\epsilon-\sqrt{(\epsilon^2+2\epsilon)} \\ b &= 1+\epsilon+\sqrt{(\epsilon^2+2\epsilon)} \end{aligned}\right\}. \tag{73}$$

(2) If $\lambda_{RM} < 0$, $$-b \leqslant \lambda_p/\alpha \leqslant -a \tag{74}$$

and λ_q/α lies in either $(-\infty, -b)$ or $(-a, +\infty)$, (75)

where a and b are defined by (73).

It is not difficult to show that (72) and (74) are equivalent to the first restrictive inequality given by Southwell (**8**).

15. Case 5

$f(\lambda) = \left(\frac{\lambda}{\alpha}+\frac{\alpha}{\lambda}\right)^2$, *where* α *is an arbitrary real constant.* The following method presents another case in which the difficulty encountered in section 13 can be removed. In this case the eigenvalues of the transformed matrix $f(A)$ are

$$\kappa_i = \left(\frac{\lambda_i}{\alpha}+\frac{\alpha}{\lambda_i}\right)^2 \quad (i = 1, 2, \ldots, n), \tag{76}$$

and they are all positive and equal to or greater than 4. The generalized Rayleigh's principle asserts that if λ_p and λ_q are defined so that

$$\left.\begin{aligned} \kappa_p &= \left(\frac{\lambda_p}{\alpha}+\frac{\alpha}{\lambda_p}\right)^2 \equiv \min\left\{\left(\frac{\lambda_i}{\alpha}+\frac{\alpha}{\lambda_i}\right)^2\right\} \\ \kappa_q &= \left(\frac{\lambda_q}{\alpha}+\frac{\alpha}{\lambda_q}\right)^2 \equiv \max\left\{\left(\frac{\lambda_i}{\alpha}+\frac{\alpha}{\lambda_i}\right)^2\right\} \end{aligned}\right\}, \tag{77}$$

then

$$\left(\frac{\lambda_p}{\alpha}+\frac{\alpha}{\lambda_p}\right)^2 \leqslant \lambda_{RM} \leqslant \left(\frac{\lambda_q}{\alpha}+\frac{\alpha}{\lambda_q}\right)^2, \tag{78}$$

where

$$\lambda_{RM} = \frac{((A^2+\alpha^2 I)w, (A^2+\alpha^2 I)w)}{\alpha^2(Aw, Aw)}. \tag{79}$$

These relations are shown graphically in Fig. 11, and we get

$$a \leqslant |\lambda_p/\alpha| \leqslant b, \tag{80}$$

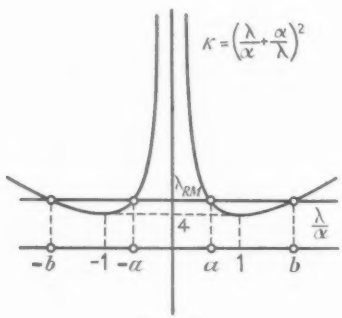

FIG. 11.

where

$$\left.\begin{aligned} a &= 1+\delta-\sqrt{(\delta^2+2\delta)} \\ b &= 1+\delta+\sqrt{(\delta^2+2\delta)} \end{aligned}\right\}, \tag{81}$$

and

$$\lambda_{RM} \equiv 4(1+\delta)^2$$

This is equivalent to the second restrictive inequality given by Southwell (**8**).

16. Final remarks

It has been shown in the latter part of the present paper that several theorems which provide the bounds of eigenvalues can be derived from the generalized Rayleigh's principle. The next problem would be to find the best and the most efficient method for locating the bounds of eigenvalues. In the above discussion all the roots on the real axis in the λ-plane were mapped on the real axis in the κ-plane by the transformation $\kappa = f(\lambda)$. The general theory of transforming λ-plane into κ-plane would be worthy of consideration.

17. Acknowledgements

The author wishes to express his thanks to Sir Richard Southwell and Professor S. H. Crandall for their very helpful discussions about this paper.

REFERENCES

1. L. Collatz, *Eigenwertaufgaben mit technischen Anwendungen* (Leipzig, 1949), Akademische Verlagsgesellschaft, Geest und Portig K.-G.
2. G. Temple and W. G. Bickley, *Rayleigh's Principle and its Application to Engineering* (London, 1933).
3. —— 'The computation of characteristic numbers and characteristic functions', *Proc. London Math. Soc.* **29** (1929), 257–80.
4. W. Kohn, 'A note on Weinstein's variational method', *Phys. Rev.* **71** (1947), 902–4.
5. T. Kato, 'On the upper and lower bounds of eigenvalues', *J. Phys. Soc. Japan*, **4** (1949), 334–9.
6. G. Temple, 'The accuracy of Rayleigh's method of calculating the natural frequencies of vibrating systems', *Proc. Roy. Soc.* A **211** (1952), 204–24.
7. K. Washizu, 'Geometrical representations of bounds of eigenvalues', *J. Japan. Soc. Appl. Mech.* **5** (1952), 29–32.
8. R. V. Southwell, 'Some extension of "Rayleigh's principle" ', *Quart. J. Mech. and Applied Math.* **6** (1953), 257–72.

HEAT TRANSFER FROM A FLAT PLATE THROUGH A TURBULENT BOUNDARY LAYER

By D. R. DAVIES (*University of Sheffield*)

[Received 28 October 1954. Revise received 21 December 1954]

SUMMARY

A similarity solution of the heat transfer equation, suggested by Townsend's recent experiments, is obtained for a turbulent boundary layer overlying a flat semi-infinite heated plate, provided that the temperature difference between the plate and the free stream is small, and an expression is derived describing the mean rate of heat transfer from a section of the plate. The application of this solution requires a knowledge of the observed mean velocity and turbulent shear stress profiles, and is based on the assumption that heat diffusivity is proportional to momentum diffusivity. The measurements made recently by Townsend of mean velocity and turbulent shear stress profiles in flow over a smooth plane wall enable the distribution of temperature in a turbulent boundary layer to be calculated. The theoretical results are compared with temperature measurements made by Elias over a heated flat plate, and the comparison indicates a value in the neighbourhood of 1·0 for the ratio of heat diffusivity to momentum diffusivity.

1. Introduction

RECENT experiments by Townsend (**1**) on the structure of a turbulent boundary layer over a smooth plane wall show that a distance x_0 may be chosen so that the mean velocity and shear stress profiles may be well expressed as functions of the non-dimensional variable $\xi = y/(x_1-x_0)$, where y denotes distance measured perpendicular to the wall and x_1 measures distance along the wall from the wind-tunnel entrance. This similarity property discovered by Townsend over his range of measurements suggests that the associated problem of heat transfer from the wall to the air stream may be solved by an extension of the method developed (**2**, p. 780) in the case of forced convection in a laminar boundary layer on a plate in a uniform stream. The temperatures of the surface of the flat plate, or wall, and free stream are taken to be maintained at constant values T_1 and T_0 respectively, and the temperature difference T_1-T_0 is taken to be sufficiently small to prevent the appearance of buoyancy effects, so that the mean velocity distribution is the same as for isothermal flow.

The experimental results giving the similarity distribution over a smooth, plane wall of mean velocity and turbulent shearing stress enabled Townsend (**1**) to calculate the distribution of the eddy momentum diffusivity or eddy viscosity. Following the Reynolds analogy between heat and momentum

transfer (**2**, p. 819), we then assume that the dependence of the eddy heat diffusivity ϵ_H and the eddy momentum diffusivity ϵ (using Townsend's notation) on the ξ variable are of the same functional form, and we write

$$\epsilon_H = \lambda\epsilon. \tag{1}$$

A formal similarity solution of the ensuing heat diffusion equation for the fully turbulent zone of flow is then obtained. An approximate method of evaluating the flow in the laminar and transition zones near the surface is then used to complete the solution, and formulae describing the distribution over the plane boundary of the mean rate of heat transfer are derived. A numerical solution based on Townsend's observed values of ϵ is discussed in relation to measurements of temperature obtained by Elias (**3**) in a turbulent boundary layer over a smooth flat plate. Comparison of theoretical and experimental temperature distributions indicates a value of λ in the neighbourhood of 1·0.

2. Similarity solution of the heat-transfer equation in the fully turbulent region of flow over a semi-infinite flat plate

Let (U, V) denote components of mean velocity, in a turbulent boundary layer, relative to coordinate axes Ox, in the plane of the plate and parallel to the direction of the free stream, and Oy at right angles to the plate. Then, denoting the mean temperature by T, the thermal diffusivity by κ, and the eddy heat diffusivity by ϵ_H, the equation describing the distribution of temperature as given by Howarth (**2**, p. 821) is

$$U\frac{\partial T}{\partial x} + V\frac{\partial T}{\partial y} = \frac{\partial}{\partial y}\left(\kappa\frac{\partial T}{\partial y} + \epsilon_H\frac{\partial T}{\partial y}\right). \tag{2}$$

The eddy viscosity ϵ in a turbulent boundary layer has been evaluated numerically by Townsend from his observations of shearing stress τ, and defined by the equation $\tau = \epsilon\,\partial U/\partial y$. We find that, except for the extremely thin region in the neighbourhood of the laminar sub-layer, ϵ_H has a considerably larger numerical value than κ, which we therefore ignore in the fully turbulent region of flow. We then write our basic diffusion equation in the form

$$U\frac{\partial T}{\partial x} + V\frac{\partial T}{\partial y} = \lambda\frac{\partial}{\partial y}\left(\epsilon\frac{\partial T}{\partial y}\right), \tag{3}$$

which relates to the mean temperature distribution in the fully turbulent region.

It was discovered by Townsend (**1**) that his experimental results for mean velocity, turbulent shear stress, and turbulent intensity distributions could be expressed as functions of the variable $\xi = yx^{-1}$, where x measures distance from a point 51 cm. beyond the entrance to the working section of

the wind tunnel. It is convenient, however, to obtain first a similarity solution using the more general form

$$\xi = y/(kx^q), \tag{4}$$

where the parameters k and q, and a convenient origin for x, are to be determined from experimental results.

Following the usual Reynolds turbulence technique of taking mean values over a sufficiently long time-interval at a point, the continuity condition for an incompressible fluid applies to the mean flow, i.e.

$$\frac{\partial U}{\partial x}+\frac{\partial V}{\partial y}=0. \tag{5}$$

We then assume the existence of a stream-function ψ in the form

$$\psi = x^r f(\xi), \tag{6}$$

so that

$$U = \frac{\partial \psi}{\partial y} = k^{-1}x^{(r-q)}f'(\xi), \tag{7}$$

and

$$V = -\frac{\partial \psi}{\partial x} = -rx^{r-1}f+qx^{r-1}\xi f', \tag{8}$$

where a prime indicates differentiation with respect to ξ.

Extending Townsend's experimental results, we write

$$\epsilon = KU_0x^ph(\xi), \tag{9}$$

where U_0 is the free stream velocity, and $h(\xi)$ is assumed to be known numerically from experimental results. Townsend finds the values

$$K = p = 1$$

to be convenient, but other values are found to be necessary in discussing the heat-transfer measurements made by Elias. We assume that similarity solutions of equation (3) exist in which T is a function of ξ. We then have

$$\frac{\partial T}{\partial x} = -q\xi x^{-1}T', \qquad \frac{\partial T}{\partial y} = k^{-1}x^{-q}T', \qquad \frac{\partial^2 T}{\partial y^2} = k^{-2}x^{-2q}T'',$$

and equation (3) becomes

$$h'T'+hT'' = -\left(\frac{krf}{K\lambda U_0}\right)T'. \tag{10}$$

This equation is easily integrated to give the formal solution

$$T = A\int_{\xi_*}^{\xi}[h(\xi)]^{-1}\exp\left(-\frac{kr}{K\lambda U_0}\int_{\xi_*}^{\xi}\frac{f(\xi)\,d\xi}{h(\xi)}\right)d\xi + B, \tag{11}$$

where ξ_* corresponds to the lower limit of the fully turbulent region.

If the plate and the free stream are kept at constant temperatures T_1 and

T_0 respectively, and if the temperature at the lower limit $\xi = \xi_*$ of the fully turbulent region is T_1^*, the boundary conditions are

$$T \to T_1 \text{ as } \xi \to 0, \quad T \to T_1^* \text{ as } \xi \to \xi_*, \quad T \to T_0 \text{ as } \xi \to \infty. \tag{12}$$

Using the form (11) and these boundary conditions, the temperature distribution in the fully turbulent region of flow is given formally by

$$\frac{T-T_1^*}{T_0-T_1^*} = \frac{\int_{\xi_*}^{\xi} F(\xi)\, d\xi}{\int_{\xi_*}^{\infty} F(\xi)\, d\xi}, \tag{13}$$

where $$F(\xi) = [h(\xi)]^{-1}\exp\left(-\frac{kr}{K\lambda U_0}\int_{\xi_*}^{\xi}\frac{f(\xi)\, d\xi}{h(\xi)}\right).$$

The parameters k, K, r, q are to be calculated from the experimental results, and $f(\xi)$ obtained from equation (7), when the observed mean velocity profile is known.

An expression for the mean rate of transfer of heat in the fully turbulent region per unit width of a plane section perpendicular to the plate may now be obtained from equation (13) by evaluating the integral

$$Q_*(x) = \rho c_p \int_{y_*}^{\infty} U(T-T_0)\, dy \tag{14}$$

at a given station $x = x_1$, where ρ is the air density, c_p is the specific heat of air, and y_* denotes the lower limit of the fully turbulent zone. Using Townsend's results, we find that the power law $U/U_0 = 1{\cdot}72\xi^{0{\cdot}15}$ fits the experimental results very closely over almost the whole range of ξ. Substituting this result, together with the temperature formula (13), into the flux expression (14) leads to the form

$$Q_*(x) = 1{\cdot}72k\rho c_p U_0(T_1^*-T_0)x^q \int_{\xi_*}^{\infty}\left[1-\left(\int_{\xi_*}^{\xi} F\, d\xi \Big/ \int_{\xi_*}^{\infty} F\, d\xi\right)\right]\xi^{0{\cdot}15}\, d\xi, \tag{15}$$

noting that the mean rate of heat transfer in the fully turbulent region of flow is proportional to x^q.

This quantity may also be evaluated by an alternative method. The upward flux of heat at a point on the lower limit $\xi = \xi_*$ of the fully turbulent zone is given by

$$-\rho c_p \lambda\epsilon\, \partial T/\partial y \quad \text{at } y = y_*, \quad \text{for a given } x.$$

Using equation (13), this expression becomes

$$\frac{K\rho c_p \lambda U_0 (T_1^* - T_0) x^{p-q}}{k \int_{\xi_*}^{\infty} F \, d\xi},$$

and consequently the rate of heat transfer through a length $x = x_1$ of the surface $\xi = \xi_*$ is given by

$$Q_*(x) = \frac{K\rho c_p \lambda U_0 (T_1^* - T_0) x_1^{1+p-q}}{k(1+p-q) \int_{\xi_*}^{\infty} F \, d\xi}. \tag{16}$$

For a consistent diffusion model we see, by comparing expressions (15) and (16), that

$$1+p-q = q, \tag{17}$$

and we note that the proportionality constants involved in expressions (15) and (16) must also agree. We note from equation (7) that, if U is to be a function of ξ, then we must write

$$q = r. \tag{18}$$

Hence, if q is determined from measurements of U/U_0, the values of p and r follow from equations (17) and (18): the values of the parameters k and K are also to be determined from the U/U_0 and ϵ/U_0 measurements.

It is also of interest to note here that, if the measurements of ϵ can be fitted to a simple power law, the temperature distribution may be obtained in terms of tabulated mathematical functions. If $h = a\xi^{\alpha}$ and $U/U_0 = b\xi^{\beta}$, then the function $F(\xi)$ may be written in the form

$$F(\xi) = a^{-1}\xi^{-\alpha} \exp\left\{ -\frac{k^2 r b (\xi^{2+\beta-\alpha} - \xi_*^{2+\beta-\alpha})}{K\lambda a (1+\beta)(2+\beta-\alpha)} \right\},$$

and consequently the temperature distribution function may be expressed in the form

$$\frac{T - T_1^*}{T_0 - T_1^*} = \frac{I\left\{ \frac{k^2 r b \xi^{2+\beta-\alpha}}{K\lambda a(1+\beta)(2+\beta-\alpha)}, \frac{-(1+\beta)}{(2+\beta-\alpha)} \right\} - I\left\{ \frac{k^2 r b \xi_*^{2+\beta-\alpha}}{K\lambda a(1+\beta)(2+\beta-\alpha)}, \frac{-(1+\beta)}{(2+\beta-\alpha)} \right\}}{1 - I\left\{ \frac{k^2 r b \xi_*^{2+\beta-\alpha}}{K\lambda a(1+\beta)(2+\beta-\alpha)}, \frac{-(1+\beta)}{(2+\beta-\alpha)} \right\}}, \tag{19}$$

where the $I(x, p)$ functions are defined and tabulated by Pearson (4).

We now require solutions of equation (2) in the laminar and transition zones of flow very near the surface in order to complete the problem.

However, similarity solutions of equation (2) in terms of the variable $y/(kx^q)$ do not exist, and, moreover, the velocity profile measurements made by Townsend and Elias do not extend into the laminar sub-layer. Consequently, we adopt an approximate method of procedure.

3. An approximate method of treatment of the heat-transfer problem in the laminar and transition zones of flow over a flat plate

Measurements of the mean velocity distribution very near a plane wall (**2**, p. 824) show that the mean velocity forms

$$U/U_\tau = U_\tau y/\nu = y_\tau \quad (y_\tau \leqslant 5) \tag{20}$$

in the laminar sub-layer,

$$U/U_\tau = -3{\cdot}05 + 5\log_e y_\tau \quad (5 \leqslant y_\tau \leqslant 30) \tag{21}$$

in the transition layer, and

$$U/U_\tau = 5{\cdot}5 + 2{\cdot}5\log_e y_\tau \quad (y_\tau \geqslant 30) \tag{22}$$

in the fully turbulent layer, may be used to give a good representation of the dependence of the mean velocity of flow on distance from the wall: U_τ is the 'friction velocity', whose value is determined by fitting the forms (20), (21), and (22) to the measured values of $U(y)$ at a given distance x from the leading edge of the wall, and ν is the kinematic viscosity. The measurements made by Elias and Townsend did not extend into the laminar layer, and we fit equation (22) to the observed values of U at values of y just inside the fully turbulent zone.

Assuming that the shear stress and the vertical heat flux at a point in the laminar and transition layers are independent of y and equal to τ_0 and q_0 respectively, we have (**2**, p. 823)

$$q_0 = \rho c_p U_\tau T_\tau, \tag{23}$$

where T_τ is the 'friction temperature'. At a point on the lower limit of the fully turbulent region this is also given by the present analysis to be

$$q_0 = \frac{K\rho c_p \lambda U_0 (T_1^* - T_0) x_1^{p-q}}{k \int_{\xi_*}^{\infty} F\, d\xi}, \tag{24}$$

at a given station $x = x_1$ from the leading edge.

The temperature at a point in the transition layer is given by the form (**2**, p. 831)

$$\frac{T_1 - T}{T_\tau} = \frac{5}{\lambda}\log_e\left(\frac{\lambda\sigma y_\tau}{5} + 1 - \lambda\sigma\right) + 5\sigma,$$

where σ is the Prandtl number. This becomes

$$\frac{T_1-T_1^*}{T_\tau}=\frac{5}{\lambda}\log_e(5\lambda\sigma+1)+5\sigma, \tag{25}$$

at $y=y_*$. Eliminating T_τ from (23), (24), (25), we obtain

$$\frac{T_1-T_1^*}{T_0-T_1^*}=-\frac{5K\lambda U_0\{(1/\lambda)\log_e(5\lambda\sigma+1)+\sigma\}}{kU_\tau x_1^{q-p}\int_{\xi_*}^{\infty}F\,d\xi}, \tag{26}$$

and finally, using equations (13) and (26), the mean temperature distribution is given by

$$\begin{aligned}\theta(\xi)=\frac{T-T_1}{T_0-T_1}&=\frac{\left(\frac{T-T_1^*}{T_0-T_1^*}\right)-\left(\frac{T_1-T_1^*}{T_0-T_1^*}\right)}{1-\left(\frac{T_1-T_1^*}{T_0-T_1^*}\right)}\\&=\frac{\left(\int_{\xi_*}^{\xi}F\,d\xi\right)\Big/\left(\int_{\xi_*}^{\infty}F\,d\xi\right)+\dfrac{5K\lambda U_0\{(1/\lambda)\log_e(5\lambda\sigma+1)+\sigma\}}{kU_\tau x_1^{q-p}\int_{\xi_*}^{\infty}F\,d\xi}}{1+\dfrac{5K\lambda U_0\{(1/\lambda)\log_e(5\lambda\sigma+1)+\sigma\}}{kU_\tau x_1^{q-p}\int_{\xi_*}^{\infty}F\,d\xi}}.\end{aligned} \tag{27}$$

An expression for the flux of heat through the region from $y=0$ to $y=y_*$ across unit width of a plane section normal to the flat plate, at a distance $x=x_1$, can be obtained from empirical velocity and temperature forms (**2**, p. 831). We find that the contribution to the flux in the transition zone from $y_\tau=5$ to $y_\tau=30$ is given, at $x=x_1$, say, by

$$\begin{aligned}&\rho c_p\int_{5\nu/U_\tau}^{30\nu/U_\tau}U(T-T_0)\,dy\\&\quad=\rho c_\mu(T_1-T_0)U_\tau\int_{5\nu/U_\tau}^{30\nu/U_\tau}\left[-3{\cdot}05+5\log_e\frac{U_\tau y}{\nu}\right]\times\\&\qquad\times\left[1-\frac{(5/\lambda)\log_e\{(\lambda\sigma U_\tau y/5\nu)+1-\lambda\sigma\}+5\sigma}{(5/\lambda)\log_e(5\lambda\sigma+1)+5\sigma+kU_\tau x_1^{q-p}\int_{\xi_*}^{\infty}F\,d\xi}\right]dy,\end{aligned} \tag{28}$$

with a similar result for the flux through the laminar region of flow from $y_\tau=0$ to $y_\tau=5$.

4. A comparison of theoretical and experimental evaluations of temperature distribution above and rate of heat transfer from a heated smooth flat plate into a turbulent boundary layer

Townsend (**1**, Fig. 2) shows that U/U_0 over a smooth plane wall is a function of y/x, x being measured from a point 51 cm. beyond the entrance to the wall, and that ϵ/xU_0 (**1**, Fig. 10) is also a function of y/x, but he gives no temperature measurements with which we can compare theoretical results. Elias (**3**), on the other hand, provides temperature and velocity profiles over a smooth flat plate for various free stream velocities and distances up to 50 cm. from the leading edge of the plate, but gives no measurements from which ϵ could be calculated. In Townsend's experiments the boundary layer is thickened by an obstruction near the entrance, and in the experiments made by Elias the boundary layer is completely laminar in the region near the leading edge, but in both cases the flow is over a smooth flat surface and temperature conditions are such that buoyancy effects are avoided. This suggests that we may extend the values of ϵ obtained by Townsend to the conditions of Elias's experiments and thus enable a quantitative comparison to be made of theoretical and measured temperature distributions.

We shall assume that the effect on the flow in the fully turbulent region due to the presence of a completely laminar layer near the leading edge of the flat plate may be allowed for by writing the similarity variable in the form $y/[k(x-x_0)^q]$, where x denotes the distance from the leading edge of the plate and x_0 denotes the distance of the virtual origin of the fully turbulent region from the leading edge.

We first discuss the results associated with the highest free stream velocity (35 m./sec.) used by Elias, so that any complicating effect due to the presence of a completely laminar region near the leading edge is as small as possible. The mean velocity measurements made by Elias are rather scattered and are not sufficiently numerous to determine exactly the best values of x_0 and q. We find that any value of q between 0·8 and 1·0 could be used with a zero x_0 value to provide a reasonably satisfactory similarity variable, and in order to compute the formal expressions (15), (16), (27), (28) we *choose* a value for q of 0·89 with $x_0 = 0$. The dependence on x of the expression (15) for the flux of heat in the fully turbulent region of flow then agrees with the measured result given by Elias (**3**); in this connexion we also note that a numerical evaluation of expressions (15) and (28) shows that 95 per cent. of the total flux at a given x value takes place in the fully turbulent region of flow. Consequently the contribution to the downwind flux of heat in the laminar and transition zone does not significantly affect the dependence on x of the net result. The numerical value of k is

taken to be 1·02, so that the velocity measurements made by Elias for $x = 20, 30, 40, 50$ cm. at $U_0 = 35$ m./sec. coincide quite well (Fig. 1) with the curve, giving the dependence of U/U_0 on ξ, plotted by Townsend.

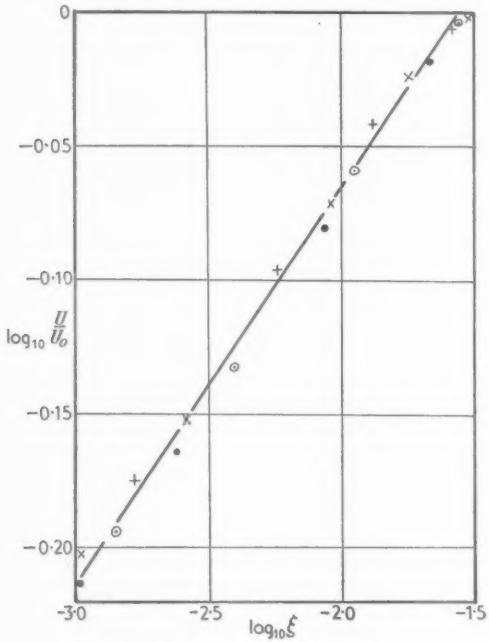

FIG. 1. Mean flow distribution U/U_0, measured by Elias at $U_0 = 35$ m./sec.

+ $x = 20$ cm. from the leading edge of the plate
⊙ $x = 30$ cm. ,, ,, ,, ,, ,, ,, ,,
× $x = 40$ cm. ,, ,, ,, ,, ,, ,, ,,
● $x = 50$ cm. ,, ,, ,, ,, ,, ,, ,,
—— $U/U_0 = 1{\cdot}72\xi^{0{\cdot}15}$

$\xi = y/(1{\cdot}02x^{0{\cdot}89})$, where x is measured from the leading edge of the plate.

The value of the parameter p is now given by equation (17) to be 0·78, and we consequently take $\epsilon/(KU_0x^{0{\cdot}78})$ to be a function of the similarity variable $y/(1{\cdot}02x^{0{\cdot}89})$. We next determine an appropriate K value by comparing with Townsend's work, in which the similarity property was demonstrated by plotting U/U_0 and $\epsilon/[(x-x_0)U_0]$ against $y/(x-x_0)$, the quantities ϵ/U_0 and y being multiplied by the same factor $1/(x-x_0)$. This suggests that we choose the value of K so that the variable $Kx^{0{\cdot}78}$ coincides

numerically as closely as possible with $1{\cdot}02x^{0{\cdot}89}$ over the range of x considered, and we find that the closest numerical agreement for values of x in the range 20 cm. to 50 cm. is obtained with $K = 1{\cdot}54$, the numerical values of $Kx^{0{\cdot}78}$ and $kx^{0{\cdot}89}$ being then within 1 per cent. of each other. Since our choice of k value brings the Elias and Townsend U/U_0 curves into coincidence, we now assume that Townsend's ϵ curve (**1**, Fig. 10) can be applied in the conditions tested by Elias with $\epsilon/(1{\cdot}54U_0x^{0{\cdot}78})$ and $y/(1{\cdot}02x^{0{\cdot}89})$ replacing $\epsilon/[(x-x_0)U_0]$ and $y/(x-x_0)$. The values of $h(\xi)$ given by Townsend are then used in the calculation of the function $F(\xi)$ for $\lambda = 0{\cdot}8$, $1{\cdot}0$, and $1{\cdot}2$, $f(\xi)$ having been obtained by integrating equation (7).

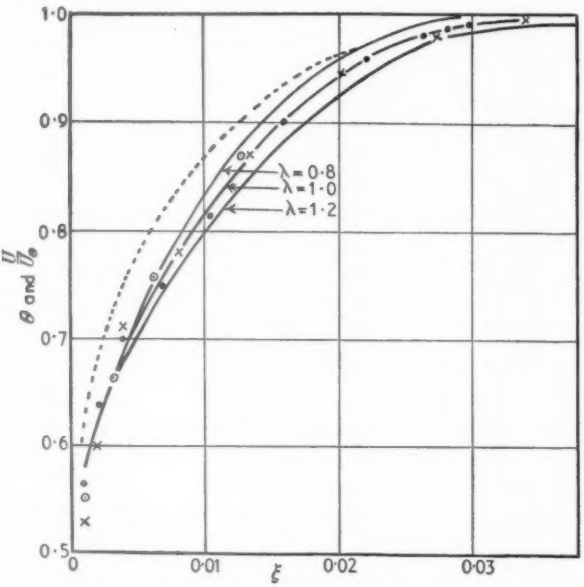

FIG. 2. Theoretical and experimental temperature distributions.

θ distribution measured by Elias:—
⊙ $x = 30$ cm. from the leading edge of the plate
× $x = 40$ cm. " " " " " " "
● $x = 50$ cm. " " " " " " "
—— calculated θ distribution for $\lambda = 0{\cdot}8$, $1{\cdot}0$, $1{\cdot}2$
--- $U/U_0 = 1{\cdot}72\xi^{0{\cdot}15}$

$\xi = y/(1{\cdot}02x^{0{\cdot}89})$, where x is measured from the leading edge of the plate.

The $\theta(\xi)$ function was then computed from equation (27), using appropriate values of U_τ and ξ_* calculated by the method described in section 3 and taking $\sigma = 0{\cdot}72$; the calculation was repeated for values of x between 20 cm. and 50 cm., no significant change being obtained in the theoretical θ values.

The results are shown in Fig. 2, together with the measured values of θ due to Elias (**3**). The theoretical $\theta(\xi)$ curve, based on $\lambda = 1{\cdot}0$, corresponds fairly closely to the measured values, and we infer this value of 1·0 for the important parameter λ, giving the ratio between the heat and momentum diffusivities. We then find that the theoretical net rate of transfer of heat $Q(x)$, obtained by adding the value calculated for $y > y_\tau$ from equation (15), with $\lambda = 1{\cdot}0$, to the value calculated for $y < y_\tau$, is in agreement with the experimental result $Q/(T_1 - T_0) = 0{\cdot}56$ watts per degree centigrade, obtained by Elias for a length $x = 50$ cm., when $U_0 = 35$ m./sec.; we also obtain the same calculated value for $Q(x)$ by adding the value computed from the alternative expression (16) for the flux in the fully turbulent region of flow, $y > y_\tau$, to the value computed for $y < y_\tau$.

Finally, we note that the dependence of the flux of heat on U_0 is given formally by expression (15) or (16), and in order to evaluate this dependence numerically we first need an accurate assessment of the variation of the k parameter with U_0. When $U_0 = 25$ m./sec. or less, the problem is complicated by the presence of an appreciable completely laminar layer extending from the leading edge of the plate: thus at $U_0 = 25$ m./sec. the velocity measurements for $x = 20$, 30, 40, 50 cm. when plotted against $y/(x - x_0)^q$ display the similarity property approximately if we choose values of x_0 between 5 cm. and 8 cm. and values of q of about 0·89. The points are, however, too scattered to determine a reasonably accurate value of x_0 and hence of k, and a similar result is obtained for U_0 values less than 25 m./sec. Elias's measurements are thus not sufficiently accurate to determine numerically the dependence of k and hence of $Q(x - x_0)$ on U_0.

5. Conclusions

In this paper it is shown that a suitable similarity solution exists of the heat diffusion equation in the fully turbulent region of flow in the boundary layer over a flat surface. Using the mean velocity profile measurements given by Elias for flow over a smooth flat plate and extending to flow over a plate the mean shearing stress measurements made by Townsend for flow over a smooth tunnel wall, the theoretical temperature distribution over, and rate of heat transfer from, a section of the plate can be calculated. We obtain the important result that the best agreement between the theoretical and measured temperature distribution is obtained if we assume a value of 1·0 for the ratio, λ, of heat diffusivity to momentum diffusivity, noting that this result is based on the assumption that Townsend's observations of shearing stress near a smooth plane wall may be extended to flow over a smooth flat plate. This is a reasonable assumption, however, as the physical conditions of flow in the two cases are similar, with no buoyancy

effects. The numerical value of the expression obtained for rate of heat transfer from a section of the plate is found to be in good agreement with the value given by Elias.

Acknowledgement

The author is indebted to the referees for their valuable suggestions concerning the revision and extension of an earlier manuscript.

REFERENCES

1. A. A. Townsend, *Proc. Camb. Phil. Soc.* **47** (1951), 375.
2. L. Howarth (Editor), *Modern Developments in Fluid Dynamics* (Oxford, 1953).
3. F. Elias, *Z. angew. Math. Mech.* **10** (1930), 1.
4. K. Pearson, *Tables of the Incomplete Gamma Function* (London: H.M.S.O., 1922).

THE INEXTENSIONAL THEORY FOR THIN FLAT PLATES

By E. H. MANSFIELD† (*Royal Aircraft Establishment, Farnborough*)

[Received 7 May 1954]

SUMMARY

This paper presents the *inextensional* theory for thin flat plates. The theory is applicable to cantilever and other plates subjected to a normal loading which is resisted primarily by the flexural rigidity of the plate rather than by the extensional rigidity. The middle surface of the plate is assumed to be inextensional so that the mode of deformation is a developable surface.

1. Introduction

In considering the behaviour of flat plates subject to normal loading it has been customary to use the classical small-deflexion theory. It can be shown, however, that for thin plates the small-deflexion theory soon breaks down and should be replaced by the von Kármán large-deflexion equations (1) which incorporate the effects of the induced middle surface forces and strains. These equations are almost intractable, but for two types of problem the equations may be appreciably simplified.

The first type of problem is characterized by the fact that the plate is supported along the boundaries so that the load tends to be taken to an increasing extent by the middle surface forces. A typical example of this first type is a rectangular plate supported along its edges and subject to, say, a uniformly distributed load. Such problems may be simplified by taking the flexural rigidity equal to zero, though the resulting equations, first derived by A. Föppl (**2**), are still difficult to solve. The equations are, of course, non-linear because the deflexion is not proportional to the load.

The second type of problem, which is considered in detail here, is characterized by the fact that the plate acts as a cantilever, being clamped along one straight boundary and free along the others. The plate tends to resist the applied loading by its flexural rigidity only; and because of the boundary conditions the middle surface forces play an insignificant part in resisting the load. A simplifying assumption which can now be made is that the middle surface strains are zero, and because of this the simplified theory will be called the *inextensional* theory since the middle surface is

† Acknowledgement is made to the Chief Scientist, Ministry of Supply, for permission to publish this paper.

inextensional. One of the differential equations for the deflexion of the plate then reduces to

$$\left(\frac{\partial^2 w}{\partial x \partial y}\right)^2 - \frac{\partial^2 w}{\partial x^2}\frac{\partial^2 w}{\partial y^2} = 0.$$

This equation expresses the fact that the surface is a developable surface; this follows from the fact that the middle surface is inextensional. The equation does not, however, prove very useful *per se* as a starting-point for solving a particular problem. It is better to start from the fact that the surface is a developable surface and to determine the generators of the surface from considerations of strain energy. It will be shown that a plate problem then reduces to the solution of a one-dimensional non-linear differential equation of the second order. Alternatively, the theory may be coupled with an energy technique to give an approximate solution. It will be shown too that because the sum of two developable surfaces with different generators is not itself a developable surface, the principle of superposition for different load systems is not generally valid, but for any one given type of loading the deflexion is proportional to the load. Examples of plate problems to which the *inextensional* theory is applicable and which cannot be classed as cantilevers include: (*a*) a square plate loaded by concentrated forces at the corners, which deforms cylindrically with the generators parallel to a diagonal and does not take up the form of the saddle which small-deflexion theory would predict; (*b*) a strip under end moment; it can be readily shown (**3**) that the anticlastic curvature predicted by small-deflexion theory has but a fleeting existence in reality; (*c*) a shallow truncated cone formed from an originally flat sheet bounded by radii and arcs of concentric circles. This last case differs from the preceding ones in that the generators are not parallel but all meet at the apex of the cone. When we come to consider the general problem of the bending of thin plates it must be realized that if adjacent generators intersect, the sheet bounded by these generators will form part of a conical surface, but the 'radius' of the cone and its 'curvature' may vary continuously over the whole plate. The locus of the cone centres i the 'edge of regression' of the developable surface (**4**).

2. List of symbols

x distance along reference axis; a *dash* denotes differentiation with respect to x

α angle made by a generator with the x-axis

η distance measured along a generator from an elemental cone apex

η_x value of η at the x-axis

η_1, η_2 values of η at the plate boundaries

M_η moment per unit length about a generator
M_α total moment about the α-generator
t thickness of plate
D_η flexural rigidity of plate at distance η along a generator, $Et^3/12(1-\nu^2)$
ε constant introduced in equation (2)
U strain energy
F $F(\alpha, x, x')$, integrand in square brackets in equation (4)
σ outer fibre stress
F_x $\partial F/\partial x$, where F is regarded as a function of independent variables α, x, x'; similarly for other suffixes
ρ η_2/η_1
μ $\rho-1$
w width of strip
M applied moment
P applied load

3. Outline of the inextensional theory

The method of solution will now be given to the problem of a thin cantilever plate of variable thickness under an arbitrary loading normal to the plane of the plate. The mode of deformation is a developable surface and attention is given to the determination of the directions of the generators of this developable surface. An arbitrary distribution for the generators is assumed and the strain energy stored in the plate is then determined. The correct distribution is to be determined from the condition that the strain energy is a maximum.

Consider the cantilever plate shown in Fig. 1. Let two adjacent generators making angles α and $\alpha+d\alpha$ with the x-axis intersect at the point H so that the elemental strip $KLL'K'$ forms part of a conical surface whose apex is at H. From geometrical considerations the distance along the generator from the apex H to the x-axis is given by

$$\eta_x = x' \sin\alpha. \tag{1}$$

3.1. Equilibrium

An equilibrium condition will now be formed by taking moments about a generator, for then the component due to the unknown middle surface forces vanishes. The moment resisted by the element $d\eta$ is $M_\eta\, d\eta$ and the total moment about the α-generator is therefore

$$\int_{\eta_1}^{\eta_2} M_\eta\, d\eta.$$

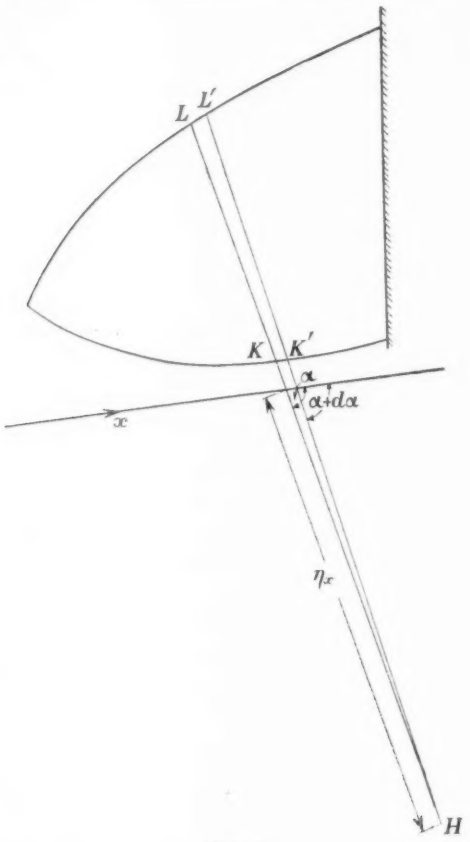

FIG. 1.

But from the conical properties of the strip the radius of curvature normal to the generator is proportional to the distance from the apex, so that

$$\frac{\eta M_\eta}{D_\eta} = c, \text{ say}, \tag{2}$$

where c is to be determined from the equilibrium condition, namely

$$\left.\begin{aligned} \int_{\eta_1}^{\eta_2} M_\eta \, d\eta &= c \int_{\eta_1}^{\eta_2} \frac{D_\eta}{\eta} \, d\eta \\ &= M_\alpha \end{aligned}\right\}, \tag{3}$$

the moment of the applied loads.

3.2. Strain energy

In calculating the strain energy in the plate it is convenient to integrate first over elemental strips bounded by generators, and then to integrate with respect to α. Thus

$$U = \tfrac{1}{2}\int\int_{\eta_1}^{\eta_2} \frac{M_\eta^2}{D_\eta}\,\eta\,d\eta\,d\alpha = \frac{1}{2}\int \left[M_\alpha^2 \Big/ \left\{\int_{\eta_1}^{\eta_2} (D_\eta/\eta)\,d\eta\right\}\right] d\alpha \tag{4}$$

from equations (2) and (3).

Now η_1 and η_2 are known in terms of α, x, and η_x, so that by virtue of equation (1) the integrand in square brackets above is a known function of α, x, x' and the applied loading. For a given loading we can therefore write

$$U = \tfrac{1}{2}\int F(\alpha, x, x')\,d\alpha, \text{ say,} \tag{5}$$

where the integration is over the whole plate.

The relation between x and α is to be determined from the condition that the strain energy U is a maximum. This condition may be expressed as a non-linear, second-order differential equation for x:

$$x''F_{x'x'} + x'F_{xx'} + F_{\alpha x'} - F_x = 0. \tag{6}$$

The derivation of equation (6) from the condition that expression (5) is a maximum is a result of the calculus of variations (**5**). In equation (6) F_x for example, stands for $\partial F/\partial x$, where F is formally regarded as a function of independent variables α, x, x'. Equation (6) is the differential equation for determining the distribution of the generators of the developable surface to which the plate deforms, but since the shape and thickness of the plate and the applied loading all enter into the equation, no further progress can be made in integrating it unless an actual plate and a definite applied loading is considered. Let us consider, therefore, a simple example, yet one apparently that classical small-deflexion theory has not yet solved.

4. Examples

4.1. Swept plate of uniform thickness

Consider a long strip one end of which is built-in at an angle α_0 as shown in Fig. 2. We require the stress distribution when a pure moment is applied at the far end.

If we take moments about a typical generator, we find

$$M_\alpha = M\sin\alpha, \tag{7}$$

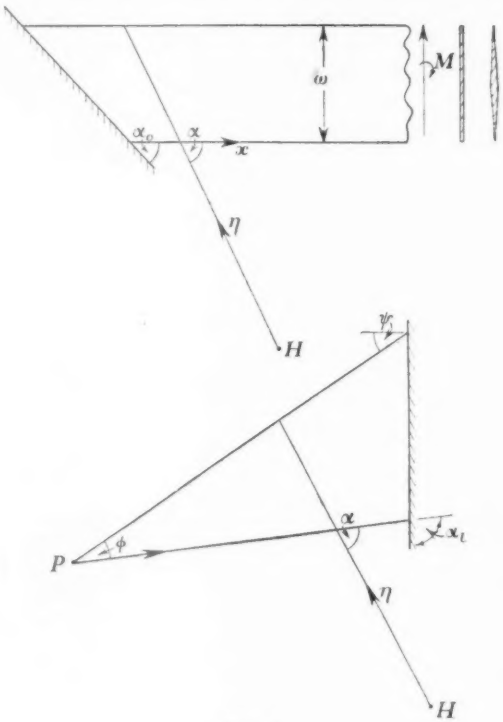

FIG. 2.

while from geometrical considerations and equation (1) we have

$$\left.\begin{aligned} \eta_1 &= x' \sin\alpha \\ \eta_2 &= \eta_1 + w \operatorname{cosec}\alpha \end{aligned}\right\}. \tag{8}$$

Thus from the definition of F we find

$$\begin{aligned} F(\alpha, x, x') &= \frac{M_x^2}{\int_{\eta_1}^{\eta_2} (D_\eta/\eta)\, d\eta} \\ &= \frac{M^2 \sin^2\alpha}{D \log(\eta_2/\eta_1)} \quad \text{(since we have assumed } D \text{ constant)} \\ &\propto \frac{\sin^2\alpha}{\log\left(1 + \dfrac{w \operatorname{cosec}^2\alpha}{x'}\right)}, \end{aligned} \tag{9}$$

and because this expression does not contain the term x, it will be found that equation (6) may be integrated once to give

$$F_{x'} = \text{a constant},$$

whence
$$x'^2\left\{1+\frac{w\,\mathrm{cosec}^2\alpha}{x'}\right\}\left[\log\left\{1+\frac{w\,\mathrm{cosec}^2\alpha}{x'}\right\}\right]^2 = K_1. \tag{10}$$

The constant K_1 may be determined from the boundary condition that, for large x, α tends to $\frac{1}{2}\pi$ and x' tends to infinity, so that on taking the limit

$$K_1 = w^2. \tag{11}$$

The further integration of equation (10) is best done graphically. If we introduce a parameter ρ equal to η_2/η_1 we can obtain a parametric relationship between α and x', namely

$$\left.\begin{aligned} \frac{x'}{w} &= \frac{1}{\sqrt{\rho}\log\rho} \\ \text{and} \qquad \alpha &= \sin^{-1}\left[\frac{\sqrt{\rho}\log\rho}{\rho-1}\right]^{\frac{1}{2}} \end{aligned}\right\}, \tag{12}$$

and x will then be given by the relation

$$x = \int x'\,d\alpha.$$

Once the (α, x) relationship has been determined the generators of the deflected surface may be drawn, as, for instance, in Fig. 3, where they have been drawn at 5° intervals.

4.1.1. **Stress distribution in the plate.** In general, once the distribution of generators over the plate has been found the stresses may be found readily from equations (1), (2), (3) and from the fact that

$$\sigma = \frac{6M_\eta}{t^2}. \tag{13}$$

The stresses so found are principal stresses and will be directed at right angles to the generators. The stresses in the direction of the generators will be ν times those given by equation (13), owing to the fact that the generator lines remain straight.

For the particular problem of the swept plate under a pure moment the outer fibre stresses some way from the root assume a constant direction and a magnitude given by

$$\sigma_\infty = \frac{6M}{wt^2}, \tag{14}$$

and it is convenient to regard this stress as our unit, so that the stresses elsewhere in the plate will be numerically the same as a stress concentration factor, and can therefore be more readily appreciated.

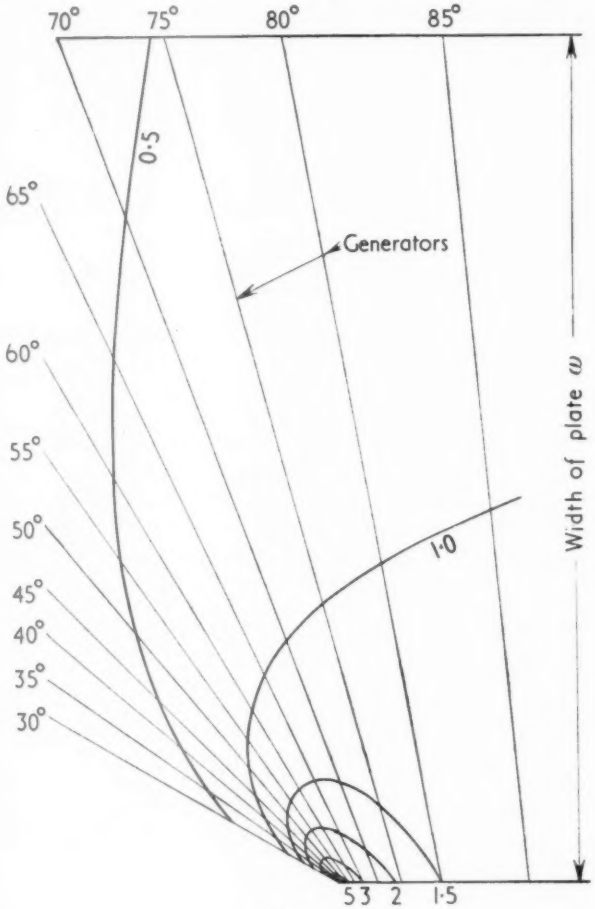

FIG. 3.

From equation (3) we have, on simplifying,

$$c = \frac{M \sin \alpha}{D \log \rho},$$

so that from equation (2)

$$\frac{\sigma}{\sigma_\infty} = \frac{M_\eta}{M/w} = \frac{w \sin \alpha}{\eta \log \rho}$$

$$= \frac{w \sin \alpha}{\{x' \sin \alpha + (\eta - \eta_1)\} \log \rho}; \qquad (15)$$

and all expressions occurring here are known from geometrical or other

considerations. The maximum stress in the plate occurs at the junction of the trailing edge and the built-in edge (where $\alpha = \alpha_0$ and $\eta = \eta_1$). Taking σ_∞ as unity, it will be found that the maximum stress is given by

$$\sigma = \sqrt{\rho},$$

so that from equation (12) the maximum stress is related to the building-in angle α_0 by the formula:

$$\alpha_0 = \sin^{-1}\left[\frac{2\sigma \log \sigma}{\sigma^2 - 1}\right]^{\frac{1}{2}}. \tag{16}$$

Some values of α_0 are given in the table below:

α_0	90°	80°	65°	55°	45°	30°
σ	1·00	1·50	3·00	5·00	8·8	26

It will be seen that as α_0 decreases σ increases rapidly, but as will be seen from Fig. 3, where contours of σ over the whole plate have been drawn, these high stress values tend to be very localized; for example, when α_0 is 55° the peak stress value of 5 has dropped to 3 in a distance of $0{\cdot}035w$. This type of phenomenon is, of course, characteristic of stress concentration problems in general.

In considering Fig. 3 it is important to note that since a generator remains straight it may be regarded as clamped so that any one of them may be regarded as a built-in root. Thus we have obtained the solution for the swept plate built-in at an angle α_0. For example, if α_0 is actually 45°, our solution is represented by the plate to the right of the 45°-generator in Fig. 3; we simply ignore the additional information contained in the rest of the figure. The fact that a whole class of problems of cantilevered plates can be solved in a single analysis is an important and useful characteristic of the *inextensional* theory.

4.2. Swept plate of varying thickness

The plate considered in the example above was of constant thickness, but the analysis is not necessarily over-complicated when the plate thickness varies. We can illustrate this by outlining the analysis for the same problem except that a cross-section of the plate is now diamond-shaped, being of thickness t at the mid-chord and tapering uniformly to zero at the leading and trailing edges.

Equations (7) and (8) will be the same since they depend on the loading and geometry. Along a generator the thickness varies linearly from zero at $\eta = \eta_1$ to t at $\eta = \frac{1}{2}(\eta_1 + \eta_2)$ and then linearly to zero at $\eta = \eta_2$. Now the

flexural rigidity varies as t^3, so that along a generator the flexural rigidity varies as follows:

$$\left.\begin{aligned} &\text{for} \quad \eta_1 < \eta < \tfrac{1}{2}(\eta_1+\eta_2) \text{ we have } 8D\left\{\frac{\eta-\eta_1}{\eta_2-\eta_1}\right\}^3 \\ &\text{for} \quad \tfrac{1}{2}(\eta_1+\eta_2) < \eta < \eta_2 \text{ we have } 8D\left\{\frac{\eta_2-\eta}{\eta_2-\eta_1}\right\}^3 \end{aligned}\right\}. \tag{17}$$

The term $\int_{\eta_1}^{\eta_2} \frac{D_\eta}{\eta}\, d\eta$ occurring in equations (4) and (9) therefore becomes

$$\frac{8D}{(\eta_2-\eta_1)^3}\left[\int_{\eta_1}^{\frac{1}{2}(\eta_1+\eta_2)} \frac{(\eta-\eta_1)^3}{\eta}\, d\eta + \int_{\frac{1}{2}(\eta_1+\eta_2)}^{\eta_2} \frac{(\eta_2-\eta)^3}{\eta}\, d\eta\right],$$

which reduces to

$$\frac{8D}{(\eta_2-\eta_1)^3}\left\{\eta_2^3 \log\left(\frac{2\eta_2}{\eta_1+\eta_2}\right) - \eta_1^3 \log\left(\frac{\eta_1+\eta_2}{2\eta_1}\right)\right\} - \frac{5D(\eta_1+\eta_2)}{\eta_2-\eta_1}, \tag{18}$$

and the function F is finally determined by the equation

$$\frac{M^2w^3}{8DF\sin^4\alpha} = (2\zeta+x')^3 \log\left(\frac{2\zeta+x'}{\zeta+x'}\right) - x'^3 \log\left(\frac{\zeta+x'}{x'}\right) - 5\zeta^2(\zeta+x') \tag{19}$$

$$= \chi, \text{ say,}$$

where $$\zeta = \tfrac{1}{2}w \operatorname{cosec}^2\alpha.$$

Equation (19) does not contain the term x, so that, as in the previous case, the differential equation for the generators integrates once to become

$$F_{x'} = \text{a constant},$$

whence

$$(2\zeta+x')^2 \log(2\zeta+x') + x'^2 \log x' - 2\{2\zeta^2+2\zeta x'+x'^2\}\log(\zeta+x') - 3\zeta^2 = K_2 \sin^4\alpha\, \chi^2, \tag{20}$$

and, for the same boundary condition as before, we find, after some algebra, that

$$K_2 = -\frac{32}{3w^4}. \tag{21}$$

Though equation (20) is fairly involved, the relation between x' and ζ (and hence x' and α) can obviously be found by graphical and numerical methods, and the final calculation for the stresses then follows a similar course to that of the first example.

4.3. Triangular cantilever plate under a tip load

The plate with a typical generator is shown in Fig. 2. This example has been chosen because the resulting differential equation for the generators is of the second order in x and α, and a different technique is needed for its solution.

Taking moments about a typical generator gives

$$M_\alpha = Px\sin\alpha, \tag{22}$$

while from geometrical considerations

$$\left.\begin{aligned}\eta_1 &= x'\sin\alpha\\ \eta_2 &= \eta_1 + \frac{x\sin\phi}{\sin(\alpha+\phi)}\end{aligned}\right\}, \tag{23}$$

so that for a plate of uniform thickness we have

$$F = \frac{P^2x^2\sin^2\alpha}{D\log\left\{1+\dfrac{x\sin\phi}{x'\sin\alpha\sin(\alpha+\phi)}\right\}}. \tag{24}$$

Substituting equation (24) in equation (6), we have an equation of the second order in x and α, but it may be written in the form

$$\frac{d\beta}{d\mu} = \frac{\cos\phi+\cos 2\beta}{\sin\phi\left\{\dfrac{N\sin 2\beta}{\mu\sin\phi}-2Q\right\}}, \tag{25}$$

where

$$\left.\begin{aligned}N &= \frac{4\mu^2(1+\mu)\log(1+\mu)}{(2+\mu)\log(1+\mu)-2\mu}\\ Q &= \frac{(1+\mu)\log(1+\mu)\left\{2+\mu-\dfrac{2(1+\mu)}{\mu}\log(1+\mu)\right\}}{(2+\mu)\log(1+\mu)-2\mu}\end{aligned}\right\}, \tag{26}$$

$$\mu = \frac{2x\sin\phi}{x'(\cos\phi+\cos 2\beta)} = \frac{\eta_2-\eta_1}{\eta_1}, \tag{27}$$

$$\beta = \alpha - \tfrac{1}{2}(\pi-\phi). \tag{28}$$

The advantage of introducing the function μ is that the differential equation relating μ and β is of the first order. The angle β has been introduced so that the boundary condition at the tip reduces to

$$\beta = 0 \quad \text{at} \quad \mu = 0. \tag{29}$$

The method of integration of equation (25) subject to condition (29) will be given shortly. It will be seen that this primary integration is the only real difficulty since, when the relationship between μ and β is determined, the formal solution for x and β is straightforward: from equation (27)

$$\frac{x'}{x} = \frac{2\sin\phi}{\mu(\cos\phi+\cos 2\beta)}, \tag{30}$$

which may be integrated to give

$$x = C\exp\left\{\int_0^\beta \frac{2\sin\phi\, d\beta}{\mu(\cos\phi + \cos 2\beta)}\right\}. \tag{31}$$

The method of integration of equation (25) is a combination of exact analysis and numerical step-by-step and trial-and-error methods.

When the limit is taken of equation (25) as μ and β tend to zero, it is found that

$$\left(\frac{d\beta}{d\mu}\right)_0 = \sin\phi\left\{\frac{1+\sqrt{(7+6\cot^2\tfrac{1}{2}\phi)}}{24}\right\}$$

$$= \gamma, \text{ say.} \tag{32}$$

A step-by-step integration of equation (25) now proceeds as follows. A small value for μ is chosen, say 0·1, and a corresponding approximate value of β (i.e. $0{\cdot}1\gamma$) determined from equation (32). Substitution in equation (25) yields $(d\beta/d\mu)_{0\cdot1}$. The value of β at $\mu = 0{\cdot}1$ may then be revised by trial and error until

$$(\beta)_{0\cdot1} \approx \frac{0{\cdot}1}{2}\left\{\gamma + \left(\frac{d\beta}{d\mu}\right)_{0\cdot1}\right\}. \tag{33}$$

The value of β at $\mu = 0{\cdot}2$ may be determined approximately from the equation

$$(\beta)_{0\cdot2} \approx (\beta)_{0\cdot1} + \frac{0{\cdot}1}{2}\left\{\left(\frac{d\beta}{d\mu}\right)_{0\cdot1} + \left(\frac{d\beta}{d\mu}\right)_{0\cdot2}\right\}, \tag{34}$$

in which $(d\beta/d\mu)_{0\cdot2}$ is obtained approximately by extrapolation from $(d\beta/d\mu)_0$ and $(d\beta/d\mu)_{0\cdot1}$. A revised value of $(d\beta/d\mu)_{0\cdot2}$ may now be obtained from equation (25) and thence a revised value of $(\beta)_{0\cdot2}$ from equation (34). Further values are found in a similar manner.

When the above calculations are completed there is a known relationship between μ and β, and from equation (30) we can regard x'/x as a known function of β. Now the expressions in equation (30) tend to infinity as β tends to zero and it is necessary to introduce $T(\beta)$ such that

$$T(\beta) = \frac{2\gamma\tan\tfrac{1}{2}\phi}{\beta} - \frac{2\sin\phi}{\mu(\cos\phi + \cos 2\beta)}, \tag{35}$$

which is finite as β tends to zero.

Equation (30) now becomes

$$\frac{x'}{x} = \frac{2\gamma\tan\tfrac{1}{2}\phi}{\beta} - T(\beta), \tag{36}$$

which may be integrated in the usual manner.

The limiting value $T(0)$ cannot be obtained numerically from equation

(35) and must be found as follows. Differentiating equation (25) and taking the limit as β tends to zero, it will be found that

$$\left(\frac{d^2\beta}{d\mu^2}\right)_0 = -\gamma, \tag{37}$$

and taking the limit of equation (35) gives

$$T(0) = -\frac{1}{\gamma}\left(\frac{d^2\beta}{d\mu^2}\right)_0 \tan\tfrac{1}{2}\phi = \tan\tfrac{1}{2}\phi. \tag{38}$$

Equation (37) may be used to give a more refined version of equation (33), i.e.

$$(\beta)_{0\cdot1} \approx \frac{0\cdot1}{3}\left\{2\left(\frac{d\beta}{d\mu}\right)_0 + \left(\frac{d\beta}{d\mu}\right)_{0\cdot1} + \frac{0\cdot1}{2}\left(\frac{d^2\beta}{d\mu^2}\right)_0\right\}. \tag{39}$$

The distribution of generators and principal stresses is shown in Fig. 4 for the case where ϕ is 60°. The solution obtained applies to the complete range of sweep-back angles ψ.

4.4. Triangular cantilever plate under a uniformly distributed load

The analysis for this case is almost identical with the previous case except that in equation (25) the expression $-2Q$ becomes $-6Q$. Solutions for triangular plates are given in greater detail in (**6**) and (**7**).

5. Verification of the theory

It would be ideal if the results of this *inextensional* theory could be compared with a number of exact solutions of cantilever plate problems. The only such problem for which an exact solution is known is the rather trivial case of a long strip under pure moment. For this problem it is found that the *inextensional* theory is appreciably more accurate than small-deflexion theory if the loading is such that

$$\left(\frac{w}{t}\right)^2 \frac{\sigma}{E} > 3, \tag{40}$$

and as the loading is further increased the results of the *inextensional* theory approach asymptotically those of exact theory. To fix ideas as to the numerical magnitude of the parameter in equation (40) it will be noted that, if w/t is 100 and σ/E is 0·004,

$$\left(\frac{w}{t}\right)^2 \frac{\sigma}{E} = 40,$$

which is well in excess of 3.

As a practical check on the adequacy of the *inextensional* theory a series of experiments was carried out and in all cases agreement with the theory was good. The first experiment was a check on the tip deflexions of six

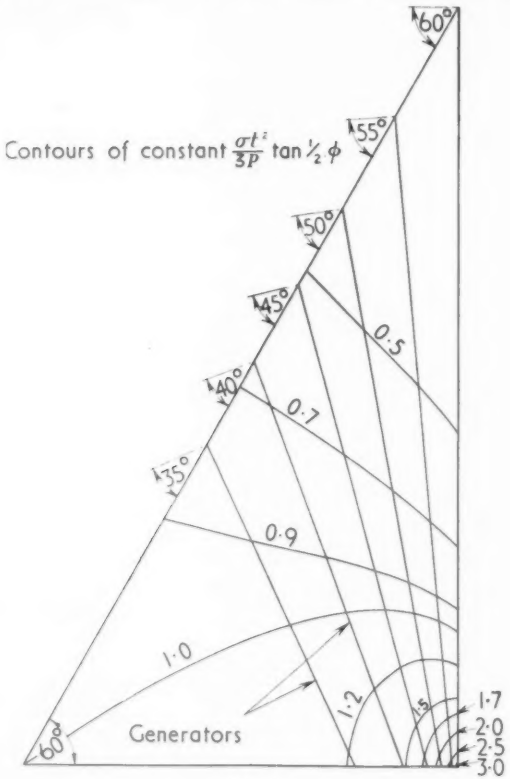

FIG. 4.

right-angled triangular plates, clamped at different angles along the hypotenuse. In all cases the load-deflexion relation was sensibly linear, although the deflexions were about 1–2 per cent. greater than those predicted by the *inextensional* theory. The second experiment was a check on the distribution of the generators for a triangular plate of angles 90°, 70°, 20° clamped along its hypotenuse. The plate was loaded at the tip and the compression surface painted with a strain lacquer. When the load was removed cracks appeared in the strain lacquer along lines of principal strain. According to the *inextensional* theory these lines should be straight and should coincide with the generators. Agreement was generally good except in the region of the 20° corner, where the stresses would be small and small-deflexion conditions would tend to prevail. In the third experiment loads were applied at the tips of five cantilever equilateral triangular plates with different t/w ratios. The smallest value of t/w tested was 0·0025

and agreement with the *inextensional* theory was apparently exact over the complete range of loading. With higher values of t/w it was possible to detect an initial decrease of about 20 per cent. in the stiffness of the plate under small loads. As the loading increased the stiffness rapidly assumed the value predicted by the *inextensional* theory. In all these experiments the plates were cantilevers and the difference between the *inextensional* theory and small-deflexion theory would be small.

6. Conclusions

A simplified large-deflexion theory has been presented for thin plates subjected to normal loading. This *inextensional* theory is applicable to plates in which the loading is resisted primarily by the flexural rigidity of the plate. In the theory the solution of a plate problem reduces to the solution of a one-dimensional non-linear differential equation of the second order. Alternatively, the theory may be coupled with an energy technique to give an approximate solution. The principle of superposition is not valid for different load systems, although for any given type of loading the deflexion is proportional to the load. For thin cantilever plates under very low loads the difference between results obtained from small-deflexion theory and from the *inextensional* theory is not large; for higher loads the results obtained from the *inextensional* theory approach asymptotically those obtained from large-deflexion theory.

REFERENCES

1. T. von Kármán, *Encyklopädie der mathematischen Wissenschaften*, **4** (1910), 349.
2. A. Föppl, *Vorlesungen über technische Mechanik*, **5** (1907), 132.
3. H. Lamb, 'On the flexure of a flat elastic spring', *Phil. Mag.* **31** (1891), 182-8.
4. Lord Kelvin and P. G. Tait, *Treatise on Natural Philosophy*, Part I, chap. I § 148 (Cambridge, 1912).
5. H. and B. S. Jeffreys, *Methods of Mathematical Physics*, chap. 10 (Cambridge, 1946).
6. E. H. Mansfield and P. W. Kleeman, 'A large-deflexion theory for thin plates' *Aircraft Engineering* (to be published).
7. —— —— 'Stress analysis of triangular cantilever plates' ibid. (to be published).

THE EQUIVALENCE OF CONTINUOUS AND DISCRETE MASS DISTRIBUTIONS IN CERTAIN VIBRATION PROBLEMS

By R. K. LIVESLEY

(*Computing Machine Laboratory, University of Manchester*)

[Received 21 October 1954]

SUMMARY

Several numerical methods for determining the natural frequencies of non-uniform shafts in torsional and transverse vibration require the replacement of any continuous distribution of matter by an 'equivalent system', in which the mass or inertia is concentrated at particular points. This paper discusses the error introduced by this process by considering a few simple cases, in which both the continuous and the discrete systems can be treated exactly. Following a brief statement of the results obtained by previous authors, an expression is derived for the frequency error in the case of a uniform simply supported beam in transverse vibration. It is shown that if the continuous mass distribution of the beam is replaced by a set of equally spaced concentrated masses, the errors in the natural frequencies are proportional to the inverse fourth power of the number of segments into which the beam is divided.

1. Introduction

ENGINEERING design work often requires an investigation of the transverse or torsional vibrations of a straight non-uniform beam or shaft. In most cases attention is concentrated on the values of the natural frequencies, the precise nature of the associated modes being of less importance. In a steam turbine, for instance, it is essential that the critical frequencies of the rotor assembly should be outside the normal range of running speeds, but the actual modes of the vibrations which occur are rarely of interest.

The various schemes of numerical analysis which are available may be classified according to the way in which the displacement of the shaft is specified. In the first group the displacement is represented by a linear combination of certain independent arbitrary functions, the latter being chosen so as to satisfy the boundary conditions. The methods of Ritz (1, p. 370) and Galerkin (2) are examples of this approach. In the second group the problem is reduced to one with a finite number of degrees of freedom by the introduction of an 'equivalent system' of concentrated masses and inertias. The motion of the shaft is then treated entirely in terms of the displacements of these mass points. This idealization is required

in the method of analysing torsional vibrations named after Holzer (1, p. 261), and also in the extension devised by Prohl (3) for treating the transverse case.

The methods of Holzer and Prohl are both 'exact' in the sense that they give all the modes and frequencies of the equivalent system to any required degree of accuracy. These frequencies, however, will not in general be identical with those of the original continuous system, and differences may also occur in the actual modes of vibration, although these are usually less important. In most cases only the lower frequencies are of interest, so that the problem facing the practical computer is the determination of the simplest equivalent system which will give a certain number of the lower frequencies to some specified degree of accuracy.

It is apparent that a quantitative expression for the frequency errors mentioned above can only be obtained in cases where both the continuous system and its discrete equivalent can be analysed exactly, and such solutions are difficult to obtain unless the shaft is in fact a uniform one, carrying a uniform mass distribution. Results for simple systems of this type are of little value in themselves, but they may be used as a rough guide in estimating the errors in more complicated cases. A few of these solutions are discussed in this paper.

2. Systems obeying the wave equation

Perhaps the simplest case in which both solutions can easily be found is the uniform elastic string in transverse vibration. This problem was completely solved by Lagrange, and an account of the analysis may be found in Rayleigh's *Theory of Sound* (4, vol. 1, p. 172). He considers an elastic string of line density ρ, held by a tensile force T between two fixed points distant L apart. He reduces the system to one with a finite number of degrees of freedom by dividing the string into m sections and splitting the mass of each section into two equal concentrated masses at the ends as shown in Fig. 1, thereby obtaining a set of $m-1$ moving mass-points each of mass $\rho L/m$.

FIG. 1

If ${}_m\omega_s$ is the natural frequency of the sth mode of vibration, Rayleigh shows that

$$ {}_m\omega_s = [(2m/L)\sin(s\pi/2m)]\sqrt{(T/\rho)}, \tag{1} $$

and hence that

$$ {}_m\omega_s/{}_\infty\omega_s = \sin(s\pi/2m)/(s\pi/2m), \tag{2} $$

where ${}_\infty\omega_s$ represents the true natural frequency of the continuous system. Thus if s/m is small

$$({}_\infty\omega_s - {}_m\omega_s)/{}_\infty\omega_s \approx (\pi^2/24)(s/m)^2. \tag{3}$$

In this particular case analysis shows that although the frequencies are in error, the normal modes for the discrete case are in fact correct, i.e. if Y_r represents the modal displacements of the mass points, then for the sth mode,

$$Y_r = A_s \sin(\pi r s/m) \quad (r = 1, 2, \ldots, m-1).$$

Similar analysis, applied to the torsional vibrations of a uniform heavy shaft, has recently been given by Duncan (**5**), who also considers the more general problem of the non-uniform shaft. In the latter case he shows that the error in each frequency remains inversely proportional to the square of the number of sections, but he does not discuss its magnitude.

It is worth noting that Duncan uses a different method of concentrating the inertias, as he replaces the distributed inertia of each segment by an equal amount placed at the centre. Fig. 2 shows how this scheme compares with the method used by Rayleigh. In the case of a uniform string or shaft it will be found that the two methods give identical results. It is clear that Rayleigh's approach has some advantages when dealing with shafts formed of several uniform sections of different diameter, as in such cases concentration of the inertias at the ends of the sections greatly simplifies the calculation of the sectional rigidities.

FIG. 2

Frequency errors of this type occur in any finite-difference method of finding the eigenvalues of a partial differential equation. The wave equation with two independent space variables, associated with the problem of the vibrating membrane, has been treated from this standpoint by Milne (**6**, p. 237). He discusses rectangular regions only, obtaining results analogous to the ones quoted above.

3. Systems obeying the vibrating beam equation

Duncan (**5**) also considers the problem of a uniform cantilever in transverse vibration, and shows from numerical calculations that the inverse square law for the frequency error still applies. Although it does not appear possible to obtain an exact analytical solution to the discrete problem in this case, such a solution can be found when the beam is simply supported. The method used in the following analysis is very similar to that employed by Rayleigh in his treatment of the vibrating string.

If we consider a beam of length L, line density ρ, and flexural rigidity EI, simply supported at its ends, the natural frequencies of vibration ω_s are given by

$$\omega_s = (\pi^2 s^2/L^2)\sqrt{(EI g/\rho)} \quad (s = 1, 2,\ldots), \tag{4}$$

and the corresponding normal modes are

$$Y_s(x) = A_s \sin(s\pi x/L). \tag{5}$$

If we now divide the beam into m equal sections, concentrating the mass of each section in accordance with Fig. 1, our mass distribution becomes one of $m-1$ equal masses μ, spaced at equal intervals a, where $\mu = \rho L/m$ and $a = L/m$. We let y_r denote the displacements of these mass points, where r runs from 1 to $m-1$, as shown in Fig. 3.

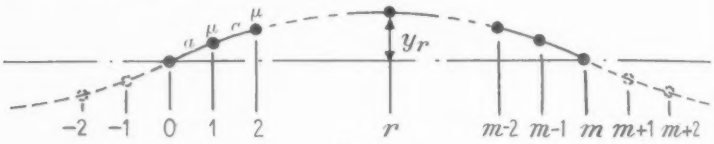

FIG. 3

Our aim is to find a solution $y_r(t)$ which satisfies exactly the equations of motion of the mass points and the boundary conditions at $r = 0$, $r = m$. These conditions are most easily dealt with if we treat the beam as part of an infinite beam of the same material, as shown in Fig. 3. By introducing 'image points' in this way, it becomes apparent that the conditions of zero deflexion and bending moment at $r = 0$, $r = m$, are satisfied exactly by any set of displacements y_r for which

$$y_{-r} = -y_r = y_{2m-r}, \tag{6}$$

where r may now take any value.

In order to write down the equations of motion of the masses we require the following result, which the present author has not been able to find explicitly stated elsewhere, although a similar idea is mentioned by Southwell (**7**, p. 183).

LEMMA. *If a uniform beam of flexural rigidity EI is loaded by concentrated loads $W_0,\ldots,W_n$, the load spacing a being constant, then for $2 \leqslant r \leqslant n-2$,*

$$\frac{6EI}{a^3}(y_{r-2} - 4y_{r-1} + 6y_r - 4y_{r+1} + y_{r+2}) = W_{r-1} + 4W_r + W_{r+1}. \tag{7}$$

Consider the section of beam shown in Fig. 4, where F and M are the shear and bending moment acting on the beam just to the right of the load W_{r-2}. For $0 \leqslant x \leqslant 4a$, the deflexion of the beam satisfies the equation

$$EI\frac{d^2y}{dx^2} = M + Fx + W_{r-1}\{x-a\} + W_r\{x-2a\} + W_{r+1}\{x-3a\}, \tag{8}$$

the brackets $\{\}$ being used to indicate terms which are only considered when positive; i.e.

$$\{x-a\} = 0, \qquad \text{if } 0 < x \leqslant a,$$

$$\{x-a\} = x-a, \quad \text{if } a < x.$$

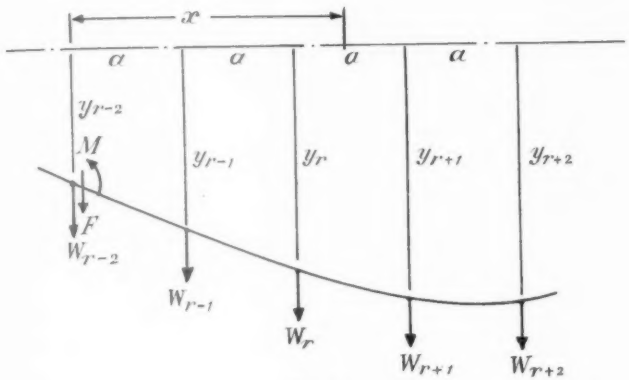

FIG. 4

On integrating (8) we obtain

$$EIy = \frac{Mx^2}{2} + \frac{Fx^3}{6} + \frac{W_{r-1}}{6}\{x-a\}^3 + \frac{W_r}{6}\{x-2a\}^3 + \\ + \frac{W_{r+1}}{6}\{x-3a\}^3 + \frac{Aa^2}{6}x + \frac{Ba^3}{6}, \qquad (9)$$

where A and B are arbitrary constants of integration. Substituting the appropriate values of x in (9) we obtain

$$\begin{aligned}
(6EI/a^3)y_{r+2} &= 48M/a + 64F + 27W_{r-1} + 8W_r + W_{r+1} + 4A + B,\\
(6EI/a^3)y_{r+1} &= 27M/a + 27F + 8W_{r-1} + W_r + 3A + B,\\
(6EI/a^3)y_r &= 12M/a + 8F + W_{r-1} + 2A + B,\\
(6EI/a^3)y_{r-1} &= 3M/a + F + A + B,\\
(6EI/a^3)y_{r-2} &= B.
\end{aligned} \qquad (10)$$

Forming the fourth difference of both sides of equations (10) we obtain the required result (7). It should be noted that this equation represents an exact solution of the original differential equation. Replacing the right-hand side by $6W_r$ gives

$$EI\,\frac{(y_{r-2} - 4y_{r-1} + 6y_r - 4y_{r+1} + y_{r+2})}{a^4} = \frac{W_r}{a}, \qquad (11)$$

which is of course the normal finite-difference form of the differential equation for the continuous-load case, with the error term omitted.

3.1. Using equation (7) we can write down immediately the equations of motion governing the mass points. It is important to realize that we are comparing exact solutions of two different physical systems, so that the approximate expression (11) must not be used. The equations of motion are

$$\frac{6EI}{a^3}(y_{r-2}-4y_{r-1}+6y_r-4y_{r+1}+y_{r+2}) = -\frac{\mu}{g}(\ddot{y}_{r-1}+4\ddot{y}_r+\ddot{y}_{r+1}). \quad (12)$$

where r may take any value, provided that the y_r satisfy equation (6). Putting $y_r = Y_r e^{i\omega t}$, we obtain

$$Y_{r-2}-4Y_{r-1}+6Y_r-4Y_{r+1}+Y_{r+2} = \frac{\mu a^3\omega^2}{6EIg}(Y_{r-1}+4Y_r+Y_{r+1}). \quad (13)$$

Following Rayleigh, we try a function Y_r giving exact agreement with the continuous case at the mass-points, i.e. $Y_r = A\sin r\beta$. This clearly satisfies equation (6) provided that $m\beta = s\pi$, where s is a positive integer. Substituting in (13) and putting $k = \dfrac{\mu a^3\omega^2}{6EIg}$, we obtain

$$\sin(r-2)\beta-(4+k)\sin(r-1)\beta+$$
$$+(6-4k)\sin r\beta-(4+k)\sin(r+1)\beta+\sin(r+2)\beta = 0,$$

and hence

$$2\sin r\beta\cos 2\beta-2(4+k)\sin r\beta\cos\beta+(6-4k)\sin r\beta = 0.$$

Since by hypothesis $\sin r\beta \neq 0$,

$$2\cos 2\beta-2(4+k)\cos\beta+6-4k = 0,$$

whence

$$k = \frac{16\sin^4(\beta/2)}{6-4\sin^2(\beta/2)}.$$

Substituting for k, β, μ, a, we finally obtain

$$\omega = {}_m\omega_s = \frac{m^2}{L^2}\frac{4\sin^2(s\pi/2m)}{\sqrt{\{1-\frac{2}{3}\sin^2(s\pi/2m)\}}}\sqrt{(EIg/\rho)}, \quad (14)$$

and comparing this with equation (4) gives

$$\frac{{}_m\omega_s}{{}_\infty\omega_s} = \left[\frac{\sin(s\pi/2m)}{(s\pi/2m)}\right]^2\frac{1}{\sqrt{\{1-\frac{2}{3}\sin^2(s\pi/2m)\}}}. \quad (15)$$

For small values of s/m this becomes

$$\frac{{}_x\omega_s - {}_m\omega_s}{{}_x\omega_s} \approx \tfrac{1}{90}(8\pi/2m)^4 = 0{\cdot}0676(s/m)^4. \tag{16}$$

Repeating the analysis using Duncan's method of mass concentration (Fig. 2) gives an identical result. We see that not only is the error an inverse fourth power one, but that it is considerably smaller than in the case of the vibrating string. For instance, if we take $m = 3$, $s = 1$, we obtain an approximate value for the lowest natural frequency of

$${}_3\omega_1 = \frac{3^2}{L^2}\sqrt{\left(\frac{6}{5}\right)}\sqrt{\left(\frac{EIg}{\rho}\right)} = \frac{9{\cdot}859}{L^2}\sqrt{\left(\frac{EIg}{\rho}\right)}.$$

Comparing this with the exact solution of the continuous case,

$${}_x\omega_1 = \frac{\pi^2}{L^2}\sqrt{(EIg/\rho)} = \frac{9{\cdot}870}{L^2}\sqrt{(EIg/\rho)},$$

we find that the error is only 0·1 per cent., as against 4·5 per cent. in the corresponding vibrating string case.

4. Conclusions

From Duncan's numerical results for the uniform cantilever we can deduce the approximate relationship

$$\frac{{}_x\omega_s - {}_m\omega_s}{{}_x\omega_s} \approx 0{\cdot}2(s/m)^2, \tag{17}$$

while the general rule (also quoted by Duncan) of 13 segments per complete wavelength for 1 per cent. accuracy corresponds to an error function of approximately $0{\cdot}5(s/m)^2$. The surprisingly small error in the case of the simply supported beam is clearly due to the fact that the modes for the discrete case are identical with those of the continuous system, while the boundary conditions are also satisfied exactly. It is unlikely that such agreement occurs with any other types of support condition, so that in most circumstances we must expect an error function similar to that appearing in equation (17).

It should be noted that even in cases where the modes agree at the mass points they will not in general agree elsewhere, and the stress distributions will therefore be different in the two cases. In the numerical example given in section 3 above, a comparison between the two modes shows that in the discrete case the displacement at the centre is 0·4 per cent. too small, while the bending moment at the same point is 5 per cent. too small. Thus a redistribution of mass which does not have a great effect on the natural frequency can produce a relatively large change in the internal stresses.

REFERENCES

1. S. P. Timoshenko, *Vibration Problems in Engineering*, 2nd edition (New York, 1937).
2. W. J. Duncan, *Galerkin's Method in Mechanics and Differential Equations*, R. & M. No. 1728 (1937).
3. M. A. Prohl, *Trans. Amer. Soc. Mech. Engrs.* **67** (1945), A142.
4. Lord Rayleigh, *The Theory of Sound*, 2nd edition (London, 1894).
5. W. J. Duncan, *Quart. J. Mech. and Applied Math.* **5** (1952), 97.
6. W. E. Milne, *Numerical Solution of Differential Equations* (New York, 1953).
7. R. V. Southwell, *The Theory of Elasticity*, 2nd edition (Oxford, 1941).

THE PRINCIPAL FREQUENCIES OF VIBRATING SYSTEMS WITH ELLIPTIC BOUNDARIES

By S. D. DAYMOND

(*Department of Applied Mathematics, University of Liverpool*)

[Received 17 June 1954]

SUMMARY

In the equation $\nabla^2\phi(x,y)+\nu\phi(x,y)=0$, which occurs in the theory of vibrations, the frequencies of the normal modes are, with a convenient choice of units, equal to the square roots of the eigenvalues ν_i appropriate to the boundary condition. Two problems are dealt with here in connexion with elliptical boundaries, all of which enclose a constant area π. In the first problem the boundary condition is $\phi=0$ and the principal frequency is $\sqrt{\lambda}$; in the second the boundary condition is $\partial\phi/\partial n=0$ and the principal frequency is $\sqrt{\mu}$. The numerical values of $\sqrt{\lambda}$ and $\sqrt{\mu}$ are determined for $e=0(0{\cdot}1)1$ and for $\sqrt{(1-e^2)}=1(0{\cdot}1)0$. By applying a simple theorem of extension it is then possible to find such values for an ellipse of any area and eccentricity.

The method is an inverse one in which zeros (ξ_0) of the modified Mathieu function $\mathrm{Ce}_0(\xi,q)$ and of $(d/d\xi)\mathrm{Ce}_1(\xi,q)$ are evaluated, when the parameter q takes each one of a conveniently chosen increasing sequence of positive values. A real zero of the former function exists for any such q, but there are no real zeros of the latter if $q>0{\cdot}89$.

It is found that as e increases from zero to unity $\sqrt{\lambda}$ increases from 2·4048... to infinity, in such a way that $\lambda\sqrt{(1-e^2)}\to\pi^2/4$, while $\sqrt{\mu}$ decreases from 1·8411... to zero.

Sections 1 and 2 contain, respectively, brief accounts of the relevant properties of eigenvalues and of the theory underlying the solutions of the two problems. Values of $\sqrt{\lambda}$ are found in section 3; in addition, brief references are made in this section to the application of an asymptotic formula, and to the accuracy of a known approximate analytical formula for $\sqrt{\lambda}$. Values of $\sqrt{\mu}$ are determined in section 4. Finally, section 5 is a brief note on the ξ-derivative of the function Ce_1.

The notation used for the Mathieu functions is in general that to be found in (**1**). Occasionally we use that accompanying the tables (**2**); thus, we frequently write s for $4q$ and we adopt in section 5 the method of normalization explained in (**2**) as this simplifies the use of these tables in evaluating the derivative mentioned above.

1. Some elementary properties of eigenvalues

Let $\phi(x,y)$ satisfy the equation

$$\nabla^2\phi+\nu\phi=0 \tag{1.1}$$

in a region R bounded by a closed curve C, where x,y are cartesian coordinates and ν is a parameter. Two problems, arising from two different boundary conditions, will be considered; they are:

Problem I, in which $\phi=0$ on C; the eigenvalues $\{\lambda_i\}$ are such that

$$0<\lambda_0\leqslant\lambda_1\leqslant\lambda_2\leqslant\ldots;$$

[Quart. Journ. Mech. and Applied Math., Vol. VIII, Pt. 3 (1955)]

and PROBLEM II, in which $\partial\phi/\partial n = 0$ on C; the eigenvalues $\{\mu_i\}$ are such that

$$0 = \mu_0 < \mu_1 \leqslant \mu_2 \leqslant \dots .$$

The property $\lambda_i \geqslant \mu_i$ is well known. Moreover, proofs of the interesting property $\lambda_0 > \mu_1$ are given in (**3**) and in the appendix, by G. Pólya, to that paper. In the theory of wave-guides (**1**, ch. xviii) the significance of the latter theorem is that for an arbitrary but constant cross-section the absolute (i.e. longest) cut-off wavelength is $2\pi/\sqrt{\mu_1}$, and hence that the dominant mode is an H-mode and not an E-mode.

Again we have the further properties (**3**) that

(i) if R and $\bar{R}$ are the areas of similar regions, corresponding eigenvalues of any order are such that

$$\bar{\lambda}_i/\lambda_i = \bar{\mu}_i/\mu_i = R/\bar{R}; \tag{1.2}$$

(ii) of all regions R enclosing a prescribed constant area the bounding curve C for which λ_0 is smallest, and also μ_1 is greatest, is a circle.

The truth of (i) follows at once from (1.1) by changing the variables to $\bar{x}, \bar{y}$, which are respectively proportional to x, y.

In (ii) let the magnitude of the constant area be π. For the circle, $\sqrt{\lambda_0}$ is $2{\cdot}4048\dots = \alpha$, say, and $\sqrt{\mu_1}$ is $1{\cdot}8411\dots = \beta$, say, where these numbers are respectively the smallest positive zeros of $J_0(x)$ and $J_1'(x)$, in the usual notation for Bessel functions.

For a rectangle whose sides are in the ratio $k{:}1$ ($k \leqslant 1$), we have

$$\lambda_0 = \pi(k + k^{-1}) \geqslant 2\pi$$

and

$$\mu_1 = \pi k \leqslant \pi.$$

Thus, as $k \to 0$, $\lambda_0 \to \infty$ in such a way that $\lambda_0 k \to \pi$, and $\mu_1 \to 0$ like k.

Consider now a family E of ellipses of which each member encloses an area π. When the eccentricity is e, the ratio of the axes is $\sqrt{(1-e^2)}$. Consideration of the above cases of the rectangle leads us to expect that $\lambda_0\sqrt{(1-e^2)}$ varies from α^2 to a finite limit l_0 and that $\mu_1/\sqrt{(1-e^2)}$ varies from β^2 to a finite limit m_1, as e increases from zero to unity. In fact it is shown later that $l_0 = \pi^2/4$ and $m_1 = 0$.

It is clear that the eigenvalues corresponding to any given elliptical boundary $\bar{E}$ can be found from those appropriate to the similar member of E by applying (1.2). In the subsequent treatment of the problems of evaluating $\sqrt{\lambda_0}$ and $\sqrt{\mu_1}$ for such a family of ellipses, over the ranges of e and $\sqrt{(1-e^2)}$ stated in the summary, we shall dispense with the suffixes, so that $\sqrt{\lambda}$ and $\sqrt{\mu}$ will represent the principal frequencies to be determined in the Problems I and II.

2. Basic theory and method of solution of the two problems

Let the region R be bounded by an ellipse of eccentricity e and area π. The semi-axes are $(1-e^2)^{\pm\frac{1}{4}}$. We express (1.1) in elliptic coordinates given by

$$x+iy = c\cosh(\xi+i\eta),$$

where $c^2 = (1-e^2)^{-\frac{1}{2}}-(1-e^2)^{\frac{1}{2}} = e^2(1-e^2)^{-\frac{1}{2}}$. Writing, in the usual way, $\phi = X(\xi)Y(\eta)$, it follows that X and Y must satisfy the Mathieu equations

$$X''-(a-2q\cosh 2\xi)X = 0, \tag{2.1}$$

$$Y''+(a-2q\cos 2\eta)Y = 0, \tag{2.2}$$

where the 'characteristic number' a is a separation constant and

$$4q = s = \nu c^2 = \nu e^2(1-e^2)^{-\frac{1}{2}}. \tag{2.3}$$

If $\xi = \xi_0$ on the boundary, we have

$$\cosh\xi_0 = 1/e, \qquad c^2 = 1/\cosh\xi_0\sinh\xi_0. \tag{2.4}$$

Now let $u = \sqrt{q}\exp\xi_0, \qquad v = \sqrt{q}\exp(-\xi_0),$

and hence $w_0 = u+v = \sqrt{s}\cosh\xi_0. \tag{2.5}$

It follows that $w_0^2 = s/e^2 = \nu(1-e^2)^{-\frac{1}{2}}$ (2.6)

and that $w_0^2-s = \nu(1-e^2)^{\frac{1}{2}}$. (2.7)

The appropriate solutions of (2.2) are the Mathieu functions of the first kind of integral order,

$$\mathrm{ce}_m(\eta, q) \quad \text{and} \quad \mathrm{se}_{m+1}(\eta, q) \quad (m = 0, 1, 2,...),$$

and those of (2.1) are the modified functions

$$\mathrm{Ce}_m(\xi, q) = \mathrm{ce}_m(i\xi, q) \quad \text{and} \quad \mathrm{Se}_{m+1}(\xi, q) = -i\,\mathrm{se}_{m+1}(i\xi, q),$$

which are respectively even and odd functions† of ξ.

The boundary condition of Problem I requires that

$$\mathrm{Ce}_m(\xi_0, q) = 0 \quad \text{and} \quad \mathrm{Se}_{m+1}(\xi_0, q) = 0$$

where $m = 0, 1, 2,...$; we require further that the appropriate zero in q should lead to a value of $\sqrt{\lambda}$ which tends to $\alpha = 2{\cdot}4048...$ as $\xi_0 \to \infty$. Now $\mathrm{Ce}_0(\xi_0, q)$, and this modified function only, tends to $J_0(\sqrt{\lambda})$, the Bessel function of order zero, as $\xi_0 \to \infty$. Thus, on making the substitutions

$$\exp\xi = \exp\xi_0 = p \quad \text{and} \quad q = \lambda/2\sinh 2\xi_0 = \lambda p^2/(p^4-1),$$

the expression

$$\mathrm{Ce}_0(\xi, q) = 1-\tfrac{1}{2}q\cosh 2\xi+\tfrac{1}{32}q^2\cosh 4\xi-\tfrac{1}{128}q^3(\tfrac{1}{9}\cosh 6\xi-7\cosh 2\xi)+... \tag{2.8}$$

† In (2) the notations for these even and odd modified functions are respectively $\mathrm{Je}_m(s, \xi)$ and $\mathrm{Jo}_{m+1}(s, \xi)$; see p. xxxviii of the Introduction.

can be reduced to the form

$$J_0(\sqrt{\lambda})+\sum_{k=1}^{\infty}(p^4-1)^{-k}f_k(\sqrt{\lambda}),$$

where the f_k are power series. Although these series are only slowly convergent, even when $\sqrt{\lambda}$ assumes its smallest value α, and therefore of no use for computing purposes, the above form makes it clear that a direct solution of this problem would require the evaluation of parametric zeros of the function (2.8), for prescribed values of ξ_0.

The boundary condition of Problem II requires that the ξ-derivatives of the functions Ce_m and Se_{m+1} should be zero when $\xi = \xi_0$. Also the corresponding parametric zero should lead to a value of $\sqrt{\mu}$ which tends to $\beta = 1{\cdot}8411...$ from below (see property (ii) of the eigenvalues) as $\xi_0 \to \infty$. Now (**1**, p. 368) both $(d/d\xi)\mathrm{Ce}_1$ and $(d/d\xi)\mathrm{Se}_1$ tend to $J_1'(\sqrt{\mu})$ as $\xi = \xi_0 \to \infty$. Closer examination on the lines of the preceding paragraph, however, shows that the frequencies which depend on parametric zeros of $(d/d\xi)\mathrm{Se}_1$ begin to increase as the eccentricity increases from zero, while those which depend on zeros of $(d/d\xi)\mathrm{Ce}_1$ possess the required property that $\sqrt{\mu}$ for the circle is the largest. Thus a direct solution of Problem II would involve parametric zeros of the function

$$[(d/d\xi)\mathrm{Ce}_1]_{\xi=\xi_0} = \sinh\xi_0 - \tfrac{3}{8}q\sinh 3\xi_0 + \tfrac{1}{64}q^2(-3\sinh 3\xi_0 + \tfrac{5}{3}\sinh 5\xi_0) - \ldots. \tag{2.9}$$

The method of solution

In either problem the direct determination of parametric zeros for given values of ξ_0 is impracticable, and the inverse procedure is adopted in which zeros are determined for prescribed values of s $(= 4q)$, as below.

The modified Mathieu functions Ce_0 and Ce_1 are expressible (**1**, pp. 159, 160) in series of Bessel functions of argument $w = \sqrt{s}\cosh\xi$. The coefficients,† functions of s only, are extensively tabulated in (**2**). Thus, with the aid of (**2**) and (**4**), we evaluate for each one of a sequence of values of s the zeros $w_0 = \sqrt{s}\cosh\xi_0$ of Ce_0 and of $(d/d\xi)\mathrm{Ce}_1$. The values of e and of ν (i.e. λ in Problem I, μ in Problem II) which correspond then follow from (2.6) or (2.7). These corresponding pairs of values of e and $\sqrt{\lambda}$, or $\sqrt{\mu}$, are of course at unequal intervals of e. Four-decimal values for the regular intervals described in the summary are derived from the above values by the method of linear cross means.‡ An account of this method is to be found in (**5**), pp. 84–86.

† The absolute values of the coefficients depend on the method of normalization of the functions; however, the A_{2k+p} of (**1**) and the D_{2k+p} of (**2**), where $p = 0$ or 1 here, are proportional for a given value of s. The factor of proportionality is unimportant in the calculation of zeros.

‡ The author is indebted to Dr. C. W. Jones for pointing out the suitability of this method.

3. The evaluation of $\sqrt{\lambda}$

Now $\mathrm{Ce}_0(\xi, q)$ is proportional to

$$\sum_0^\infty (-1)^k A_{2k}(q) J_{2k}(w),$$

where J_{2k} as usual denotes Bessel functions of the first kind, w is $\sqrt{s}\cosh\xi$, and the coefficients are functions of q $(= s/4)$. This expression is in turn proportional to

$$\sigma = \sum_0^\infty C_{2k}(s) J_{2k}(w), \tag{3.1}$$

where $C_{2k} \equiv (-1)^k D_{2k}$, and the D_{2k} are the functions of s tabulated in (2), pp. 41–57. It is clear from the tables that the C_{2k} are positive for all positive s.

As a preliminary step in the evaluation of a zero w_0 of (3.1) for a given value of s, equations (2.6) and (2.7) can be used to find a good approximation. Thus, since $\nu \equiv \lambda \geqslant \alpha^2$ for all eccentricities, we get $w_0\sqrt{(w_0^2 - s)} \geqslant \alpha^2$; that is

$$w_0^2 \geqslant \tfrac{1}{2}s + \sqrt{\{(\tfrac{1}{2}s)^2 + \alpha^4\}} = w_1^2, \text{ say,} \tag{3.2}$$

where $\alpha^4 = 33{\cdot}4452\ldots$. The fact that $w_0 - w_1$ is quite small (not greater than 0·18 for any s) is very helpful in the exact calculations of w_0, particularly for values of s greater than about unity. As the chosen value of s is increased from zero, it is found, during the process of evaluating w_0 exactly, that $w_0 - w_1$ increases from zero to a maximum of 0·176 when s is 25 and then decreases. When, for example, s is 100 (the largest value for which the coefficients in (3.1) are tabulated), w_1 is 10·017 and w_0 is 10·136. In fact, if it is assumed at this stage that $(w_0^2 - s) \to \pi^2/4$ as $s \to \infty$ (see the end of this section), it follows quite easily from (3.2) that, for large values of s,

$$(w_0 - w_1) \sim \pi^2/8\sqrt{s}.$$

Returning now to the precise determination of zeros of (3.1), it is clear that for a positive value of s less than unity, $w_0 - w_1$ is so small that the evaluation of the exact zero presents no difficulty; the function σ is tabulated in the neighbourhood of the approximate zero w_1 and then w_0 is found by inverse interpolation. For a larger value of s, the value of $w_0 - w_1$ found during the previous stage of the calculations serves as a useful estimate of the zero. Thus, when $s = 16$, $w_1 = 4{\cdot}227$ and $w_0 - w_1$ is a little greater than 0·15, its value at $s = 13$. The approximate values of σ when $w = 4{\cdot}39$ and 4·40 are respectively 0·0038 and −0·0041, and they suggest tabulation around the value 4·395, as follows:

w	4·393	4·394	4·395	4·396	4·397
σ	·00171 211	·00084 443	−·00002 209	−·00088 747	−·00175 170

Thus, when $s = 16$, $w_0 = 4{\cdot}39497\ 449$ and, therefore,

$$e = \sqrt{s}/w_0 = 0{\cdot}91013\ 042, \qquad \lambda\sqrt{(1-e^2)} = w_0^2 - s = 3{\cdot}31580\ 08.$$

For certain suitable values of s ranging from zero to 100, the w-zeros of (3.1), and hence the pairs of corresponding values of e and $\lambda\sqrt{(1-e^2)}$, are evaluated in the manner described above. The results are contained in Table I. In each case σ changes from positive to negative as w increases through the zero; this is obvious when s is small since the function is then dominated by the first term $C_0 J_0(w)$ and C_0 is slightly greater than unity.

TABLE I

s	w_0	$e = \sqrt{s}/w_0$	$\sqrt{(1-e^2)}$	$\lambda\sqrt{(1-e^2)} = w_0^2 - s$
0·00	2·40482 56...	0	1	5·78318 6...
0·02	2·40690 731	·05875 646	·99827 235	5·77320 28
0·04	2·40899 425	·08302 220	·99654 770	5·76325 33
0·08	2·41318 360	·11720 729	·99310 747	5·74345 51
0·12	2·41739 354	·14329 903	·98967 944	5·72379 15
0·16	2·42162 393	·16517 841	·98626 370	5·70426 25
0·20	2·42587 463	·18435 149	·98286 038	5·68486 77
0·40	2·44742 871	·25841 632	·96603 365	5·58990 73
0·80	2·49198 300	·35892 187	·93336 761	5·40997 93
1·00	2·51494 409	·39762 315	·91754 882	5·32494 38
2·00	2·63568 177	·53656 461	·84385 924	4·94681 84
3·00	2·76403 068	·62663 950	·77930 927	4·63986 56
4·00	2·89696 612	·69037 742	·72344 939	4·39241 27
5·60	3·11310 696	·76015 118	·64974 625	4·09143 49
7·00	3·30110 576	·80147 427	·59802 926	3·89729 92
10·00	3·68987 087	·85701 581	·51529 011	3·61514 70
13·00	4·05430 973	·88931 323	·45729 857	3·43742 74
16·00	4·39497 449	·91013 042	·41432 188	3·31580 08
25·00	5·30150 516	·94312 838	·33242 871	3·10595 70
36·00	6·24316 979	·96105 027	·27637 362	2·97716 90
50·00	7·27227 227	·97233 265	·23360 053	2·88594 40
64·00	8·17493 080	·97860 156	·20576 442	2·82949 36
100·00	10·13646 1	·98653 8	·16353	2·7478
↓	↓	↓	↓	↓
∞	∞	1	0	$\pi^2/4 = 2{\cdot}46740\ 11$

The value of $\lambda\sqrt{(1-e^2)}$ for $s = 100$ is liable to an error of a unit or so in the fourth decimal place; this entry, however, is not necessary for subsequent calculations.

The values of $\lambda\sqrt{(1-e^2)}$ at equal intervals in e, and in $\sqrt{(1-e^2)}$, are now constructed from Table I by the method of linear cross means to which reference has been made in section 2. (A method dependent upon divided differences is unsuitable owing to the very slow convergence of these differences.) For example, in the calculation of the value of this function when $e = 0{\cdot}7$ the convergence of the successive cross means proved to be

less satisfactory than in all other cases; the convergence of the process towards the finally assumed value of 4·35281 2 is shown in the Table II.

TABLE II

e_i	$\lambda\sqrt{(1-e^2)}$	$e = 0{\cdot}7$						$e_i - e$
0·39762 315	5·32494 38							−·30237 685
0·53656 461	4·94681 84	4·50203 34						−·16343 539
0·62663 950	4·63986 56	·42041 54	4·35394 25					−·07336 050
0·69037 742	4·39241 27	·36176 12	5298 57	4·35284 12				−·00962 258
0·76015 118	4·09143 49	·29610 05	5150 23	260 17	4·35280 82			+·06015 118
0·80147 427	3·89729 92	·25601 85	5025 51	239 53	80 26	4·35281 64		+·10147 427
0·85701 581	3·61514 70	·19953 84	4775 60	197 25	79 11	88	4·35281 20	+·15701 581

The final values are liable to be in error by two or three units in the sixth place of decimals. It is of interest to note here that the method of linear cross means, when applied to evaluate $\lambda\sqrt{(1-e^2)}$ when $e = 1$, gives the value 2·4674, and this is correct to five figures for the theoretical limit $\pi^2/4$.

Numerical values of the principal frequency $\sqrt{\lambda}$ at one-tenth intervals in e and in $\sqrt{(1-e^2)}$ respectively are shown in columns 3 and 6 of Table III. These final values can be given correct to four places of decimals only.

TABLE III

1 e	2 $\lambda\sqrt{(1-e^2)}$	3 $\sqrt{\lambda}$	4 $\sqrt{(1-e^2)}$	5 $\lambda\sqrt{(1-e^2)}$	6 $\sqrt{\lambda}$
0	5·78318 6	2·4048	1·0	5·78318 6	2·4048
0·1	5·75426 6	2·4048	0·9	5·23220 8	2·4111
0·2	5·66745 8	2·4051	0·8	4·73579 6	2·4330 5
0·3	5·52261 0	2·4061	0·7	4·29352 3	2·4766
0·4	5·31943 5	2·4091	0·6	3·90444 3	2·5510
0·5	5·05744 3	2·4166	0·5	3·56672 8	2·6708 5
0·6	4·73579 6	2·4330 5	0·4	3·27708 8	2·8623
0·7	4·35281 2	2·4688	0·3	3·03009 8	3·1781
0·8	3·90444 3	2·5510	0·2	2·81807 0	3·7537
0·9	3·37582	2·7829	0·1	2·63265 7	5·1309
1·0	2·46740 1	∞	0	2·46740 1	∞

It is significant that over the major part of the range of the eccentricity the principal frequency increases remarkably slowly, and even when $\sqrt{(1-e^2)} = 0{\cdot}1$, that is when $e = 0{\cdot}995$, $\sqrt{\lambda}$ is only 5·1309.

A method of evaluating $\sqrt{\lambda}$ when $0{\cdot}1 > \sqrt{(1-e^2)} > 0$ is outlined below.

Applications of an asymptotic formula

When $s = 4q >> 0$, we have (**1**, p. 385)

$$\mathrm{Ce}_0(\xi_0, q) \sim C\{(1+x_0)\cos\chi_0 + z_0 \sin\chi_0\}, \tag{3.3}$$

where C is a constant,

$$1/x_0 = (\sinh\xi_0)/z_0 = 4\sqrt{s}\cosh^2\xi_0,$$

and

$$\chi_0 = \sqrt{s}\sinh\xi_0 - \tan^{-1}(\tanh\tfrac{1}{2}\xi_0).$$

The zeros of (3.3) are such that

$$\cot \chi_0 = \tan(\tfrac{1}{2}\pi - \chi_0) = -\{1+(1/x_0)\}^{-1}\sinh \xi_0,$$

that is

$$\sqrt{s}\sinh \xi_0 = \tfrac{1}{2}\pi + \tan^{-1}(\tanh \tfrac{1}{2}\xi_0) + \tan^{-1}\{\sinh \xi_0/(1+4\sqrt{s}\cosh^2\xi_0)\}. \quad (3.4)$$

Firstly, we note that the right side of (3.4) tends to $\frac{1}{2}\pi$. Hence, as s tends to infinity,

$$\lambda\sqrt{(1-e^2)} = s\sinh^2\xi_0 \to \pi^2/4,$$

as previously stated, and assumed in Table I.

Secondly, we can apply (3.4) to evaluate $\sqrt{\lambda}$ with considerable accuracy when $0{\cdot}1 > \sqrt{(1-e^2)} > 0$. Thus, when $\sqrt{(1-e^2)} = 0{\cdot}1$, we get

$$\exp \xi_0 = 11/\sqrt{99},$$

and therefore

$$\sqrt{s}\sinh \xi_0 = \sqrt{(s/99)} = \tfrac{1}{2}\pi + \tan^{-1}(10-\sqrt{99}) + \tan^{-1}\{\sqrt{99}/(99+400\sqrt{s})\},$$

approximately. By a method of successive approximations the consecutive values of $\sqrt{s}$, and those of $\sqrt{\lambda}$, obtained by using one, two, and three terms of this expression, are respectively:

$\sqrt{s}$	15·62923	16·12755	16·14267
$\sqrt{\lambda}$	4·96729	5·12567	5·13048

Comparison of the third approximation 5·1305 with the corresponding entry in Table III shows an error of only four units in the fourth decimal place. Thus the error incurred by use of the asymptotic formula over the range of $\sqrt{(1-e^2)}$ stated above is certain to be less than this amount.

A note on a known formula for $\sqrt{\lambda}$ and its range of applicability

Herriot (**6**) has derived the following formula for this principal frequency in terms of the eccentricity:

$$b\sqrt{\lambda} = 2{\cdot}4048\ldots \times (1-0{\cdot}25e^2-0{\cdot}034640e^4-0{\cdot}010355e^6-0{\cdot}004650e^8). \quad (3.5)$$

No greater claim is made for the formula than its accuracy for 'small' eccentricities. However, using the expression $(1-e^2)^{\frac{1}{2}}$ for the semi-minor axis b of an ellipse of area π, the following pairs of values can be derived from (3.5):

e	0·4	0·6	0·8
$\sqrt{\lambda}$	2·40915	2·4331	2·5530

These compare very favourably with the exact four-figure values in Table III; even when $e = 0{\cdot}8$, the error is probably small enough to be unimportant in practical applications of the formula. That the formula can in fact be used for quite 'large' values of e is not surprising, now that the extremely slow rate of increase of $\sqrt{\lambda}$ over the major part of the full range of the eccentricity has been established.

4. The evaluation of $\sqrt{\mu}$

In this problem $\partial\phi/\partial n$, and therefore $\partial\phi/\partial\xi$, are zero on the boundary $\xi = \xi_0$. In the notation of section 2, ν is equal to μ, the principal eigenvalue, and zeros are required of the function expressed in (2.9).

We use an expansion for $\mathrm{Ce}_1(\xi, q)$ equivalent to that given in (**1**), p. 160; the coefficients $(-1)^k A_{2k+1}$ used there are proportional, for a given s, to the coefficients $C_{2k+1} = (-1)^k D_{2k+1}$ which are in effect tabulated in (**2**), pp. 58–68. The C_{2k+1} are positive for all positive s. Thus the function (2.9) is proportional to

$$\sqrt{s}\sinh\xi_0 \sum_0^\infty C_{2k+1} J'_{2k+1}(\sqrt{s}\cosh\xi_0).$$

Ignoring for the moment the zero $\xi_0 = 0$, which exists for all s, and applying a recurrence relation for the Bessel function derivative, it becomes clear that we now require zeros w_0 of the expression

$$\sigma' = \sum_0^\infty C_{2k+1}\{J_{2k}(w) - (2k+1)w^{-1}J_{2k+1}(w)\} \qquad (4.1)$$

for given values of s.

The range of values of s for which real zeros exist is, however, in this case limited by the condition that $e = \sqrt{s}/w_0$ must not exceed unity, i.e. that $w_0^2 - s = (u-v)^2 \not< 0$. This condition restricts s to the range $0 \leqslant s \leqslant 3{\cdot}56$, the right side of the inequality corresponding to $e = 1$, $\xi_0 = 0$. Thus, after dividing (2.9) by ξ_0 and then making $\xi_0 \to 0$, we get the following equation for q:

$$9q = 8 - (q^2/12) + (97q^3/1152) + \ldots .$$

The approximate root is 0·890 and corresponds to the value 3·56 of s.

An alternative method capable of greater accuracy makes use of the expression

$$\sum_0^\infty \mathrm{De}_{2k+1}(s)\cosh(2k+1)\xi,$$

which is proportional to $\mathrm{Ce}_1(\xi, q)$. From this expression we derive our equation for s, namely,

$$0 = \lim_{\xi=\xi_0\to 0}(\xi^{-1}\mathrm{Ce}'_1) \propto \sum_0^\infty (2k+1)^2 \mathrm{De}_{2k+1} = \Sigma, \text{ say.}$$

The appropriate value of s (i.e. 3·55928) is then found from the following table of values of Σ:

s	2	2·5	3·0	3·5	4·0	4·5	5·0
Σ	·46676 7	·32229 2	·17297 6	·01863 9	−·14089 2	−·30578 2	−·47618 4

As s increases from zero over its limited range, the zero w_0 of (4.1) increases from $\beta = 1{\cdot}8411\ldots$ to the slightly greater value $\sqrt{(3{\cdot}55928)} = 1{\cdot}8866$. As

the latter interval is so small, the evaluation of w_0 for a given s, by tabulation and inverse interpolation, presents no special difficulty. However, because the values of $\sqrt{\mu}$ decrease quite rapidly to zero as s increases from 3·50 to its upper limit, sub-tabulation of the coefficients C_{2k+1} is necessary within this range. Their values are given in the table below:

s	C_1	C_3	C_5	
3·51	1·13303 207	0·13815 87	0·00522 3	
3·52	348 799	865 71	25 7	
3·53	394 442	913 71	29 1	$C_7 = 0{\cdot}00010$
3·54	440 134	962 73	32 5	
3·55	485 876	0·14011 80	35 9	

Column 2 of Table IV gives zeros of (4.1) for values of s from zero to 3·55. The other columns of the table give corresponding pairs of values of e, or of $\sqrt{(1-e^2)}$, and $w_0^2 = \mu/\sqrt{(1-e^2)}$, the intervals being, of course, unequal. (The values of w_0^2 and e are liable to errors of 2 units in the seventh and eighth places of decimals respectively.)

TABLE IV

1 s	2 w_0	3 e	4 $\sqrt{(1-e^2)}$	5 w_0^2
0·0	1·84118 38	0	1	3·38995 78
0·1	1·84229 59	·17164 874	·98515 822	3·39405 42
0·25	1·84398 10	·27115 247	·96253 641	3·40026 59
0·5	1·84683 40	·38287 512	·92380 011	3·41079 58
1·0	1·85271 21	·53974 927	·84182 583	3·43254 21
2·0	1·86517 95	·75821 848	·65200 057	3·47889 46
2·5	1·87178 12	·84472 417	·53520 189	3·50356 49
3·0	1·87863 50	·92197 303	·38725 409	3·52926 95
3·5	1·88574 53	·99208 981	·12553 012	3·55603 53
3·51	1·88589 01	·99342 979	·11444 326	3·55658 15
3·52	1·88603 83	·99476 575	·10218 172	3·55714 05
3·53	1·88618 02	·99610 282	·08819 957	3·55767 57
3·54	1·88632 53	·99743 601	·07156 406	3·55822 31
3·55	1·88647 05	·99876 694	·04964 474	3·55877 09

The values of w_0^2 and subsequent values of $\sqrt{\mu}$, at one-tenth intervals in e, and in $\sqrt{(1-e^2)}$, are here again evaluated by linear cross means, and are shown in Table V.

The nature of the convergence of the cross means, and differencing of the final values, strongly suggest that the entries in columns 2 and 5 of Table V will have only slight errors in the fifth place of decimals, and hence that the values of $\sqrt{\mu}$ can confidently be given correct to four places of decimals, as in the table.

TABLE V

1 e	2 w_0^2	3 $\sqrt{\mu}$	4 $\sqrt{(1-e^2)}$	5 w_0^2	6 $\sqrt{\mu}$
0·0	3·38996	1·8412	1·0	3·38996	1·8412
0·1	3·39134	1·8369	0·9	3·41719	1·7537
0·2	3·39553	1·8240	0·8	3·44329	1·6597
0·3	3·40261	1·8016	0·7	3·46783	1·5580
0·4	3·41276	1·7686	0·6	3·49030	1·4471
0·5	3·42621	1·7225 5	0·5	3·51029	1·3248
0·6	3·44329	1·6597	0·4	3·52733	1·1878
0·7	3·46446	1·5729	0·3	3·54103	1·0307
0·8	3·49030	1·4471	0·2	3·55108	0·8427
0·9	3·52157	1·2390	0·1	3·55723	0·5964
1·0	3·55928	0	0·0	3·55928	0

5. A note on the function $(d/d\xi)\mathrm{Ce}_1(\xi, q)$

The function $\mathrm{Ce}_0(\xi, q)$ involved in Problem I has a positive zero in ξ for any assigned positive value of q, and consequently the principal frequency $\sqrt{\lambda}$ increases without limit as the eccentricity of the ellipse tends to unity. The derivative of Ce_1, however, has a positive zero in ξ only if $0 < q < 0{\cdot}89$, and thus $\sqrt{\mu}$ is such that $\beta \geqslant \sqrt{\mu} \geqslant 0$ for all values of the eccentricity.

To illustrate the latter functional property, parametric curves of the function $(d/d\xi)\mathrm{Ce}_1$ are shown in Fig. 1, for $s = 4q = 0, 1, 2, 3$, and 4.

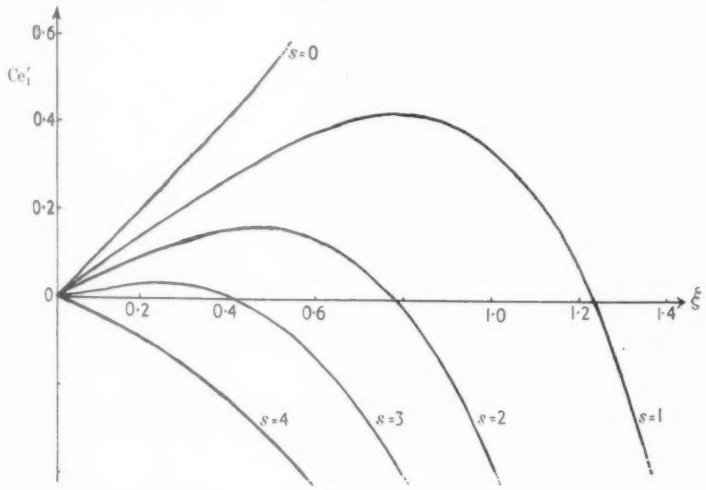

FIG. 1.

The absolute values of this function depend on the way in which Ce_1 itself is normalized; for convenience the normalization to be found in (**2**), p. xix, is adopted here. Thus

$$\mathrm{Ce}_1(0, q) = 1.$$

It then follows (pp. xx and xxii) that

$$\mathrm{Ce}_1(\xi, q) = \sqrt{(\tfrac{1}{2}\pi)} g_{e,1}(s) \sum_0^\infty C_{2k+1} J_{2k+1}(\sqrt{s}\cosh\xi),$$

where $g_{e,1}$ is the 'joining factor'. Finally we have

$$(d/d\xi)\mathrm{Ce}_1 = \sigma' \sqrt{(\tfrac{1}{2}\pi)} \sinh\xi \sqrt{s}\, g_{e,1}, \tag{5.1}$$

where σ' is the infinite series (4.1).

The function $\sqrt{s}\, g_{e,1}$ is tabulated in (**2**) (see p. 219).

When s is zero, σ' is equal to $\frac{1}{2}$ and $\sqrt{s}\, g_{e,1}$ is in fact equal to $2\sqrt{(2/\pi)}$; hence

$$(d/d\xi)\mathrm{Ce}_1(\xi, 0) \equiv \sinh\xi,$$

and this is in agreement with (2.9).

The positive zeros of the function (5.1) for $s = 1$, 2, and 3 are respectively 1·228, 0·779, and 0·409. Also it follows from (2.1) that the maxima occur for values of ξ satisfying

$$(a_1 - \tfrac{1}{2}s\cosh 2\xi)\mathrm{Ce}_1 = 0, \tag{5.2}$$

where in this case a_1 is the 'characteristic number'; the corresponding number as defined and tabulated in (**2**) (see p. 4) is $\mathrm{be}_1 = a_1 + \frac{1}{2}s$. It is of interest in connexion with (5.2) to note that the three appropriate values of ξ are not zeros of Ce_1 but are found from the equation

$$\cosh 2\xi = 2a_1/s = 2(\mathrm{be}_1/s) - 1.$$

For $s = 1$, 2, and 3 we get, therefore, $\xi = 0{\cdot}780$, 0·466, and 0·238 respectively at the maxima. The maximum values of the function could, if required, be found by direct substitution of s, ξ, and $w = \sqrt{s}\cosh\xi = \sqrt{(\mathrm{be}_1)}$ into (5.1).

REFERENCES

1. N. W. McLachlan, *Theory and Application of Mathieu Functions* (Oxford, 1947).
2. *Tables Relating to Mathieu Functions* (New York; Columbia University Press, 1951).
3. E. T. Kornhauser and I. Stakgold, 'A variational theorem for $\nabla^2 u + \lambda u = 0$ and its application', *J. of Math. and Phys.* **31** (1952–3), 45–54.
4. *Tables of the Bessel Functions*, The Annals of the Computation Laboratory of Harvard University, vols. iii to viii (Harvard University Press).
5. D. R. Hartree, *Numerical Analysis* (Oxford, 1952).
6. J. G. Herriot, *The Principal Frequency of an Elliptic Membrane*, Navy Contract N6–ORI–106, Task Order 5, Stanford, 1949.

TRANSIENT FLEXURAL STRESSES IN AN INFINITE BEAM

By R. P. N. JONES

(*Applied Mechanics Department, University of Sheffield*)

[Received 7 May 1954]

SUMMARY

A solution is obtained for the problem of an infinite beam under the action of a point load $PH(t)$, where $H(t)$ is the Heaviside unit function. The solution, which is based on Timoshenko's theory of transverse vibrations of beams, is obtained by the use of Fourier transforms, from which asymptotic approximations are obtained by the method of stationary phase. The solution shows that three wave-fronts are propagated in each direction from the loading point, and the stress distribution behind the slowest wave-front does not differ greatly from that given by ordinary beam theory.

1. Notation

C	shear rigidity of beam section
c	$\frac{1}{k}\sqrt{\left(\frac{EI}{m}\right)} = \sqrt{\frac{E}{\rho}}$
E	Young's modulus
F	shear force
$H(t)$	Heaviside unit function
I	moment of inertia of beam section
k	radius of gyration of beam section
m	mass of beam per unit length
M	bending moment
p	inversion parameter used in Fourier transforms
P	transverse point load
$q(x)$	transverse distributed load
s	x/k
t	time
u	y/k
x	distance along beam
y	transverse deflexion of beam
y_b	deflexion component due to bending
y_s	deflexion component due to shear
z	$\frac{s^2}{4\tau} = \frac{x^2}{4ctk}$

ρ density of beam material

γ $\dfrac{EI}{Ck^2}$

τ ct/k

λ wavelength

2. Introduction

The solution of the problem of an infinite uniform beam under the action of a transverse point-load $PH(t)$ has an important application in problems of transverse impact on finite beams. Solutions for similar infinite-beam problems have been obtained by Boussinesq (**1**) and others, using the ordinary equation for vibrations of beams, viz.

$$EI\frac{\partial^4 y}{\partial x^4}+m\frac{\partial^2 y}{\partial t^2}=q(x). \tag{1}$$

This equation, however, leads to an incorrect solution, in which there is instantaneous propagation of disturbances along the beam, whereas it is known (Prescott (**2**)) that an exact solution to such a problem exhibits wave-fronts which are propagated with finite velocity.

The solution given here by the author is based on Timoshenko's more accurate theory (**3**), (**4**), in which (1) is modified by the introduction of additional terms representing the effects of shear deflexion and rotary inertia. These modifications lead to a solution exhibiting wave-fronts similar to those expected in an exact solution. A similar problem, also using Timoshenko's equation, has been investigated by Dengler and Goland (**5**) by means of Fourier–Laplace transforms. Their solution, however, is in integral form, and not suitable for computation. In an earlier paper Robinson (**6**) gives a method for a step-by-step numerical solution which is, however, tedious except for investigating the initial spread of the disturbance.

In the present paper the solution is obtained by means of Fourier transforms, and, by using the method of stationary phase, asymptotic approximations are obtained for the shear force and bending moment in the beam. These approximations have the advantage of giving directly the amplitude and wavelength of the stresses which, owing to dispersion, are highly oscillatory. Special approximations are also obtained for the stresses in the region of the wave-fronts.

3. Equations of motion

The equations of motion used are those derived by Timoshenko taking into account shear deflexion and rotary inertia, the total transverse

deflexion being resolved into two components y_b and y_s due to bending and shear respectively.

The stress–strain relationships are

$$M = -EI\frac{\partial^2 y_b}{\partial x^2} \tag{2}$$

for the bending moment and

$$F = C\frac{\partial y_s}{\partial x} \tag{3}$$

for the shear force, where C is the effective shear rigidity of the beam section, that is, the shear force required to produce unit shear strain at the neutral axis.

The equations of motion† of the beam are

$$C\frac{\partial^2 y_s}{\partial x^2} - m\frac{\partial^2}{\partial t^2}(y_b + y_s) + q(x) = 0, \tag{4}$$

$$EI\frac{\partial^3 y_b}{\partial x^3} - mk^2\frac{\partial^3 y_b}{\partial x \partial t^2} + C\frac{\partial y_s}{\partial x} = 0. \tag{5}$$

A simplification can be obtained by introducing non-dimensional variables, s, u, and τ, defined by

$$\left.\begin{aligned} s &= \frac{x}{k} \\ u &= \frac{y}{k} \\ \tau &= \frac{ct}{k} \end{aligned}\right\}. \tag{6}$$

Making these substitutions, equations (2) to (5) become

$$M = -\frac{EI}{k}\frac{\partial^2 u_b}{\partial s^2}, \tag{7}$$

$$F = C\frac{\partial u_s}{\partial s}, \tag{8}$$

$$\frac{1}{\gamma}\frac{\partial^2 u_s}{\partial s^2} - \frac{\partial^2}{\partial \tau^2}(u_b + u_s) + \frac{k^3}{EI}q(x) = 0, \tag{9}$$

$$\frac{\partial^3 u_b}{\partial s^3} - \frac{\partial^3 u_b}{\partial s \partial \tau^2} + \frac{1}{\gamma}\frac{\partial u_s}{\partial s} = 0. \tag{10}$$

The quantity $\gamma = EI/Ck^2$ measures the effective ratio of flexural to shear stiffness. For a beam of rectangular section, $\gamma = 4$ approximately, but for

† In his original derivation Timoshenko obtains a single equation for the total deflexion $(y_b + y_s)$. It is more convenient, however, to treat the problem as one of coupled vibrations governed by the equations (4) and (5).

flanged sections, which are designed for flexural rather than shear strength, γ is considerably larger.

4. Fourier transforms

Multiplying equations (9) and (10) by e^{ips} and integrating with respect to s from $-\infty$ to $+\infty$, we get

$$\frac{p^2}{\gamma}\bar{u}_s+\frac{d^2}{d\tau^2}(\bar{u}_b+\bar{u}_s)-\frac{k^3}{EI}\int_{-\infty}^{\infty} q(x)e^{ips}\,ds = 0 \tag{11}$$

and

$$p^2\bar{u}_b+\frac{d^2\bar{u}_b}{d\tau^2}-\frac{1}{\gamma}\bar{u}_s = 0, \tag{12}$$

where $\bar{u}$ is the Fourier transform of u defined by

$$\bar{u}(p,\tau) = \int_{-\infty}^{\infty} u(s,\tau)e^{ips}\,ds. \tag{13}$$

Also, because of the point load $PH(t)$ applied at $x = 0$, we have in equation (11)

$$\int_{-\infty}^{\infty} q(x)e^{ips}\,ds = \frac{P}{k}H(\tau). \tag{14}$$

The complete solution of equations (11) and (12) satisfying the initial conditions $\bar{u} = 0$ and $d\bar{u}/d\tau = 0$ at $\tau = 0$ is

$$\bar{u}_b = \frac{Pk^2}{EIp^4}\{1+A_1(p)\cos\omega_1\tau+A_2(p)\cos\omega_2\tau\}, \tag{15}$$

$$\bar{u}_s = \frac{\gamma Pk^2}{EIp^2}\{1+B_1(p)\cos\omega_1\tau+B_2(p)\cos\omega_2\tau\}, \tag{16}$$

where

$$\left.\begin{aligned} A_1(p) &= -\frac{\omega_2^2}{\omega_2^2-\omega_1^2} \\ A_2(p) &= \frac{\omega_1^2}{\omega_2^2-\omega_1^2} \\ B_1(p) &= \frac{p^2-\gamma\omega_2^2}{\gamma(\omega_2^2-\omega_1^2)} \\ B_2(p) &= \frac{\gamma\omega_1^2-p^2}{\gamma(\omega_2^2-\omega_1^2)} \end{aligned}\right\} \tag{17}$$

and ω_1, ω_2 ($\omega_2 > \omega_1$) are the positive roots of the equation

$$(\gamma\omega^2-p^2)(\omega^2-p^2)-\omega^2 = 0. \tag{18}$$

The solution of the problem is now obtained by inversion of the Fourier transforms according to the usual inversion formula

$$u(s,\tau) = \frac{1}{2\pi}\int_{-\infty}^{\infty} \bar{u}(p,\tau)e^{-ips}\,dp. \tag{19}$$

Thus the bending moment and shear force are given by

$$M = \frac{Pk}{2\pi} \int_{-\infty}^{\infty} \{1 + A_1(p)\cos\omega_1\tau + A_2(p)\cos\omega_2\tau\} e^{-ips} \frac{dp}{p^2} \tag{20}$$

and

$$F = \frac{P}{2\pi i} \int_{-\infty}^{\infty} \{1 + B_1(p)\cos\omega_1\tau + B_2(p)\cos\omega_2\tau\} e^{-ips} \frac{dp}{p}. \tag{21}$$

The deflexion of the beam is, of course, symmetrical about $s = 0$ and further analysis will therefore be restricted to the region $s \geqslant 0$.

It may be shown that, when $s > \tau$, the integrals (20) and (21) are identically zero. The integrands are single-valued and have no poles throughout the p-plane, and the path of integration may therefore be deformed into an infinite semicircle in the lower half-plane. Along this path the integrals are readily shown to be zero when $s > \tau$.

5. Stationary-phase approximations—the general case

It is convenient to resolve the bending moment into two components, viz.

$$M_1 = \frac{Pk}{2\pi} \int_{-\infty}^{\infty} \{1 + A_1(p)\cos\omega_1\tau\} e^{-ips} \frac{dp}{p^2}, \tag{22}$$

$$M_2 = \frac{Pk}{2\pi} \int_{-\infty}^{\infty} A_2(p)\cos\omega_2\tau\, e^{-ips} \frac{dp}{p^2}, \tag{23}$$

and similarly the shear force,

$$F_1 = \frac{P}{2\pi i} \int_{-\infty}^{\infty} \{1 + B_1(p)\cos\omega_1\tau\} e^{-ips} \frac{dp}{p}, \tag{24}$$

$$F_2 = \frac{P}{2\pi i} \int_{-\infty}^{\infty} B_2(p)\cos\omega_2\tau\, e^{-ips} \frac{dp}{p}. \tag{25}$$

None of the integrands has a pole within the range of integration, and asymptotic approximations for the integrals may therefore be obtained by the method of stationary phase (Lamb (**7**)).

Consider the integral

$$\int_{-\infty}^{\infty} A_1(p)\exp[if(p)] \frac{dp}{p^2}, \tag{26}$$

where

$$f(p) \equiv \omega_1\tau - ps. \tag{27}$$

The approximation given by the stationary-phase method is

$$\sqrt{(2\pi)}\frac{A_1(p_1)}{p_1^2}\{|f''(p_1)|\}^{-\frac{1}{2}}\exp[if(p_1)\pm i\tfrac{1}{4}\pi]. \tag{28}$$

The $+$ or $-$ sign is taken according as $f''(p_1)$ is $+$ or $-$, and p_1 is the value of p satisfying the stationary-phase condition

$$f'(p_1) = 0 \tag{29}$$

which may be written in the form

$$\left[\frac{d\omega_1}{dp}\right]_{p=p_1} = \frac{s}{\tau}. \tag{30}$$

The approximation (28) is valid provided that $A_1(p)/p^2$ is not varying rapidly at $p = p_1$ and also that

$$|f'''(p_1)| \ll \{|f''(p_1)|\}^{\frac{3}{2}}, \tag{31}$$

that is, provided

$$\left|\frac{d^3\omega_1}{dp^3}\right|_{p=p_1} \ll \sqrt{\tau}\left\{\left|\frac{d^2\omega_1}{dp^2}\right|\right\}^{\frac{3}{2}}_{p=p_1}. \tag{32}$$

Except for certain values of p, this criterion is satisfied for large values of $\tau \equiv ct/k$ and the solutions obtained are therefore asymptotic approximations, which are valid provided the disturbance has spread over a distance large compared with the depth of the beam.

Using the procedure outlined above, the following approximations are obtained:

$$M_1 \simeq \frac{Pk}{\sqrt{(2\pi\tau)}}\left[\frac{A_1(p)}{p^2}\left\{\left|\frac{d^2\omega_1}{dp^2}\right|\right\}^{-\frac{1}{2}}\cos(\omega_1\tau - ps \pm \tfrac{1}{4}\pi)\right]_{p=p_1}, \tag{33}$$

and

$$M_2 \simeq \frac{Pk}{\sqrt{(2\pi\tau)}}\left[\frac{A_2(p)}{p^2}\left\{\left|\frac{d^2\omega_2}{dp^2}\right|\right\}^{-\frac{1}{2}}\cos(\omega_2\tau - ps \pm \tfrac{1}{4}\pi)\right]_{p=p_2}, \tag{34}$$

where p_2 is the root of the equation

$$\left[\frac{d\omega_2}{dp}\right]_{p=p_2} = \frac{s}{\tau}. \tag{35}$$

Similar approximations may be obtained for F_1 and F_2.

6. It will be understood that if the equation (30), for example, has two real roots, then there will be two corresponding contributions, each of the form (33), to the approximation for M_1. Should there be no real root, then the asymptotic approximation is zero.

Fig. 1 shows the variation of $d\omega_1/dp$ and $d\omega_2/dp$ with p. These curves have been plotted for the particular case when $\gamma = 4$, but the same essential features are obtained in the general case when $\gamma > 1$. It is seen that there

is a value of s/τ ($= \alpha$, say) for which equation (30) has repeated roots. For other values of s/τ the number of real roots of the equation are as follows:

$$\begin{aligned} s/\tau &> \alpha && \text{no root,} \\ \alpha &\geqslant s/\tau \geqslant \gamma^{-\frac{1}{2}} && \text{two roots,} \\ \gamma^{-\frac{1}{2}} &> s/\tau \geqslant 0 && \text{one root.} \end{aligned}$$

Equation (35), on the other hand, has only one real root throughout the range $1 \geqslant s/\tau \geqslant 0$.

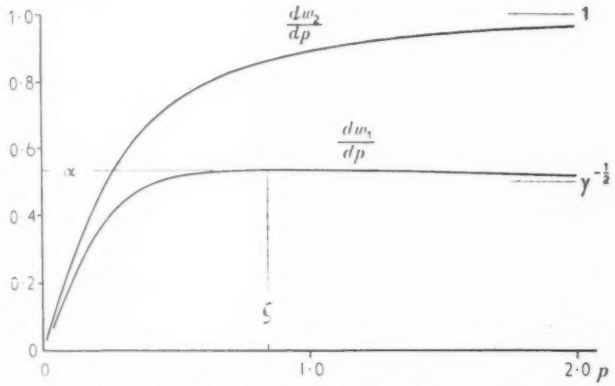

FIG. 1. Variation of $d\omega_1/dp$, $d\omega_2/dp$, with p.

The numerical evaluation of the above approximations has been undertaken for the particular case when $\gamma = 4$, and the results are presented in Figs. 2 to 4, which show the amplitude and wavelength of $M_1\sqrt{(2\pi\tau)}/Pk$ and $M_2\sqrt{(2\pi\tau)}/Pk$ plotted against s/τ. The component M_1' is the additional contribution due to the second root of equation (30) in the region

$$\alpha \geqslant s/\tau \geqslant \gamma^{-\frac{1}{2}}.$$

It will be noted that the component M_2 is comparatively small.

Here again, the same essential features of the solution are obtained in the general case when $\gamma > 1$ and it is seen that there is a wave-front at $s = \tau\gamma^{-\frac{1}{2}}$ in addition to that at $s = \tau$, together with an additional singularity at $s = \alpha\tau$. At all three points the condition (32) is not satisfied, and the general approximations hitherto obtained break down. Special approximations will now be obtained for these points.

7. Approximations when $s \simeq \tau$, $s \simeq \tau\gamma^{-\frac{1}{2}}$

Consider the integral

$$\int_{-\infty}^{\infty} A_2(p) \exp[i\omega_2\tau - ips] \frac{dp}{p^2}. \tag{36}$$

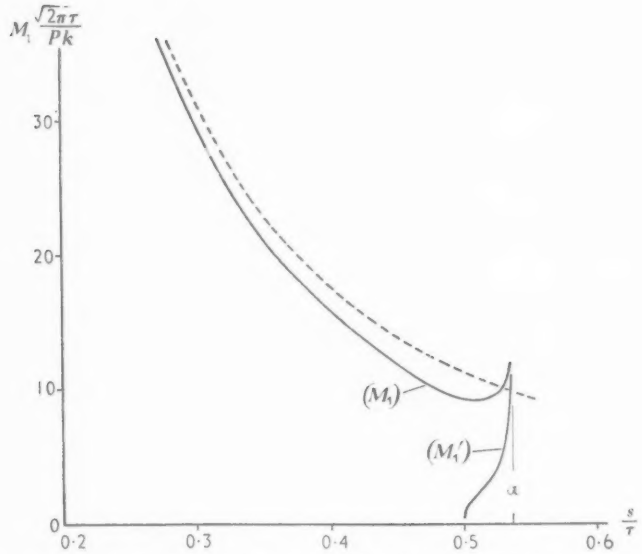

FIG. 2. Variation of amplitude of $M_1\sqrt{(2\pi\tau)}/Pk$ with s/τ ($\equiv x/ct$). (The dotted curve gives the solution by ordinary beam theory.)

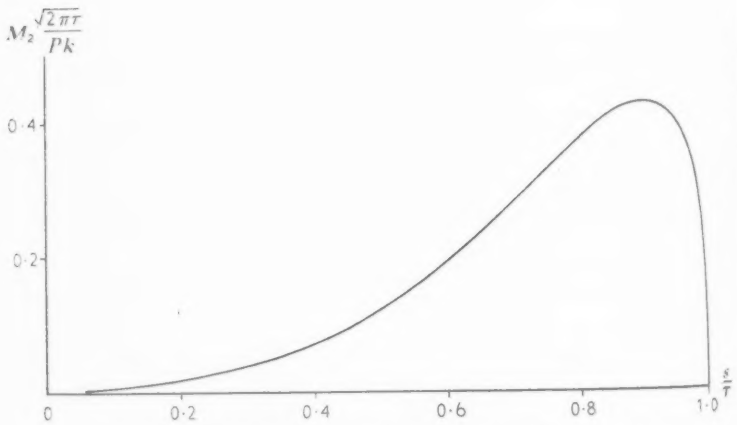

FIG. 3. Variation of amplitude of $M_2\sqrt{(2\pi\tau)}/Pk$ with s/τ.

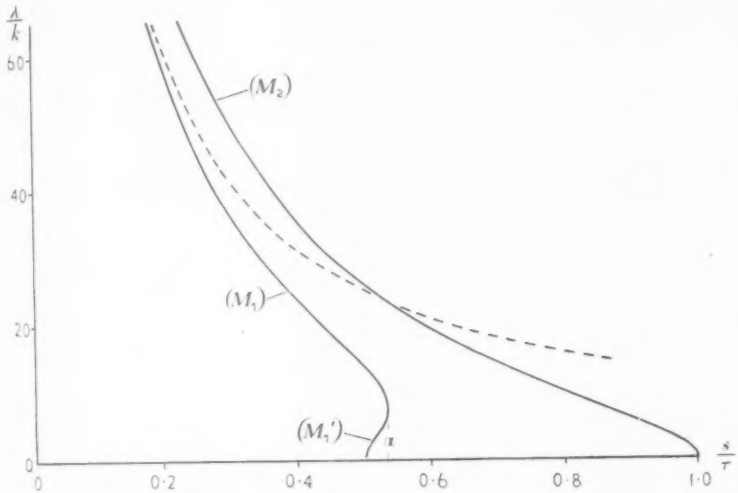

FIG. 4. Variation of wavelength with s/τ. (The dotted curve gives the solution by ordinary beam theory.)

As $s/\tau \to 1$, $p_2 \to \infty$, and the bulk of the contribution to the integral occurs for large values of p. Now, when $|p|$ is large,

$$\left.\begin{aligned} \omega_2 &\sim |p| + \frac{1}{2|p|(\gamma-1)} \\ A_2(p) &\sim \frac{1}{\gamma-1} \end{aligned}\right\}, \tag{37}$$

and therefore, when $s \simeq \tau$, the integral (36) has an asymptotic approximation

$$\frac{1}{\gamma-1}\int_0^\infty \exp\left[ip\tau - ips + \frac{i\tau}{2p(\gamma-1)}\right]\frac{dp}{p^2}. \tag{38}$$

The use of the zero lower limit here is necessary to exclude an unwanted contribution to the integral (38) in the region $p = -\infty$.

Similarly, when $s \simeq \tau$ the bulk of the contribution to the integral

$$\int_{-\infty}^{\infty} A_2(p)\exp[-i\omega_2\tau - ips]\frac{dp}{p^2} \tag{39}$$

occurs in the region $p = -\infty$ and therefore an asymptotic approximation is

$$\frac{1}{\gamma-1}\int_{-\infty}^{0} \exp\left[ip\tau - ips + \frac{i\tau}{2p(\gamma-1)}\right]\frac{dp}{p^2}. \tag{40}$$

Hence

$$M_2 \simeq \frac{Pk}{4\pi(\gamma-1)} \int_{-\infty}^{\infty} \exp\left[ip(\tau-s)+\frac{i\tau}{2p(\gamma-1)}\right]\frac{dp}{p^2} \tag{41}$$

$$\simeq -Pk\sqrt{\left(\frac{\tau-s}{2\tau(\gamma-1)}\right)}J_1\left[\sqrt{\left(\frac{2\tau(\tau-s)}{\gamma-1}\right)}\right]H(\tau-s), \tag{42}$$

and similarly

$$F_2 \simeq P\left(\frac{\tau-s}{\tau(\gamma-1)}\right)J_2\left[\sqrt{\left(\frac{2\tau(\tau-s)}{\gamma-1}\right)}\right]H(\tau-s). \tag{43}$$

Approximations for M_1' and F_1' in the region $s \simeq \tau\gamma^{-\frac{1}{2}}$ may also be obtained in the forms

$$M_1' \simeq Pk\gamma\sqrt{\left(\frac{s\sqrt{\gamma}-\tau}{2\tau(\gamma-1)}\right)}J_1\left[\sqrt{\left(\frac{2\tau(s\sqrt{\gamma}-\tau)}{\gamma(\gamma-1)}\right)}\right]H(s\sqrt{\gamma}-\tau), \tag{44}$$

$$F_1' \simeq \frac{P}{2}J_0\left[\sqrt{\left(\frac{2\tau(s\sqrt{\gamma}-\tau)}{\gamma(\gamma-1)}\right)}\right]H(s\sqrt{\gamma}-\tau). \tag{45}$$

Equation (45) shows that there is a discontinuity of magnitude $\frac{1}{2}P$ in the shear force at $s = \tau\gamma^{-\frac{1}{2}}$.

8. Approximations when $s = \alpha\tau$

When $s = \alpha\tau$, equation (30) has repeated roots, $p_1 = p_1' = \xi$, say, and $d^2\omega_1/dp^2 = 0$.

Consider again the integral (26). Since both $f'(\xi)$ and $f''(\xi)$ are zero, we can write

$$f(p) = f(\xi)+\frac{(p-\xi)^3}{6}f'''(\xi)+\ldots \tag{46}$$

and therefore, when $s = \alpha\tau$, an asymptotic approximation for the integral (26) is

$$\frac{A_1(\xi)}{\xi^2}\exp[if(\xi)]\int_{-\infty}^{\infty}\exp\left[\frac{i(p-\xi)^3f'''(\xi)}{6}\right]dp \tag{47}$$

$$= \frac{A_1(\xi)}{\xi^2}\exp[if(\xi)]\{\tfrac{1}{2}|f'''(\xi)|\}^{-\frac{1}{3}}\int_{-\infty}^{\infty}\exp\left[\frac{i\psi^3}{3}\right]d\psi. \tag{48}$$

The value of the integral in the expression (48) is 2·230 approximately, and thus it may be shown that, when $s = \alpha\tau$,

$$M_1 \simeq 2{\cdot}230\frac{Pk}{2\pi}\left[\frac{A_1(p)}{p^2}\left\{\frac{\tau}{2}\left|\frac{\partial^3\omega_1}{\partial p^3}\right|\right\}^{-\frac{1}{3}}\cos(\omega_1\tau-ps)\right]_{p=\xi}, \tag{49}$$

and similarly

$$F_1 \simeq 2{\cdot}230\frac{P}{2\pi}\left[\frac{B_1(p)}{p}\left\{\frac{\tau}{2}\left|\frac{\partial^3\omega_1}{\partial p^3}\right|\right\}^{-\frac{1}{3}}\sin(\omega_1\tau-ps)\right]_{p=\xi}. \tag{50}$$

For the particular case when $\gamma = 4$, $\alpha = 0{\cdot}536$, $\xi = 0{\cdot}844$, and these approximations become

$$M_1 \simeq -1{\cdot}26Pk\tau^{-\frac{1}{2}}\cos(0{\cdot}354\tau - 0{\cdot}844s), \tag{51}$$

$$F_1 \simeq -0{\cdot}883P\tau^{-\frac{1}{2}}\sin(0{\cdot}354\tau - 0{\cdot}844s). \tag{52}$$

9. Approximations when s is small

Finally, when $s/\tau \to 0$, $p_1 \to 0$ and the approximation (33) breaks down owing to the presence of a pole at $p = 0$ in the integrand of (26).

Now, when p is small,

$$\left.\begin{aligned} \omega_1 &\simeq p^2 \\ A_1 &\simeq -1 \\ B_1 &\simeq -1 \end{aligned}\right\}. \tag{53}$$

Asymptotic approximations for M_1 and F_1 in the region $s/\tau \simeq 0$ are therefore

$$M_1 \simeq \frac{Pk}{2\pi}\int_{-\infty}^{\infty}(1-\cos p^2\tau)e^{-ips}\frac{dp}{p^2}, \tag{54}$$

$$F_1 \simeq \frac{P}{2\pi i}\int_{-\infty}^{\infty}(1-\cos p^2\tau)e^{-ips}\frac{dp}{p}. \tag{55}$$

The integral (55) is of standard form, giving

$$F_1 \simeq -\frac{P}{2}\{1-C(z)-S(z)\}, \tag{56}$$

where

$$z \equiv \frac{s^2}{4\tau} \equiv \frac{x^2}{4ctk} \tag{57}$$

and $C(z)$, $S(z)$ are Fresnel's integrals defined by

$$C(z)+i\,S(z) = \int_0^z e^{i\psi}\frac{d\psi}{\sqrt{(2\pi\psi)}}. \tag{58}$$

The integral (54) may be derived from (55) by integrating with respect to s giving

$$M_1 \simeq -\frac{Psk}{2}\left\{1-C(z)-S(z)+\frac{\sin z-\cos z}{\sqrt{(2\pi z)}}\right\}. \tag{59}$$

Expressions (56) and (59) are identical with those obtained for the shear force and bending moment by ordinary beam theory, using equation (1) (Jones (**8**)).

By using the asymptotic expansions for $C(z)$, $S(z)$ (Watson (**9**)), expression (59) can be written in the following form, valid for large values of z:

$$M \sim -\frac{2Pk}{\sqrt{(\pi\tau)}}\left(\frac{\tau}{s}\right)^2\cos(z-\tfrac{1}{4}\pi). \tag{60}$$

This asymptotic approximation is given by the dotted curves in Figs. 3 and 4. It is seen that, when $\gamma = 4$, the solution by ordinary theory gives a good approximation (apart from a discrepancy in the wavelength) in the region $0 \leqslant s < \tau\gamma^{-\frac{1}{2}}$.

10. Application to other loading conditions

The formal extension of the present solution to problems in which the external load has any given time-variation may be achieved by the use of Duhamel's integral.

Of particular interest is the case when the beam is subjected to an impulsive load. If the impulse is taken in the form of a Dirac δ-function, the solution may be formally obtained by differentiating the present solution with respect to t. It follows that there will be an impulsive shear force of magnitude $\frac{1}{2}I_0$ at the point $s = \tau\gamma^{-\frac{1}{2}}$, I_0 being the magnitude of the applied impulse. From equations (41) and (44) it may also be shown that there will be discontinuities in the bending moment of magnitude

$$\frac{I_0 c}{2(\gamma-1)} \quad \text{at } s = \tau \tag{61}$$

and

$$\frac{I_0 c\sqrt{\gamma}}{2(\gamma-1)} \quad \text{at } s = \tau\gamma^{-\frac{1}{2}}. \tag{62}$$

From the point of view of technical applications, it is evident that, when the beam is subjected to a sustained load, the maximum stresses will ultimately occur at the loading point and will be given satisfactorily by ordinary beam theory. For a highly impulsive load, however, the maximum stresses are likely to occur at the wave fronts, in which case the ordinary theory will be inadequate.

REFERENCES

1. J. Boussinesq, *Application des potentiels* (Paris, 1885), 435.
2. J. Prescott, *Phil. Mag.* **33** (1942), 703.
3. S. P. Timoshenko, ibid. **41** (1921), 744.
4. —— ibid. **43** (1922), 125.
5. M. A. Dengler and M. Goland, *Proc. First U.S. Nat. Congress of Applied Mechanics* (1951), 179.
6. A. Robinson, Aeronautical Research Council, R. & M. No. 2265 (1950).
7. H. Lamb, *Hydrodynamics* (Cambridge, 1932), 395.
8. R. P. N. Jones, *J. Applied Mech.* **21** (1954), 75.
9. G. N. Watson, *Theory of Bessel Functions* (Cambridge, 1922), 545.

EAM

in Figs. 1
eory gives
gth) in the

which the
y the use

ed to an
function,
e present
ive shear
de of the
own that
e

(61)

(62)

at, when
sses will
orily by
aximum
rdinary

Applied

THE QUARTERLY JOURNAL OF MECHANICS AND APPLIED MATHEMATICS

VOLUME VIII PART 3 SEPTEMBER 1955

CONTENTS

The Editorial Board gratefully acknowledge the support given by: Bristol Aeroplane Company; Courtaulds Scientific and Educational Trust Fund; English Electric Co., Ltd.; General Electric Company; Imperial Chemical Industries Ltd.; Unilever Ltd.
